Institute for
WATER RESOURCES
AND WATER SUPPLY

TUHH
Hamburg University of Technology

New applications of Fine-Grained Iron Oxyhydroxides as Cost-effective Arsenic Adsorbents in Water Treatment

Doctoral Dissertation

2020

Muhammad Usman

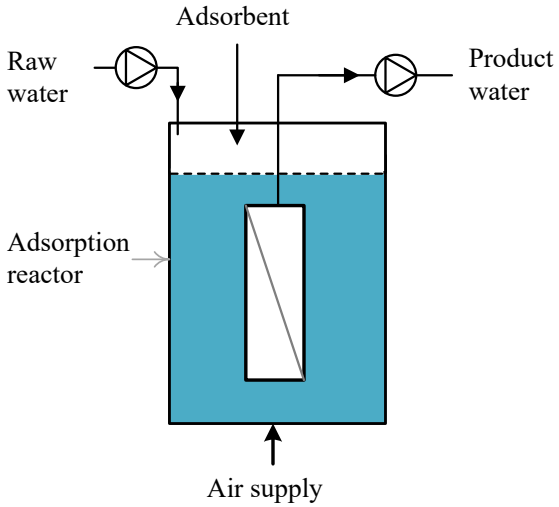

New applications of fine-grained iron oxyhydroxides as cost-effective arsenic adsorbents in water treatment

Vom Promotionsausschuss der

Technischen Universität Hamburg

zur Erlangung des akademischen Grades

Doktor-Ingenieur (Dr.-Ing.)

genehmigte Dissertation

von

Muhammad Usman (M.Sc.)

aus

Multan, Pakistan

2020

Examiners

Prof. Dr.-Ing. Mathias Ernst

Prof. Dr.-Ing. Martin Jekel

Chairman of Examination Board

Prof. Dr.-Ing. Frank Schmidt-Döhl

Date of Oral Examination

October 20, 2020

DOI: https://doi.org/10.15480/882.3388

https://orcid.org/0000-0002-8977-7523

Acknowledgement

I would like to express very sincere gratitude to my advisor Prof. Dr.-Ing- Mathias Ernst for the extraordinary support in successful completion of this dissertation. He gave me a lot, the freedom to choose a research area that inspire me, the motivation, the support and the light in some dark periods. In addition to this, the advices and comments of Prof. Ernst contributed significantly in my Ph.D. process. I would like to thank Prof. Dr.-Ing. Martin Jekel on the acceptance to be part of examination committee and to co-review this doctoral dissertation. My very sincere thanks to Prof. Dr.-Ing. Frank Schmidt-Döhl for taking over the chair of the examination committee. At the organisational level, I would like to thank Higher Education Commission (HEC) of Pakistan, German Academic Exchange Service (DAAD) for the financial support and and the Hamburg University of Technology for resources that led to successful completion of this dissertation.

During my Ph.D., I had the opportunity to collaborate with many different people. All of them offered me an optimum research conditions to achieve my professional goals. I am profoundly grateful to all of them for their contribution and support. In the very beginning of this research, I "inherited" the experimental setup for batch adsorption experiments and low-pressure membrane filtration unit from Dr.-Ing. Martin Schulz. I would like to thank him for introducing me to these experimental setups. I greatly appreciated the help of Dorota Bruniecka-Sulewski, Thorsten Dorsch, Daniel Steinbarth and Jens-Uwe Stoß, whenever something needed to be constructed, repaired or any computer issue needed to be solved. Special thanks to Dr.-Ing. habil. Klaus Johannsen not only for his support in understanding mass transfer-based kinetic models but also for his prudent and pointed guidance. Ute Schuppert and Ilona Düring were of great help solving any administrative issue. I acknowledge the valuable suggestions of Tomi Mantel for thesis writing. Dr.-Ing. Carsten Bahr (GEH Wasserchemie) and Prof. Dr. Manasis Mitrakas are thanked for supply of GFH and TMF materials.

Many thanks also to Alberto Bueno Morales from the Insitute of Thermal Separation Processes for his help with the BET surface measurements. The construction and automation of the experimental setups would not have been possible without the efficient support of the employees of the TUHH's central research service, particularly Hans Wilhelm Mehrkens from the electrical workshop, and Marin Schulz and Volker Klatt from central laboratory.

This dissertation would not have been possible without the hard-working and excellent students which I had the pleasure to work with (in alphabetical order): Bruna Alves, Aida Idrissi Belkasmi, Sumbal Tasawwar, Josma Henna Rodrigues, Muhammad Waseem. It was a great pleasure to work with all of you. Special thanks to Ioannis A. Katsoyiannis for proof-reading and critically reviewing the manuscripts including pre- or post-publication stages. I would also like to thank Dr. Mohsen Zarebanadkouki for his enthusiasm and programming skills which resulted in the development of mathematical model for arsenic adsorption in the slurry reactor. I still remember the days we spent understanding and comparing adsorption models and completing our joint paper in journal of hazardous materials.

I wish to express my gratitude to all of my co-workers at the the Institute for Water Resources and Water Supply (TUHH) and the DVGW Research Centre TUHH, who create this special atmosphere which makes working there very enjoyable. The last four years have been a very good time for me. Many thanks to all of you.

Last and most important, I would like to express my thanks to my whole family particularly my wife, Ayesha Anwar, mother, and brother, Muhammad Yasin. Without all of you, successful completion of this doctoral dissertation would have not been possible. You have not only supported me but also motivated me with great understanding and constant positivity throughout this challenging journey.

Abstract

Arsenic pollution of drinking waters across the world is one of the most serious water-related problems due to its well-established consequences on human health even at very low concentrations in the lower µg/L range. Among different well-established options for arsenic remediation, the adsorption onto highly efficient commercial iron oxyhydroxide-based adsorbent such as granular ferric hydroxide (GFH). However, GFH is a cost-extensive material. During the industrial production of granular fractions of conventional adsorbents, the fine-grained fraction (individual particle size of < 250 µm) is generated as by-product/waste as this fraction of granular adsorbents cannot be applied in fixed-bed adsorption filters because of high clogging potential in filter-bed.

In this doctoral thesis, an integrated water process combining the adsorption and submerged microfiltration (MF) unit (abbreviated as SMAHS) was investigated to employ fine-grained iron oxyhydroxides. Air bubbling was applied in the slurry reactor of a SMAHS to introduce shear at the membrane surface for fouling control. Moreover, the powdered-sized fractions (individual particle size of ~ 3 µm) of iron oxyhydroxides were applied to form the pre-deposited dynamic membrane (DM) and the effectiveness of the formed DM was assessed in MF process.

n addition to the fine fraction of the GFH, arsenic adsorption on µTMF (fine-grained tetravalent manganese feroxyhyte) was investigated through batch adsorption tests at pH 8 in three different water matrices and different adsorption isotherms were applied. The physical and chemical characteristics of the adsorbents were also fully investigated. The Freundlich isotherm describes the equilibrium isotherm data better than Langmuir isotherm, indicating a heterogeneous nature of the applied adsorbents. The isotherm data shows characteristics of favorable arsenic adsorption onto µGFH and µTMF. Further, adsorption efficiency of applied adsorbents depends strongly on the water quality parameters (pH and water matrix). Arsenic adsorption onto both adsorbents is mostly reversible, with a small proportion of irreversible adsorption.

The findings from SMAHS indicate that the arsenic adsorption efficiency is comparable to that found in a fixed-bed adsorption filter packed with conventional adsorbents of the same type, with potential benefits of simultaneous removal of micro-organisms and turbidity. The material cost is estimated to be as low as 0.30 €/m^3 of product water when the arsenic concentration in the product water is below the drinking water regulation limit (10 µg/L). The outcomes further suggest that iron oxyhydroxides as forming materials of DMs may be applied in water treatment to achieve arsenic removal rates of greater than 90 % if operating conditions are well controlled. Moreover, arsenic removal rates of the SMAHS and DM can be predicted/modeled using a mathematical model based on a homogenous surface diffusion model (HSDM). In conclusion, it is expected that the new applications of fine-grained iron oxyhydroxides would not only increase the sustainable footprint of the conventional adsorbent production process as the by-product will be utilized but also be efficient solutions for arsenic remediation using the highly efficient low-cost adsorbents in water treatment.

Zusammenfassung

Die Anwesenheit von Arsen in Grundwässern stellt in vielen Regionen der Welt ein ernsthaftes Problem für die Trinkwasseraufbereitung dar. Schon bei regelmäßigen Aufnahme sehr geringerer Arsen-Konzentrationen im unteren µg/L-Bereich ist mit gesundheitliche Folgen zu rechnen. Neben anderen Verfahren, stellt die Adsorption an granulierten Eisenhydroxid (GEH) eine geeignete Methode zur Entfernung von Arsen aus dem Rohwasser dar. Jedoch besitzt diese Methode den Nachteil, dass herkömmliches GEH kostenintensiv ist. Während des Produktionsprozesses von GEH fällt eine bisher nicht genutzte Fraktion an, die als Feinfraktion bezeichnet wird (Patrikelgröße < 250µm). Diese Fraktion kann auf Grund ihres Verblockungspotentials für die Poren des Filterbetts, nicht in konventionellen GEH-Festbett-Adsorbern verwendet werden und gilt daher als Neben- bzw. Abfallprodukt.

Im Rahmen der vorliegenden Arbeit wurde zum einen die Adsorption von Arsen mittels GEH-Feinfraktion untersucht und zum anderen inwiefern man die GEH-Partikel anschließend mittels getauchter Mikrofiltration zurückhalten werden können (SMAHS-Verfahren). Der Adsorptionsreaktor wurde mit Gasblasen belüftetet, um Membranfouling zu vermindern. Die GEH Partikel (~ 3 µm) bildeten auf der Membran eine Deckschicht, welche als dynamische Membran fungierte.

Neben der Feinfraktion des GEH wurden Adsorptionsversuche mit µTMF (Feinfraktion Tetravalentes Mangan-Eisenhydroxid) durchgeführt und miteinander verglichen. Diese Versuche wurden als Batchversuche bei pH 8 mit drei verschiedenen Wassermatrizen und unter Anwendung verschiedener Adsorptionsisothermen durchgeführt. Dabei stellte sich heraus, dass die Freundlich-Isotherme besser geeignet war, um das Adsorptionsgleichgewicht abzubilden als die Langmuir-Isotherme, was auf eine heterogene Beschaffenheit des verwendeten Adsorbens hinweist. Die Isothermen zeigen für beide Adsorptionsmittel eine hohe Affinität für die Arsen-Adsorption. Weiterhin konnte gezeigt werden, dass die Adsorption stark von der Wassermatrix und dem pH-Wert abhängt. Die Adsorption war an beiden Adsorptionsmitteln weitgehend reversibel.

Darüber hinaus hat diese Arbeit gezeigt, dass das SMAHS-Verfahren eine mit dem GEH-Festbett-Adsorber vergleichbare Arsen Abscheidung aufweist, wobei durch die Mikrofiltration der SMASH-Verfahrens zusätzlich Mikroorganismen und Partikel aus dem Rohwasser entfernt werden. Bei Einhaltung des Arsen-Grenzwertes im Permeat von 10 µg/L, liegen die Materialkosten für die Aufbereitung bei ca. 0,30 €/m³ filtrierten Wassers. Weiterhin hat diese Arbeit gezeigt, dass durch die Bildung einer dynamischen Membran aus GEH, Arsen-Entfernungsraten von mehr als 90 % möglich sind, wenn die Prozessbedingungen richtig abgestimmt sind. Durch die Anwendung eines mathematischen Modells (Homogeneous Surface Diffusion), konnte die Arsen-Entfernungsleistung im SMASH-Verfahren erfolgreich prognostiziert werden.

Die Verwendung der GEH-Feinfraktion im SMASH-Verfahren würde die Produktion von GEH insgesamt ökologischer und ökonomischer werden lassen, da ein bisheriges Abfallprodukt nutzbar gemacht wird. Darüber hinaus stellt das SMASH Verfahren eine effektive und kostengünstige Alternative zu herkömmlichen Technologien der Arsen-Entfernung aus Trinkwässern dar.

Table of Contents

List of Figures

List of Tables

Abbreviations and Quantities

Abbreviations

AC	Activated carbon
B_i	Biot number
DOC	Dissolved organic carbon
DI water	Deionized water
DM	Dynamic membrane
t_e	Equilibrium time
GFH	Granular ferric hydroxide
HSDM	Homogenous surface diffusion model
HH	Hamburg
HMP	Hybrid membrane process
Fe	Iron
LPM	Low-pressure membrane
µGFH	Micro-sized granular ferric hydroxide
µTMF	Micro-sized tetravalent manganese feroxyhyte
MF	Microfiltration
NSF	National Sanitation Foundation
PAC	Powdered activated carbon
pH_{IEP}	pH value at isoelectric point
RO	Reverse osmosis
SEM	Scanning electron microscopy
SMAHS	Submerged membrane adsorption hybrid system

SSE	Sum of square of error
SSP	Specific system productivity
TMF	Tetravalent manganese feroxyhyte
TMP	Trans-membrane pressure
UF	Ultrafiltration
WHO	World health organization

Quantities

d_p	μm	Particle diameter
$d_{p,mean}$	m	Mean particle diameter
C_o	μg/L	Initial arsenic liquid phase concentration
C_{in}	μg/L	Influent arsenic liquid phase concentration
C	μg/L	Liquid phase concentration
C_s	μg/L	Liquid phase concentration at the exterior surface of the particle
C_e	μg/L	Equilibium liquid phase concentration
Q_e	μg/mg	Equilibium solid phase concentration
T_{10}	h	Time taken to reach arsenic concentration to 10 μg/L
Q_{max}	μg/mg	Maximum loading of Langmuir equation
Q_{DR}	μg/mg	Theoretical saturation loading of Dubinin–Radushkevich equation
Q	μg/mg	Solid phase concentration
Q_o	μg/mg	Solid phase concentration in equilibrium with initial liquid phase concentration

Q_{10}	µg/mg	Adsorption capacity at C_e = 10 µg/L
k_f	m/s	Liquid-phase mass transfer coefficient
D_s	m^2/s	Intraparticle surface diffusion coefficient
K_F	$(\mu g/mg_{ad})/(\mu g/L)^n$	Freundlich isotherm coefficient
n	-	Freundlich isotherm constant
b	L/mg	Langmuir constant
M_a	mg/cm^2	Mass of adsorbent per unit area of the primary membrane
V	L	Volume
Q_v	m^3/s	Volumetric flow rate
R_g	J/mol. K	Gas constant
t	-	Time coordinate
r	m	Radial length
R	m	Particle radius
Q_t	µg/mg	Solid phase concentration at any time (t)
ε_B	-	Filter bed porosity
v_f	m/s	Filter velocity
ρ_p	Kg/m^3	Particle density
k_1	L/(mg·h)	Pseudo-first-order rate constant
k_2	L/(mg·h)	Pseudo-second-order rate constant
n	-	Freundlich isotherm exponent
K_{DR}	mol^2 /kJ	Dubinin–Radushkevich constant
R_L	-	Langmuir separation factor

J	$L/(m^2 \cdot h)$	Membrane water flux
A_m	m^2	Membrane area
M_{ad}	g or mg	Mass of adsorbent
EBCT	min	Empty bed contact time
T	°C	Temperature
HRT	h	Hydraulic residence time
E	kJ/mol	Energy of adsorption from
R^2	-	Coefficient of deterimation
ΔG°	kJ/mol	Gibbs free energy

1 Introduction

1.1 Background

Water, the core of life that helps us to exist, is essential for all to drink clean and pure water. Due to natural and anthropogenic sources, water becomes polluted that results in the origin of different water pollutants (Shannon et al. 2008; Singh et al. 2020). Water pollution is one of the most critical environmental problems nowadays, especially those involving heavy metal contamination (Thanawatpoontawee et al. 2016). Further, Scientific development has raised awareness of water pollutant forms and has reawakened the necessity for its effective purification (Usman et al. 2018a). Among all the pollutants contributing to the increased pollution of the water, heavy metals like arsenic, lead, cadmium, nickel, mercury, chromium, cobalt, zinc, and selenium have received paramount attention to environmental chemists due to their toxic nature (Cornelis et al. 2008). Heavy metals are usually present in trace amounts in natural waters but many of them are toxic even at very low concentrations such as arsenic (Herawati et al. 2000). The increasing quantity of heavy metals in our resources is currently an area of greater concern, especially since a large number of industries are discharging their metal containing effluents into freshwater without any adequate treatment (Salomons et al. 2012).

With its well-established consequences to human health, the presence of arsenic in water has become an important issue in water and wastewater treatment. The presence of arsenic at elevated concentrations in natural environments can be attributed to both natural and anthropogenic inputs (Hindmarsh and McCurdy 1986; Violante et al. 2006). Arsenic pollution is primarily caused by natural processes, such as weathering of rocks and minerals, followed by leaching and by industrial activities that lead to pollution of soil and groundwater (Hindmarsh and McCurdy 1986; Tantry et al. 2015). The discharge of arsenic polluted waters from mining or mining-related activities, pharmaceutical industry, and agricultural activities plays an important role in anthropogenic arsenic pollution in Asia (Mukherjee et al. 2006). However, the introduction of arsenic into groundwater is expected to occur mainly as a result of its natural geological presence in rocks (Garelick et al. 2009). Of the approximately 200 contaminants that have been detected in US public groundwater supplies, arsenic is the chemical contaminant with the highest priority (Knox and Canter 1996).

Arsenic is a naturally occurring element that is tasteless and odourless. It enters the food chains through either drinking water or eating plants and cereals that have absorbed the minerals including arsenic (Pal 2001). It is globally considered as one of the major pollutants of drinking water sources and a worldwide concern, because of its toxicity and carcinogenicity (Hindmarsh and McCurdy 1986; Podgorski and Berg 2020; Smith et al. 1992). Elevated concentration of arsenic in groundwater have been reported in most of countries including USA, India, China, Bangladesh and Pakistan (Figure 1.1).

It is estimated in 2020 that about 94 million to 220 million people around the world (of which 85 to 90 % are in South Asia, Figure 1.2) are potentially exposed to high concentrations of arsenic (> 10 µg/L) in groundwater from their domestic water supply (Podgorski and Berg 2020). Comparing this to an estimate of 130 million people in 2001, a substantial increase in the number of people affected has been estimated. For the past few decades, several studies have shown in India that drinking arsenic-polluted water should be one of the major concerns for the health of humans (Guha Mazumder and Dasgupta 2011; Maity et al. 2012). Due to its high toxicity on humans the World Health Organization, WHO (Organization 2004) has lowered the guideline value for arsenic in drinking water from 50 to 10 µg/L, aiming to minimize the health-related problems, associated with arsenic pollution. The same standards apply also for the European Commission, as well as for the US Environmental Protection Agency.

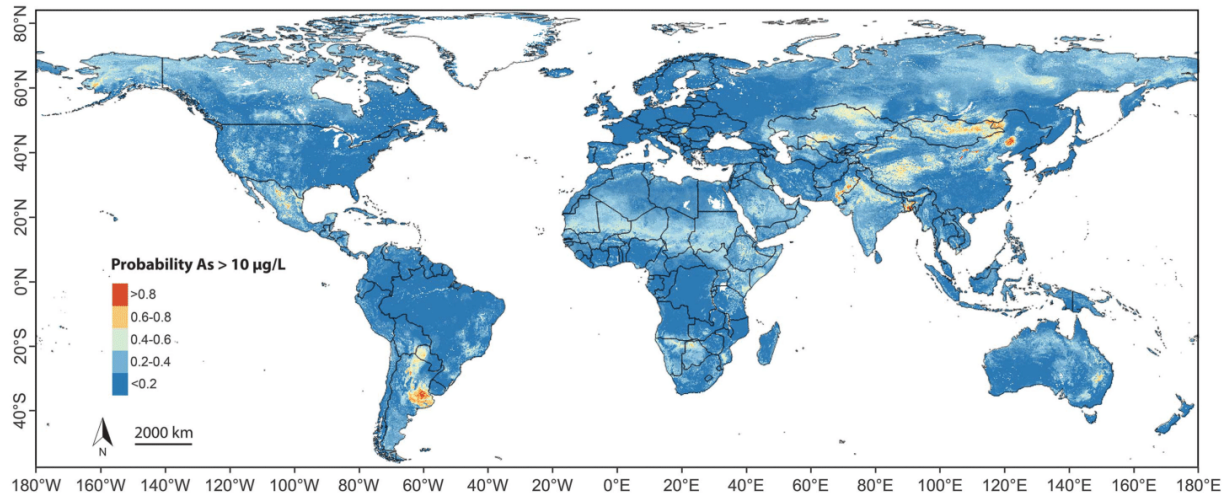

Figure 1.1. Global prediction of arsenic concentration in groundwater exceeding 10 µg/L (taken from Podgorski and Berg (2020)).

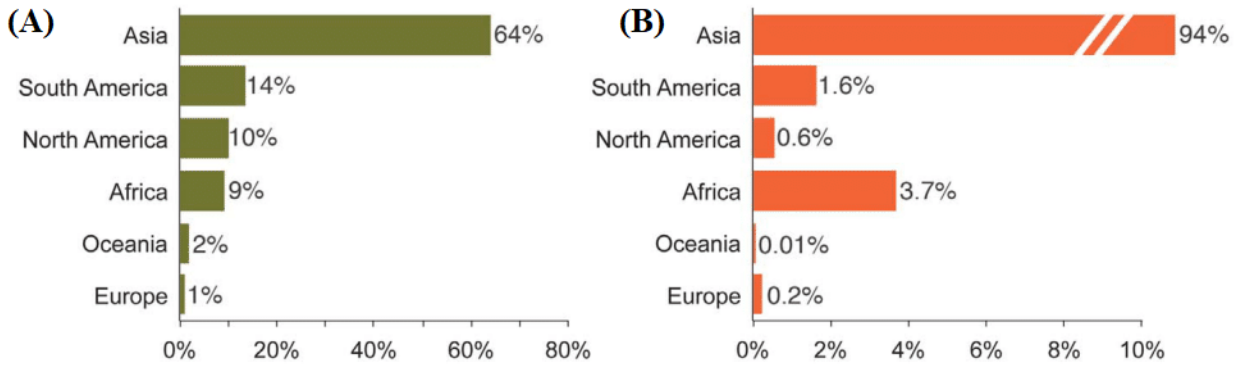

Figure 1.2. Proportions of **(A)** land area; **(B)** total population potentially effected by arsenic concentrations in groundwater exceeding 10 µg/L by each continent (taken from Podgorski and Berg (2020)).

Among other countries, arsenic pollution of groundwater is considered as a particularly serious health-related problem in Pakistan (Figure 1.3). Arsenic concentration exceeds the WHO guideline in large parts and consequently, approximately 50 to 60 million people relying on groundwater as a source of drinking water in the Indus Valley are at high health risk (Podgorski et al. 2017).

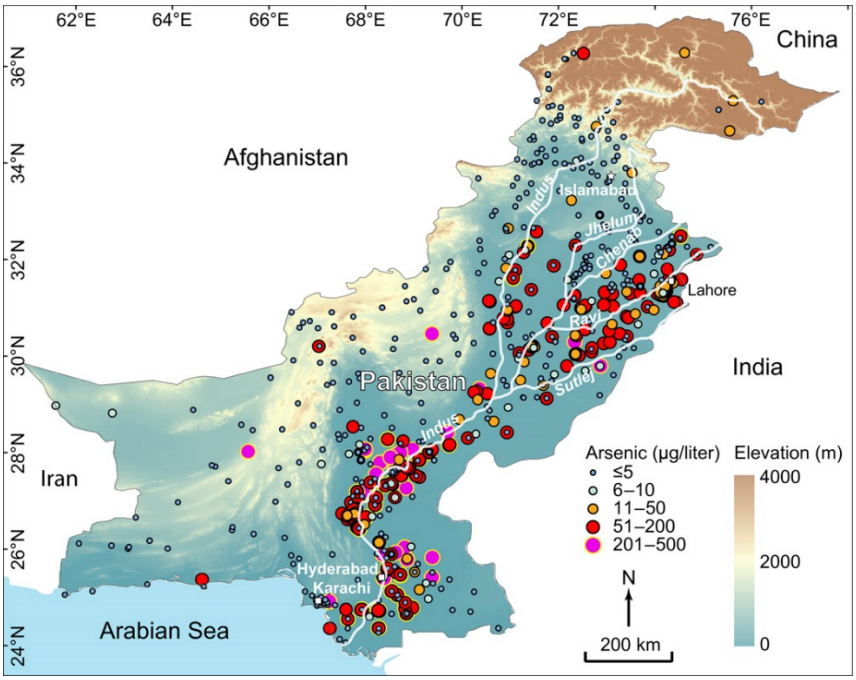

Figure 1.3. Arsenic concentrations measured in Pakistan groundwater (taken from Podgorski et al. (2017)).

Arsenic pollution of drinking water is a global environmental problem that requires innovative solutions. Therefore, the development of low-cost arsenic treatment system to reduce the health risks associated with the intake of arsenic-contaminated water and/or to alleviate the impact of such pollution are need of the time.

1.2 Objective and structure of the thesis

Packed-bed adsorption systems are widely adopted for arsenic removal from groundwater because it offers many advantages including simple and stable operation, easy handling of waste, absence of continuously added reagents, compact facilities, and generally lower labour cost (Wang et al. 2011). The use of fixed-bed adsorption media filters packed with granular ferric hydroxide (GFH, Wasserchemie, GmbH) has gained considerable attention, especially for the treatment of waters with relatively low initial arsenic concentrations (i.e., in the range of 20 to 50 µg/L) due to the simplicity of operation and the efficiency of arsenic removal (Driehaus 2002; Pal 2001). However, GFH is prohibitively expensive, which limits its application by the industries and waterworks in the developing countries.

Further, these filters usually use the granular size of the adsorbents, i.e., higher than 250 µm (Bretzler et al. 2020; Callegari et al. 2018; Thirunavukkarasu et al. 2003; Tresintsi et al. 2013a).

However, micro-sized fractions (particle sizes of 1 to 250 µm) of GFH cannot be used in fixed-bed filters because of high clogging potential in fixed-bed adsorption filters, rapidly causing an increased pressure head, and thereby increasing energy costs and maintenance (Kalaruban et al. 2018b; Vieira et al. 2017). However, considerable amounts of fine-grained fraction of GFH, termed µGFH and tetravalent manganese feroxyhyte (TMF), termed µTMF are generated as a by-product from the industrial production of GFH, while µTMF produced during kilogram-scale production at the laboratory scale and currently disposed of. The fine-grained fractions of iron oxyhydroxides are available at cheaper prices than conventional ones. Since the major part of the total cost of an adsorption process (> 80 %) arises from adsorbent's price (Wang et al. 2011). Thus, the availability of µGFH at an affordable price together with faster adsorption kinetic makes it a target candidate to be applied in arsenic treatment systems. Additionally, the application of these by-products in water treatment for drinking water production and/or groundwater remediation not only to reduce the cost of water treatment and increase the sustainable footprint of the production process but also be an efficient solution for arsenic removal and to supply methods for by-product utilization. One of the possible solutions to remove arsenic in potable water systems is to combine adsorption with the low–pressure membrane processes, often referred to as the hybrid membrane process. The objective of this thesis is the hybridization of adsorption and microfiltration (MF) membrane to create an innovative cost-effective hybrid membrane system using fine-grained fractions of conventional iron oxyhydroxides. The experimental approach was divided into following parts:

- **Characterization and investigations of the adsorption potential of fine-grained iron oxyhydroxides as arsenic adsorbents (Chapter 4).** Adsorption of arsenic onto an adsorbent depends heavily on many properties such as specific surface area and surface chemistry. Accordingly, the fine-grained iron oxyhydroxides were fully characterized in terms of their physical and chemical properties to understand the arsenic adsorption (Chapter 4.1). Moreover, the effect of equilibrium pH on arsenic adsorption by two applied adsorbents namely µGFH and µTMF was investigated through batch adsorption tests (Chapter 4.2). The adsorption of arsenic onto two applied adsorbents was thoroughly studied in three different water matrices at pH 8 and different adsorption isotherms are applied to investigate the adsorption efficiency and adsorption mechanism (Chapters 4.3 and 4.4). Finally, arsenic desorption potential using batch experiments was studied under strong alkaline conditions (Chapter 4.5).
- **Arsenic adsorption onto fine-grained iron oxyhydroxides in a submerged membrane adsorption hybrid system (Chapter 5).** Effect of contact time on arsenic adsorption by two applied adsorbents is first assessed by applying reaction kinetic models (Chapter 5.1). An integrated water treatment concept consisting of adsorption in a slurry-bed reactor and submerged MF unit (termed submerged membrane adsorption hybrid system, abbreviated as SMAHS henceforth) was developed and different operating parameters were studied to find out the optimum conditions (Chapter 5.2). The concluding chapter focuses on comparing the adsorption efficiency of two applied fine-grained adsorbents in a SMAHS with adsorption efficiency of conventional granular iron oxyhydroxide packed adsorption filter (Chapter 5.3).

Finally, an *in-situ* integrated procedure for regeneration and employment of regenerated media in a SMAHS was developed (Chapter 5.4).

- **Mathematical modeling of arsenic adsorption onto fine-grained oxyhydroxides in a submerged membrane adsorption hybrid system (Chapter 6).** The mathematical model based on the mass transfer model, e.g., homogenous surface diffusion model (HSDM) was formulated (Chapter 6.1) and subsequently, was applied to describe the arsenic adsorption in a batch and continuous mode slurry-bed reactor. The two mass transfer coefficients, i.e., surface diffusion coefficient (D_s) and liquid film mass transfer (k_f) of the HSDM were obtained through a number of bench-scale adsorption kinetic experiments (Chapter 6.2). Two sizes of adsorbate particles were tested in order to acquire a better insight into the adsorption process. The developed model was verified using the two mass transfer coefficients estimated from kinetic data with the experimentally determined arsenic breakthrough curves (Chapter 6.3). After validation at varying adsorbent doses and membrane fluxes, the developed mathematical model was applied to predict the arsenic breakthrough curves in a slurry reactor of the SMAHS at different operation conditions.
- **Dynamic membrane formed from microparticles of iron oxyhydroxides to remove arsenic from water (Chapter 7).** The mathematical model based on the HSDM was formulated (Chapter 7.1). The pre-coated dynamic membrane was formed *in-situ* from microparticles of applied iron oxyhydroxides and subsequently, used for arsenic removal from water (Chapter 7.2). In the end, experimentally determined arsenic removal rates are mathematically modeled with a model based on the HSDM (Chapter 7.3).

2 Theoretical background

This chapter first presents the arsenic chemistry including arsenic speciation, occurrence, and health effects (Chapter 2.1). Chapter 2.2 focuses on commonly used arsenic removal technologies in water treatment. Chapter 2.3 presents a brief overview on the type of iron oxyhydroxides used in water and wastewater treatment. Chapter 2.4 presents the fundamentals of adsorption, adsorption equilibrium, and commonly used different adsorption isotherm models. Chapter 2.5 exclusively focuses on adsorption kinetic models such as mass transfer and reaction kinetic models. Low-pressure membrane filtration processes are also briefly overviewed along with the hybrid membrane processes in Chapter 2.6. Concluding chapter 2.7 presents the fundamentals of the dynamic membranes and different materials used as dynamic membrane-forming materials.

2.1 Arsenic chemistry

Arsenic, a global environmental toxicant, is the 20th naturally abundant element, 14th in the seawater and 12th position in the human body (Mohan and Pittman 2007). Arsenic is the 4th period and group VA element. The other elements in the group VA are nitrogen (N), phosphorous (P), antimony (Sb), bismuth (Bi), and Moscovium (Mc). The atomic number of arsenic is 33, atomic weight is 74.91, melting point is 817 °C and boiling point is 633 °C. It is a silver-grey brittle crystalline solid, presents 0.5 - 2.5 mg/kg in most rocks. The higher concentration of arsenic has found in finer grained argillaceous sediments and phosphorites (Mandal 2002). The size of the arsenic radii various from 0.34 to 2.22 angströms (Å) (Henke 2009).

Arsenic mobility in the natural environment largely depends on the parent mineral form, oxidation state, and mobilization mechanisms (Al-Abed et al. 2007). In the natural environment, inorganic arsenic can exist in four oxidations forms, which are arsenite (As(III))/ As^{+3}), arsenate (As(V))/ As^{+5}), arsenic (As^{0}), and arsine (As(III) / As^{-3}). Among these four arsenic species, the most prevalent forms, which are commonly found in natural water, are the As(III) and As(V) and are considered as the main oxidation states of inorganic arsenic. As(V) are predominant and stable in oxygen-rich environments, whereas As(III) are existing mainly in moderately reducing environments, i.e., in anaerobic or anoxic groundwater. As(III) is more harmful to human health than As(V), being more toxic, soluble, and mobile.

Oxidation and reduction of arsenic species mainly depend on redox potential and pH conditions. In the water environment, arsenic predominantly exists as oxyanions of either As(III) or As(V) (Flora 2015; Mohan and Pittman 2007). Under oxidizing conditions and at pH values relevant to drinking water treatment, As(V) is present as an oxyanion in the forms of $H_2AsO_4^-$ and/or $HAsO_4^{2-}$, whereas at low Eh values, arsenic becomes dominant as H_3AsO_3 and up to pH 9, H_3AsO_3 does not dissociate and therefore, As(III) in most natural waters is present as the uncharged arsenious acid (Ware et al. 2005). The redox-pH chemistry of arsenic under controlled redox-pH conditions are shown in Figures 2.1- 2.3. These figures suggest the significance of pH and redox potential in

the formation and occurrence of different forms of arsenic in the water environment. Given a pH and redox potential, the speciation of arsenic including its oxidation state

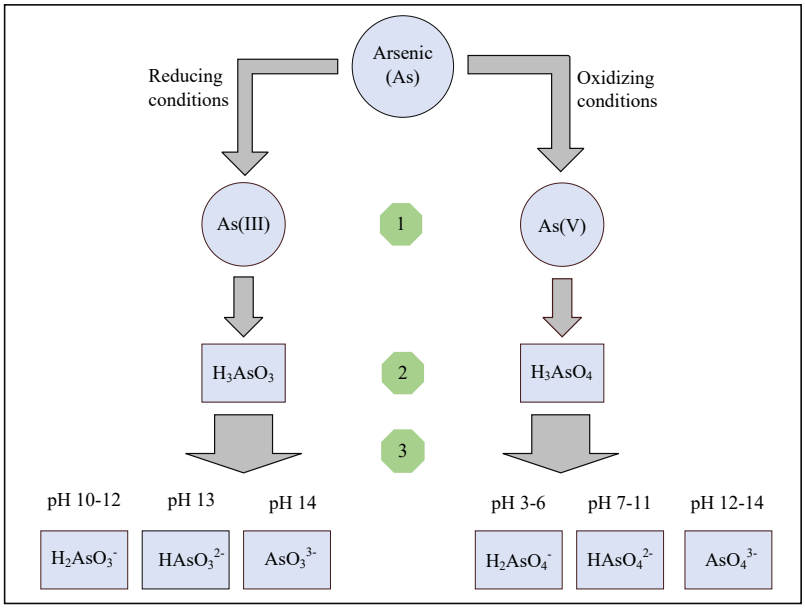

Figure 2.1. Pictorial depiction of (1) oxidation of arsenic under oxidizing and reducing conditions; (2) formation of acids by As(III) and As(V) under different pH conditions; (3) dissociation of acids to oxyanions under various sets of pH conditions (adopted from Flora (2015)).

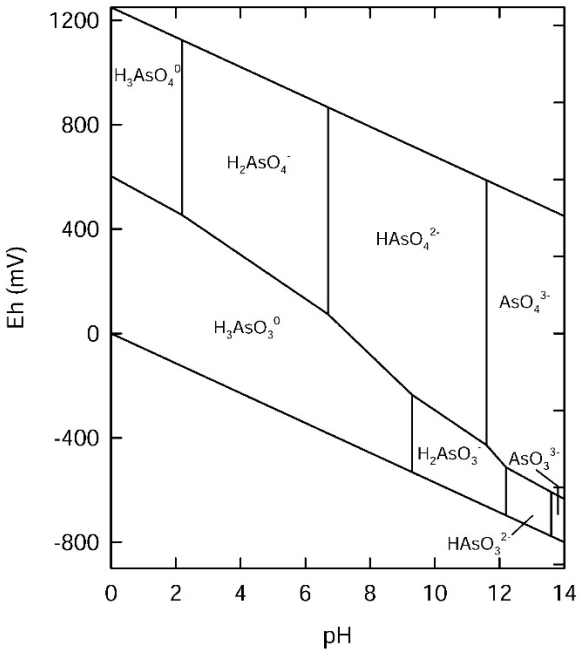

Figure 2.2. The Eh-pH diagram for arsenic at 25 °C and one atmosphere with total arsenic 10^{-5} mol/L and total sulfur 10^{-3} mol L^{-1}. Solid species are enclosed in parentheses in cross-hatched area, which indicates solubility less than $10^{-5.3}$ mol L^{-1} (Ferguson and Gavis (1972)).

can be determined through Figure 2.2. For instance, at pH > 7 and under moderately reducing conditions (Eh >100 mV) - which can be induced by flooding (Masscheleyn et al. 1991) - As(V) can be reduced to As(III). However, because of slow redox transformations, As(III) and As(V) are present in both reduced and oxidized /either environments (Al-Abed et al. 2007).

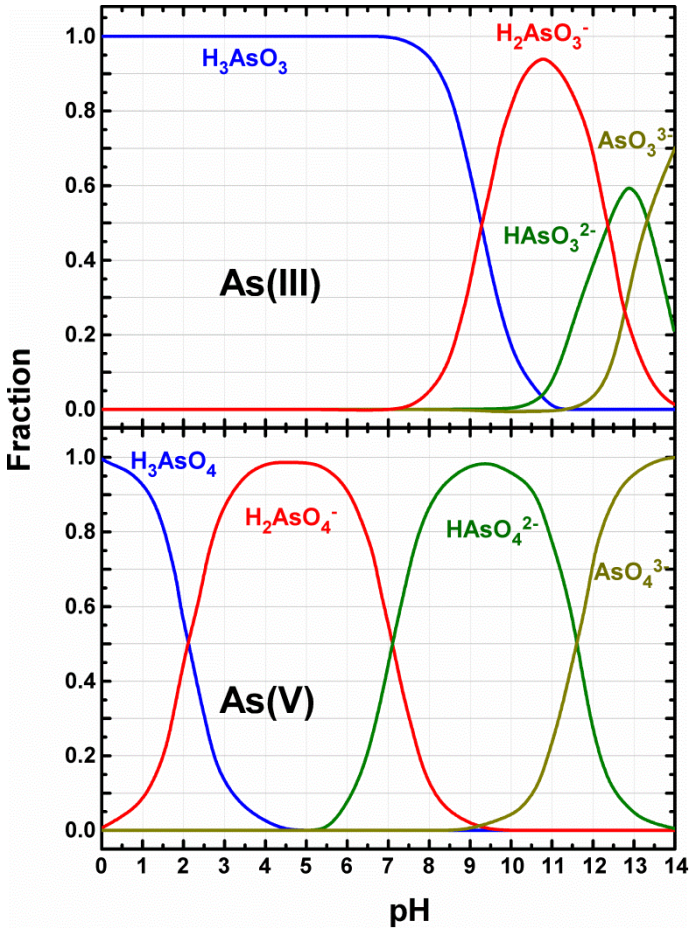

Figure 2.3. As(III) and As(V) speciation vs. pH in water.

Further, the presence of As(III) vs. pH of the solution can be explained in terms of the As(III) species and equilibrium constant. The dissociation reactions and corresponding equilibrium constants of H_3AsO_3 (Eqs. 2-1 – 2-3) are as shown below:

$$H_3AsO_3 \longleftrightarrow H_2AsO_3^- + H^+ \qquad \text{pKa: 9.2} \qquad (2\text{-}1)$$

$$H_2AsO_3^- \longleftrightarrow HAsO_3^{-2} + H^+ \qquad \text{pKa: 12.1} \qquad (2\text{-}2)$$

$$HAsO_3^{-2} \longleftrightarrow AsO_3^{-3} + H^+ \qquad \text{pKa: 13.4} \qquad (2\text{-}3)$$

In addition, possible As(V) species present under different pH conditions along with their equilibrium constant can also be described below

$$H_3AsO4 \longleftrightarrow H_2AsO_4^- + H^+ \quad \text{pKa: 2.2} \tag{2-4}$$

$$H_2AsO_4^- \longleftrightarrow HAsO_4^{-2} + H^+ \quad \text{pKa: 6.7} \tag{2-5}$$

$$HAsO_4^{-2} \longleftrightarrow AsO_4^{-3} + H^+ \quad \text{pKa: 11.5} \tag{2-6}$$

The introduction of arsenic into groundwaters is expected to occur mainly as a result of its natural geological presence in rocks and minerals (Garelick et al. 2008). Arsenic naturally occurs in over 200 different mineral forms, of which approximately 60% are arsenates, 20% sulfides and sulfosalts and the remaining 20% include arsenides, arsenites, oxides, silicates and elemental arsenic (Wedepohl et al. 1969).

2.2 Arsenic removal technologies

Several treatment technologies for arsenic removal from drinking water have been applied worldwide (Hering et al. 2017), and the most commonly used are chemical coagulation using metals (iron) salts (Mitrakas et al. 2009; Tubić et al. 2010; Zouboulis and Katsoyiannis 2002), sorption on activated alumina (Chwirka et al. 2000; Tripathy and Raichur 2008; Wang et al. 2002), iron oxides and iron oxyhydroxides (Amy 2005; Bretzler et al. 2020; Ćurko et al. 2016; Mohan and Pittman 2007; Tresintsi et al. 2012; Tresintsi et al. 2013a), electrocoagulation with Fe/Al electrodes (Khan et al. 2020), preliminary arsenic oxidation by ozonation or biological oxidation (Katsoyiannis et al. 2015a), ion exchange using polymer resins (Ghurye et al. 1999) and pressure-driven membrane processes, such as nanofiltration (Sato et al. 2002) and reverse osmosis (Abejón et al. 2015; Kang et al. 2000; Víctor-Ortega and Ratnaweera 2017). Other treatment methods include the application of oxidation and arsenic removal by using zero-valent iron (especially in Bangladesh) (Katsoyiannis et al. 2015b), biosorption on modified natural adsorbents and agricultural by-products (Asere et al. 2019; Tajernia et al. 2014) and electrocoagulation (Nidheesh and Singh 2017).

Previous studies have identified high-pressure membrane processes as an emerging technology, due to their high removal efficiencies and easy operation features, but these high-pressure membrane processes are rather energy (and cost) intensive, subjected to the fouling of membrane and the disposal of produced brine (high salts concentrations and hazardous arsenic) is also a considerable challenge.

Among the several existed arsenic removal technologies, chemical precipitation by ferric coagulation followed by filtration, and adsorption onto iron oxides and iron oxyhydroxides appear to be cost-effective for large-scale arsenic treatment plants to comply with established WHO guideline value of 10 µg/L (Bretzler et al. 2020; Tresintsi et al. 2013a; Wang et al. 2011). Chemical precipitation by ferric coagulation has significantly higher arsenic removal efficiencies compared to iron oxyhydroxides packed adsorption filters. However, the efforts required for handling the wastes from coagulation-filtration prevents its application when the treatable volume of product water corresponds to the one produced for a small town (Tresintsi et al. 2013a; Wang et al. 2011).

Tresintsi et al. (2013a) reported the WHO guideline value for drinking water can be achieved at affordable prices by chemical precipitation using ferric salts. The operational costs were estimated between 0.09 and 0.16 €/m^3 for initial As(V) concentrations ranging between 19 and 208 μg/L and the major part (> 90%) of treatment costs was attributed to the management of produced sludge since $FeClSO_4$ coagulation costs are estimated to be as low as 2 €/kg.

Adsorption technology using iron oxyhydroxides is considered as an economical and effective technique for arsenic removal because of its lower cost, and availability of suitable commercial adsorbents and their regeneration (Chen et al. 2015). Studies have revealed that iron(III) has a strong affinity toward inorganic arsenic species and it is very selective in the sorption process (Deliyanni et al. 2003). Removal has been attributed to ion exchange, specific adsorption to surface hydroxyl groups or coprecipitation (Chen et al. 2007). In the following section, the iron oxyhydroxides are discussed.

2.3 Iron oxyhydroxides

The iron oxyhydroxides (FeOOH) are chemical compounds that commonly form in aqueous environments with different content in iron cations (Fe^{2+} and Fe^{3+}), oxygen, hydroxyl, water and some amounts of SO_4^{2-}, CO_3^{2-} and Cl^-. They are present in igneous and metamorphic rocks (Cornell and Schwertmann 2003). Iron oxyhydroxides can be directly obtained from natural sources (rocks, soils) or chemically synthesized by the precipitation either of Fe^{3+} or Fe^{2+} salts.

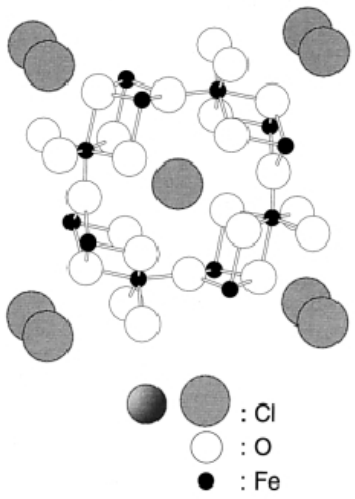

Figure 2.4. Structure of akagenéite (Cornell and Schwertmann (2003)).

The basic structural formula of iron oxyhydroxides is FeOOH. They encompass up to 6 different species including Goethite (α-FeOOH), Lepidocrocite (γ-FeOOH), Akagenéite (β-FeOOH), Feroxyhyte (δ-FeOOH) and Ferrihydrite (Cornell and Schwertmann 2003), which are characterized by differences in the anion and mineral structure. The oxidation state of iron in iron oxyhydroxides, in most cases, is trivalent. Deliyanni et al. (2003) reported that varieties of iron oxyhydroxides differ in their affinity for arsenic. Deliyanni et al. (2003) indicated that akagenéite

had higher arsenate adsorption capacity than other iron mineral phases such as hydrous ferric oxide, ferrihydrite and goethite.

The hydrolysis and oxidation rate of the iron salts mainly determine the obtained iron oxyhydroxide structure during chemical synthesis. In addition, the chemical environment and the reaction parameters may determine the critical factors such as specific surface area and available adsorption sites (Tresintsi et al. 2012). GFH, Akagenéite-type adsorbent (Bahr 2012), is a synthetically produced material from a ferric chloride solution by neutralization and precipitation with sodium hydroxide (Thirunavukkarasu et al. 2003). Akagenéite shows a tunnel-like crystal structure with tetragonal unit cells (Figure 2.4). The tunnels in the akageneite structure are considered to be stabilized by chloride ions (Cornell and Schwertmann 2003).

Like GFH, TMF (feroxyhyte-type adsorbent) is prepared in the laboratory and involves the co-precipitation of $FeSO_4$ and $KMnO_4$ in a continuous process. Its production in a laboratory two-stage continuous flow reactor includes the coprecipitation into the water of the iron source ($FeSO_4 \cdot H_2O$) at pH 4 and the manganese source ($KMnO_4$), which is an oxidant for the process and also used to adjust the reaction's redox to 850 mV (Tresintsi et al. 2013b). In TMF, tetravalent manganese (Mn(IV)) is homogeneously distributed into the crystal unit. According to this structuration, the oxyhydroxide maintains the high adsorption capacity for As(V) of a single iron oxyhydroxide combined with enhanced As(III) removal based on the oxidizing mediation of Mn(IV) (Figure 2.5). The primary benefit of Mn(IV) in TMF that it combines the oxidation property of Mn(IV) and increases removal capacity for As(III) species by complete As(III) oxidation and adsorption in As(V) form. It was reported that Mn(IV) oxidizes As(III) to As(V) and the removal of As(III) by TMF was believed to involve redox reactions and not merely correspond to a simple adsorption processes (Tresintsi et al. 2014b).

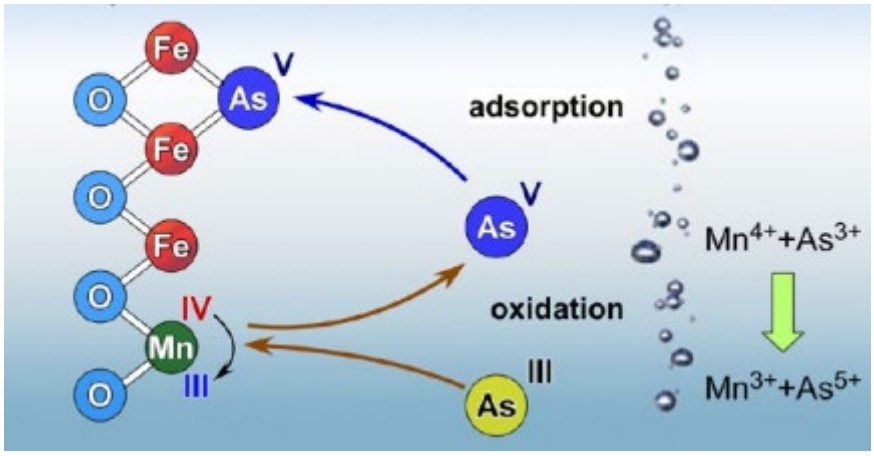

Figure 2.5. TMF structure showing homogeneously distribution of Mn(IV) into its crystal unit, and oxidizing mediation of Mn(IV) by complete As(III) oxidation and adsorption in As(V) form. (Tresintsi et al. 2013b).

In water treatment, the use of iron oxyhydroxides is promoted by their availability and affordability, their amorphous structure which gives high specific surface area values and their strong affinity and relative high selectivity for the most frequently occurring As(V) species under natural pH-values of a potable water (Henke 2009; Tresintsi et al. 2012). In this process, As(V) oxyanions are retained onto the surface of the adsorbent through various physical or chemical mechanisms resulting in a stable and non-reversible linkage (Henke 2009; Tresintsi et al. 2012). Typically, arsenic is adsorbed onto iron oxyhydroxides by the formation of monodentate and bidentate inner-sphere complexes depending on water pH and oxidation state of arsenic (Banerjee et al. 2008; Manning et al. 1998). Goldberg and Johnston (2001) reported that As(V) interactions with iron hydroxides are dominated by the formation of strong inner-sphere complexes and to a lesser extent by weaker ion-exchange reactions.

2.4 Adsorption

Adsorption is a phase transfer process in which molecules or ions, being removed from the liquid, present in a liquid phase accumulate onto a solid surface (Sperlich 2010; Worch 2012). Whereas, in the absorption process the molecules or ions to be removed (e.g., NH_3) is transferred from the gas phase to the liquid phase. (Wilcox 2012). Solid surfaces are characterized by active energy-rich sites that are able to interact with solutes in the adjacent aqueous phase due to their specific electronic and spatial properties. Typically, the active sites have different energies, or – in other words – the surface is energetically heterogeneous (Worch 2012). In adsorption, some basic adsorption terms are shown in Figure 2.6. The solid material that provides the surface for adsorption is referred to as adsorbent, while the species that will be adsorbed are named adsorbate.

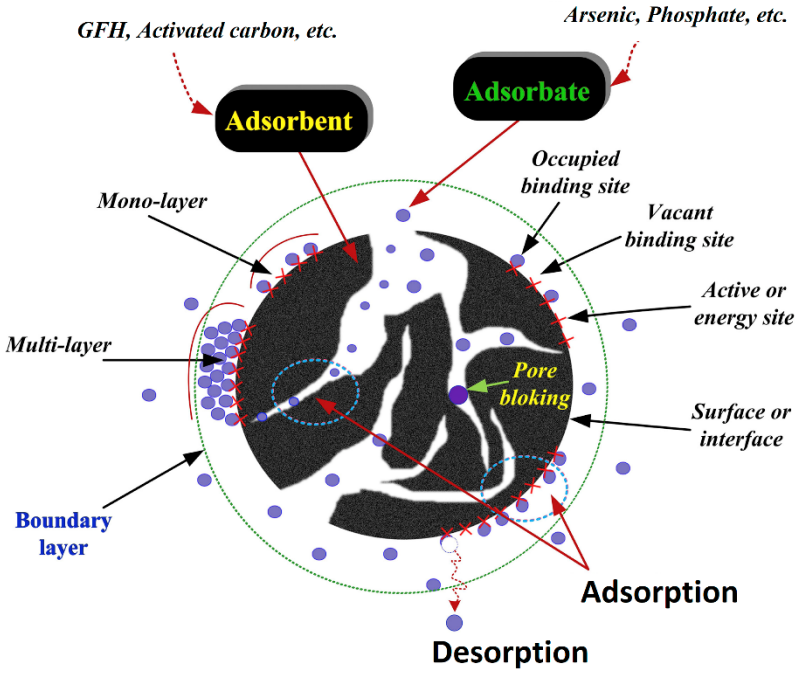

Figure 2.6. Some basic terms used in adsorption technology (Tran et al. 2017).

As adsorption is a surface process and therefore the adsorbents with surface area in the range of 10^2 - 10^3 m^2/g are considered as highly porous materials (Worch 2012). In water treatment, the adsorption process using the high internal surface area has proven to be an efficient process for removal of organic and inorganic compounds including arsenic. Activated carbon (AC), either granular or powered, - with the surface area of as large as 1500 m^2/g - is by far the most powerful adsorbent for trace organics removal. It is generally considered that AC is a universal adsorbent for the removal of diverse types of aquatic pollutants, especially organic pollutants. However, it shows poor adsorption towards oxyanion forming elements (Bhatnagar and Sillanpää 2011).

2.4.1 Adsorption equilibrium for measuring adsorption performance

To determine the adsorption potential, it is essential to determine the adsorption equilibrium data (Foo and Hameed 2010). To determine the adsorption equilibrium data, a set of (8 - 10) bottles containing adsorbent and adsorbate is used to determine a larger number of isotherm points in parallel. Each bottle is filled with the adsorbate solution of known volume and known initial concentration (C_o) of adsorbate. After adding a defined adsorbent mass, the solution is shaken or stirred until the state of equilibrium (t_e) is reached (Figure 2.7).

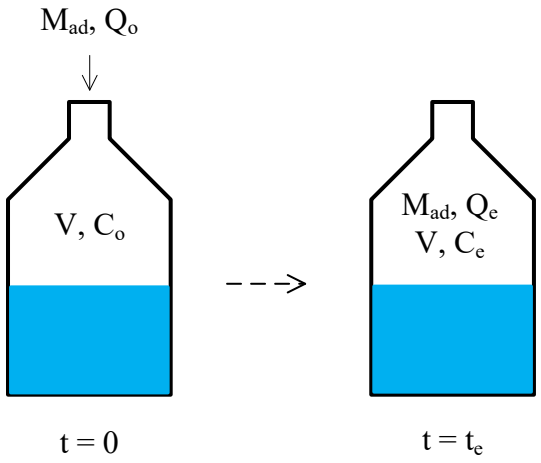

Figure 2.7. Experimental determination of adsorption equilibrium data.

The time required to reach the equilibrium (t_e) is typically between some hours and some weeks (Worch 2012). Many studies have investigated the effect of contact time on adsorption process (Simonin 2016). Figure 2.8 represents the influence of contact time on adsorption of atrazine by polypyrrole core-shell nanofibers (Yang et al. 2015).

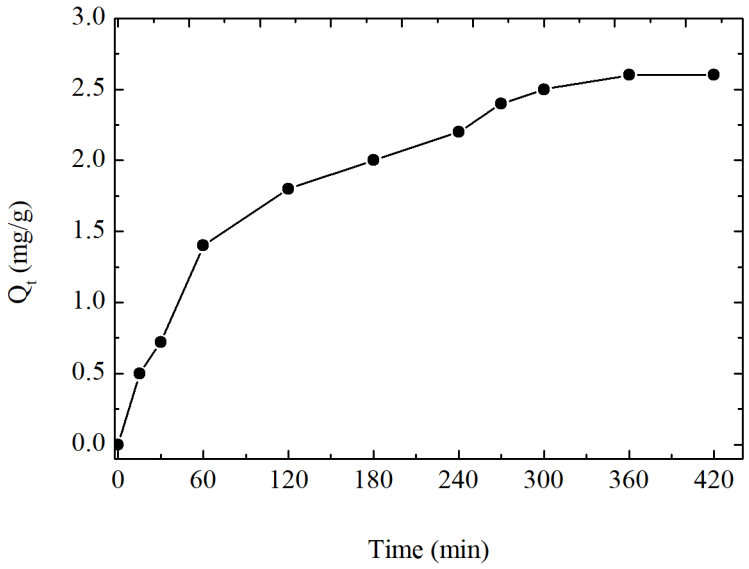

Figure 2.8. Effect of contact time on adsorption process of atrazine (Yang et al. 2015).

After the equilibrium has been established, equilibrium (residual) liquid phase concentration is determined. The material balance (Eq. 2-7) of the adsorption system can be written as:

$$M_{ad}\,(Q_0 - Q_e) = (C_o - C_e)\,V \tag{2-7}$$

where C_o and C_e are the liquid phase initial and equilibrium adsorbate concentration, Q_0 and Q_e are the solid phase initial and equilibrium adsorbate concentration, M_{ad} is the mass of adsorbent added, V is volume of the adsorbate solution in the flask. M_{ad}/V is the solid-liquid ratio. At time (t) = 0, the material is fresh (without adsorbate loaded), mass balance of the system reduces to

$$Q_e = \frac{(C_o - C_e)\,V}{M_{ad}} \tag{2-8}$$

Adsorbent capacity at the equilibrium (adsorbate equilibrium loading) can be calculated using Eq. 2-8 when solid-liquid ratio (adsorbent dose), and liquid and solid phase concentrations at equilibrium are known.

The adsorption performance can also be expressed as the percentage of the removed adsorbate from the solution using the following relationship

$$\text{Adsorbate removal (\%)} = \frac{(C_o - C_e)}{C_o} \text{ x } 100 \tag{2-9}$$

measured adsorption isotherm data (Figure 2.9) obtained through batch adsorption tests at constant temperature are subsequently described by an appropriate adsorption isotherm model (Worch 2012).

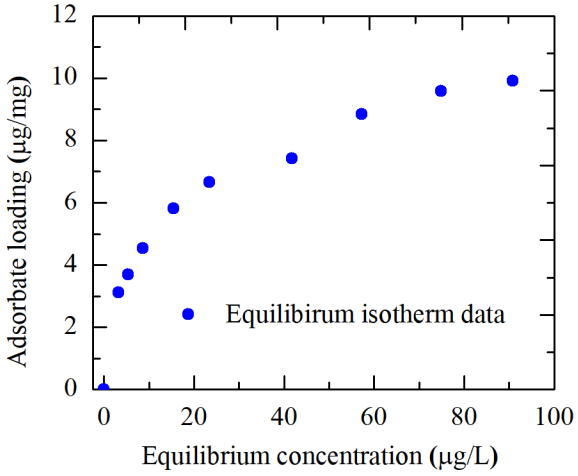

Figure 2.9. Adsorption equilibrium data obtained from batch isotherm tests. Symbols reflect the experimental data. Adsorbent dosage of 5 - 25 mg/L and constant initial concentration of arsenic (adsorbate) = 190 µg/L at pH 8 ± 0.1.

The characterization of adsorbents and their suitability assessment required the simultaneous determination of adsorption kinetic and equilibrium properties (Douven et al. 2015; Foo and Hameed 2010; Tran et al. 2017). The adsorption equilibrium parameters are usually determined by adsorption isotherms model.

2.4.2 Adsorption isotherm models

Adsorption isotherms describe how pollutants interact with the adsorbent materials and are also indispensable for the practical design and operation of adsorption systems. (El-Khaiary 2008; Foo and Hameed 2010). The constants of the isotherms express adsorption capacities, the surface properties, and the type of adsorption (ionic exchange or physical adsorption) (El-Khaiary 2008; Saldaña-Robles et al. 2017). There are many adsorption isotherms well documented in the literature. However, the Freundlich (1906) and Langmuir (1916) isotherms are the most commonly used, followed by the Dubinin-Radushkevich (Radushkevich 1947) isotherm model, because of the usefulness of their model parameters, their simplicity and their interpretability (Tran et al. 2017). Among different isotherm models, the D-R isotherm model provides the information about the adsorption mechanism being either ionic exchange adsorption or physical adsorption (Saldaña-Robles et al. 2017).

***Freundlich isotherm model**:* The Freundlich equation is the one of earliest empirical equation used to describe equilibrium data and adsorption characteristics of an adsorbent with heterogenous surface. This empirical model can be applied to multilayer adsorption, with non-uniform distribution of adsorption affinities over the heterogeneous surface (Freundlich 1906). This model can describe neither the linearity range at low concentration nor the saturation effect at very high concentration (Wang 2009). This implies that the Freundlich equation cannot be used to describe the saturation behavior of an adsorbent. The non-linear form of the Freundlich equation can be expresses by Eq. 2-10:

$$Q_e = K_F C_e^n \tag{2-10}$$

where K_F and n is Freundlich capacity constant and Freundlich intensity parameter, respectively. n indicates the magnitude of adsorption driving force and/or the surface heterogeneity. According to the Freundlich theory, adsorption efficiency of the adsorption process can be predicted using the value of n. For instance, when n < 1, the adsorption is favorable. Similarly, different shapes of isotherm can be predicted by n values as summarized in Table 2.1.

Langmuir adsorption isotherm: Langmuir adsorption isotherm is a two parameter isotherm and refers to homogeneous adsorption, which each molecule possesses constant enthalpies and sorption activation energy (all sites possess equal affinity for the adsorbate. This isotherm originally was developed to describe gas–solid-phase adsorption onto activated carbon. It has traditionally been used to quantify the adsorption performance of different bio-sorbents (Langmuir 1916). In its formulation, this empirical model assumes monolayer adsorption (the adsorbed layer is one molecule in thickness) and therefore, cannot be applied to multilayer adsorption. The monolayer adsorption can only occur at a finite (fixed) number of definite localized sites, that are identical and equivalent, with no lateral interaction and steric hindrance between the adsorbed molecules, even on adjacent sites (Vijayaraghavan et al. 2006). The Langmuir isotherm equation can be described by Eq. 2-11:

$$Q_e = \frac{Q_{max} b\, C_e}{1 + b\, C_e} \tag{2-11}$$

where Q_{max} is the maximum adsorption capacity, and b is Langmuir constant related to energy of adsorption. When liquid and solid phase adsorbate concentration at equilibrium, C_e and Q_e are liquid-phase and solid-phase adsorbate concentration at equilibrium. Q_{max} and b values can be calculated by non-linear optimization technique. Q_{max} can also be graphically characterized by a plateau, an equilibrium saturation point where once a molecule occupies a site, no further adsorption can take place. Additionally, a dimensionless constant, separation factor (R_L) originally proposed and defined by Hall et al. (1966), can be represented as:

$$R_L = \frac{1}{1 + b\, C_o} \tag{2-12}$$

where b (L/μg) refers to the Langmuir constant and C_o is the adsorbate initial concentration. Like Freundlich constant (n), R_L can be used to predict the isotherm shape (Worch 2012).

Table 2.1. Relationship between isotherm parameters and isotherm shapes (information are taken from Worch (2012)).

Freundlich exponent (n)	Langmuir separation factor (R_L)	Isotherm shape	Remarks
0	0	Irreversible	Horizontal
< 1	< 1	Favorable	Concave
1	1	Linear	Linear
>1	> 1	Unfavorable	Convex

Dubinin–Radushkevich isotherm model: D-R isotherm is an empirical model initially conceived for the adsorption of subcritical vapors onto micropore solids following a pore filling mechanism (Radushkevich 1947). It is generally applied to express the adsorption mechanism with a Gaussian energy distribution onto a heterogeneous surface and is temperature dependent isotherm model (Foo and Hameed 2010). Dubinin (1960) applied this isotherm to distinguish the physical and chemical adsorption of metal ions. The non-linear of this empirical model is expressed as follows:

$$Q_e = Q_{DR} \exp[-K_{DR} \left(R_g T \ln\left(1 + \frac{1}{C_e}\right)\right)^2] \quad (2\text{-}13)$$

where Q_{DR} is the theoretical saturation adsorption capacity, K_{DR} is a constant related to the adsorption energy, R_g is the gas constant and T is the temperature. K_{DR} is related to the free energy of adsorption per mole of adsorbate. The value of E can be evaluated using the relationship given in Eq. 2-14 according to Hobson (1969):

$$E = \frac{1}{\sqrt{2K_{DR}}} \quad (2\text{-}14)$$

where E is the mean free energy per molecule of adsorbate (for removing a molecule from its location in the sorption space to the infinity or the free energy change when one mole of the ion is transferred from infinity in the solution to the surface of the solid). The value of E is useful for estimating the type of adsorption. If the free energy ranges from 8 to 16 kJ /mol, the adsorption can be explained by chemical adsorption. When E value is lower than 8 kJ /mol, then the adsorption process is due to physical adsorption (Mahramanlioglu et al. 2002).

2.5 Adsorption kinetic

2.5.1 Fundamentals of adsorption kinetics

The time progress of the adsorption process is known as adsorption kinetics. Typically, adsorption equilibrium (when adsorption and desorption are equal) are not established instantaneously particular for porous adsorbents (Worch 2012). The adsorption process for inorganic and organic contaminants onto porous adsorbents (AC, GFH, biochar) can take longer (i.e., days or weeks) to approach true equilibrium than non-porous adsorbents. The difference in adsorption rate is associated to different adsorption mechanism of different adsorbents (Tran et al. 2017). In case of porous adsorbents, the mass transfer from the solution to the adsorption sites within the adsorbent particles is constrained by mass transfer resistances that determine the time required to reach the state of equilibrium (adsorption equilibration time) (Worch 2012). Surface and pore diffusion are the most common adsorption mechanisms for porous adsorbents together with other interactions, e.g., electrostatic attraction, and inner-surface complexes. The adsorption equilibration time depends not only on characteristics of interaction between adsorbent and adsorbate but also on adsorbent particle size (Tran et al. 2017; Worch 2012). The kinetic parameters of mass transfer models, together with the equilibrium parameters, are essential input data to design the optimum contact times for adsorption process in slurry reactor setup as well as in fixed-bed adsorption filter.

2.5.2 Mass transfer resistances for porous adsorbents

In general, the adsorption kinetic process of adsorbate onto porous adsorbent can be characterized by four consecutive steps: (1) transport of adsorbate from the bulk solution to stagnant boundary layer; (2) diffusion through the boundary layer to the external surface of a particle, termed liquid film mass transfer or external film diffusion; (3) diffusion in the adsorbed state along the internal surface of a particle, termed intraparticle surface diffusion; (4) adsorption between the adsorbate molecules and adsorption sites in the pores. Since first and the fourth step are very fast. So the total rate of the adsorption process is determined by either external film diffusion (step 2) or surface diffusion (step 3) as demonstrated in Figure 2.10.

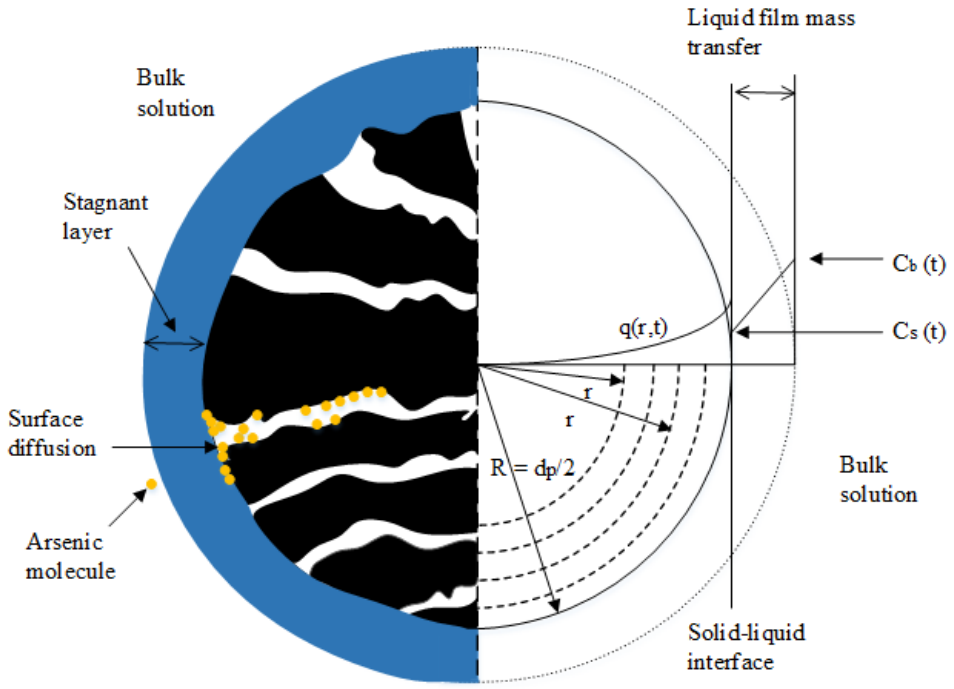

Figure 2.10. Schematic of metal ion (arsenic ion) or molecule mass transport from the bulk solution into porous adsorbent.

As the film diffusion and surface diffusion occur in succession, the slower process then determines the total adsorption rate (Jia et al. 2009a; Traegner and Suidan 1989; Worch 2012).

2.5.3 Homogeneous surface diffusion model

The homogenous surface diffusion model (HSDM) is a mass transfer model for describing the adsorption process. This model incorporates both film and surface diffusion and envisages an adsorbent particle as a sphere surrounded by a stagnant liquid boundary layer. Further, the gradient of the solid-phase concentration within the particle acts as a driving force for the transport.

In the HSDM, some assumptions are incorporated (Worch 2012):

- Adsorbent is assumed to be spherical.
- Mass transfer occurs in the adsorbed state along the internal surface of the adsorbent particle.
- The film diffusion is the previous transport step to surface diffusion.
- The film diffusion is much faster than the surface diffusion, and the mass transfer resistance in the boundary layer can be neglected. In this case, there is no concentration difference between the external surface and the bulk solution, and the adsorption rate can be described by the HSDM alone.

According to the HSDM, solid phase adsorbate concentration in the particle is:

$$\frac{\partial q(r,t)}{\partial t} = D_s\left[\frac{\partial^2 q(r,t)}{\partial r^2} + \frac{2}{r}\frac{\partial q(r,t)}{\partial r}\right] \quad (2\text{-}15)$$

The initial and boundary conditions of Eq. 2-15 are:

For a fresh or virgin adsorbent particle,

$$q(r, t = 0) = 0 \tag{2-16}$$

As there is no flux at particle center,

$$\frac{\partial q(r=0,t)}{\partial r} = 0 \tag{2-17}$$

At the external adsorbent surface ($r = d_p/2$) to connect the liquid phase to the solid phase, the following boundary condition needs to be satisfied to ensure the continuity between external mass transfer and surface diffusion fluxes at the solid-liquid interface (mass transport of arsenic molecule from the bulk solution into porous adsorbent is reported in Figure 2.10. Schematic of metal ion (arsenic ion) or molecule mass transport from the bulk solution into porous adsorbent.

$$\rho_p D_s \frac{\partial q(r=d_p/2\,,t)}{\partial r} = k_f(C - C_s) \tag{2-18}$$

At $r = d_p/2$, it is assumed that instantaneous equilibrium occurs at the external surface of adsorbent between the adsorbate molecules in the liquid phase (C_s) and solid phase adsorbate concentration (Q_s). This instantaneous equilibrium relationship at the solid liquid interface (Figure 2.10) can be described by the Freundlich adsorption isotherm (Eq. 2-19):

$$q_s = K_F(C_s)^n \tag{2-19}$$

The resultant boundary condition for the particle surface is:

$$\frac{\partial q(r=d_p/2\,,t)}{\partial r} = \frac{k_f}{\rho_p D_s}\{C - \left(\frac{q_s}{K_F}\right)^{\frac{1}{n}}\} \tag{2-20}$$

where $q(r, t)$ donates the adsorbate radial concentration within the particle over time, D_s is the intraparticle diffusion along the inner adsorbent surface. k_f denotes liquid film mass transfer coefficient when the arsenic diffuse through the stagnant liquid film surrounding the adsorbent particle, ρ_p is particle density, d_p is particle diameter, C is the liquid phase adsorbate concentration in the bulk solution at any time.

The dimensionless Biot number (Bi) characterizes the ratio of the transport rate across the liquid film layer to the diffusion rate within the particle. Bi defined as:

$$Bi = \frac{k_f\, d_p C_o}{2\, D_s\, \rho_p\, Q_o} \tag{2-21}$$

where $C_o$and Q_o represent the initial liquid and adsorbed phase adsorbate concentrations, and $Q_o$is in equilibrium with C_o. The higher the Bi, the higher is the rate of film diffusion in comparison to

surface diffusion. If Bi > 30, the influence of the film diffusion on the overall adsorption rate is negligible, and the surface diffusion alone is rate limiting (Sontheimer 1988).

2.5.4 Reaction kinetic models

The diffusion models like HSDM are widely accepted as appropriate models to describe adsorption kinetics for porous adsorbents. However, several papers focusing on adsorption of arsenic onto porous adsorbents have described the adsorption kinetics by simple models based on chemical reaction kinetics (Banerjee et al. 2008; Saldaña-Robles et al. 2017; Xie et al. 2007). It is generally believed that adsorption of arsenic species onto iron (oxyhydr)oxide is known to take place via Coulombic as well as Lewis acid–base interactions (ligand exchange reactions) and to form monodentate and bidentate inner sphere complexes (Banerjee et al. 2008; Manning et al. 1998).

The kinetic models based on surface reactions involving inner-sphere complexation can serve a role in fitting of kinetic data involving another rate limiting step (e.g., diffusion). The possible ligand exchange reaction for adsorption of As(V) and As(III) at pH between 6 and 8 by (oxyhydr)oxide-based adsorbent may include (Banerjee et al. 2008):

$$H_2AsO_4^-{}_{(aq)} + Fe - OOH_{(s)} \longrightarrow Fe - H_2AsO_{4(s)} + OH^- \quad (2\text{-}22)$$

$$H_3AsO_{3(aq)} + Fe - OOH_{(s)} \longrightarrow Fe - H_2AsO_{3(s)} + H_2O \quad (2\text{-}23)$$

In general form, the kinetics of adsorption from the above two reactions can be written as:

$$As_{(aq)} + Fe - OH_{(s)} \xrightarrow{k_{ad}} Fe - As_{(s)} + OH^- \quad (2\text{-}24)$$

where As is the liquid phase arsenic concentration, Fe–OH is the available reactive surface of the media for arsenic adsorption (i.e., adsorption sites), Fe–$As_{(s)}$ is the solid phase arsenic concentration of arsenic in the solid phase and k_{ad} is the adsorption reaction rate constant. The rate law is then written as:

$$\frac{d[As]}{dt} = -k_{ad}[As]^n\,[Fe-OH]^m \quad (2\text{-}25)$$

where, n and m are the constants representing order(s) of reaction, and t is time. Thus the kinetics can be viewed as nth order with respect to As, mth order with Fe–OH, and (n+m)th order overall. Usually the adsorbent dose is 1000-fold greater than that of the either As(V) or As(III), the available sorption surface site would virtually remain unchanged during the process (i.e., the rate law can be treated as a pseudo-order reaction). Therefore, Eq. 2-25 can be written in simplified form as follows:

$$\frac{d[As]}{dt} = -k\,[As]^n \quad (2\text{-}26)$$

where $k = k_{ad}$ [Fe-OH]^m. Then, Eq. 2-26 becomes

For a pseudo-first-order reaction: $$\frac{d[As]}{dt} = -k_1\,[As]^1 \quad (2\text{-}27)$$

For a pseudo-second-order reaction: $$\frac{d[As]}{dt} = -k_2\,[As]^2 \quad (2\text{-}28)$$

The linear forms of Eqs. 2-27 and 2-28 after by applying the integration are

For a pseudo-first-order reaction: $$\ln\left(\frac{As_t}{As_0}\right) = -k_1\,t \quad (2\text{-}29)$$

For a pseudo-second-order reaction: $$\frac{1}{As_t} - \frac{1}{As_o} = -k_2\,t \quad (2\text{-}30)$$

where k_1 and k_2 are rates constant of pseudo-first and second-order reactions. As_o and As_t are liquid phase arsenic concentrations at t= 0 and at any time, t, respectively.

2.5.5 Reusability of adsorbents

The major drawback of the adsorption process is the high cost of the applied adsorbent (Tresintsi et al. 2013a) and the cost of applied adsorbent is a function of the cost of the media and the life of the media (Chen et al. 2015). Currently, on-site regeneration and reuse of the adsorptive media is rarely considered (Chen et al. 2015), and most arsenic adsorbents are preferably employed solely replacement (throw-away) basis (Tresintsi et al. 2014a). For efficient water treatment, the adsorbent should have good stability and regeneration characteristics (Liu et al. 2018). The regeneration characteristics of the adsorbent increases the efficiency of adsorption and its possible regeneration could not only drastically decrease the operation and maintenance cost but also the total cost of water treatment. Therefore, the regeneration of arsenic saturated adsorbent is very important in real water treatment systems. The adsorption depends on the surface charge of applied adsorbent, and the surface charge is controlled by the pH of the solution. Further, the adsorption and desorption of arsenic depend on the pH of the solution, so changes in the pH of the solution can lead to regeneration of the arsenic adsorbent (Siddiqui and Chaudhry 2018). It was shown that arsenic saturated adsorbents such as iron (oxy)hydroxides and GFH can be regenerated under strong alkaline conditions using NaOH solutions, which efficiently leaches adsorbed arsenic and phosphate (Mohan and Pittman 2007; Sperlich 2010). The success of the regeneration process is assessed by the recovery degree of adsorption capacity in the regenerated adsorbent compared to the fresh one (Tresintsi et al. 2014a).

However, the main challenge of the regeneration process is the handling of the arsenic-rich solution. It is possible to use recovered arsenic from the regeneration solution as arsenic sulfide in certain circumstances (Manna et al. 2003). Additionally, this process is complicated and increases the labor cost by setting up the regeneration process by quite expensive materials and chemicals. Some studies have reported that magnesium oxide (MgO) with isolectic point ($pH_{IEP} \approx 12$) , a low-cost and an alkaline earth metal oxide with simple production process from abundant natural

minerals, is a potentially attractive adsorbent and present high adsorption affinity towards As(V) and As(III) under strong alkaline conditions (pH ≥ 11) (Liu et al. 2011; Yu et al. 2011). Adsorption mechanism is explained by the intermediate hydration to $Mg(OH)_2$ and the following As(V) oxy-anions adsorption on its surface through the formation of monodentate inner-sphere complexes. Some studies have applied MgO in the arsenic adsorption process to adsorb the arsenic-rich solution produced during the regeneration process and demonstrated the use of the arsenic saturated MgO as an additive in building materials (Li et al. 2014; Zhang et al. 2015). The produced building material containing 3 and 5 wt% saturated MgO demonstrated successful arsenic stabilization in concrete and therefore, comply with European standards for safe disposal of toxic waste materials (Tresintsi et al. 2014a).

2.6 Low-pressure membrane filtration processes

Both microfiltration (MF) and ultrafiltration (UF) are low-pressure membrane (LPMs) with similar operating principles: pressure drives the water through the membrane element while pollutants bigger than the pore size are retained. MF is characterized by a membrane pore size ≥ 50 nm and trans-membrane pressure (Δp) below 1 bar. MF is used primarily to separate particles and bacteria from other smaller solutes. UF is characterized by a membrane pore size of nearly between 10 and 50 nm with Δp < 5 bars. UF is used to separate viruses, colloids like proteins from small molecules like sugars and salts (Jekel and Czekalla 2017; Pal 2015). Both MF and UF do not have rejection properties for mono- and divalent ions such as As(V) and As(III) species (Figure 2.11).

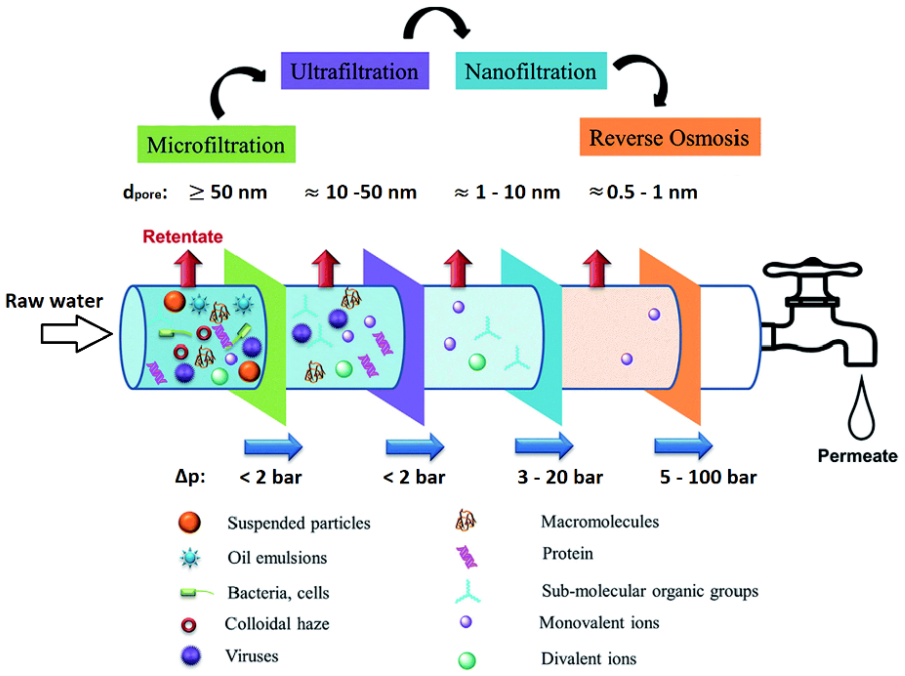

Figure 2.11. Pressure-driven membrane filtration processes for water treatment technologies, showing the particles effectively captured by each process along with the pore sizes (d_{pore}) of the membranes and trans-membrane pressure (Δp) used for each process (adapted from Selatile et al. (2018)).

However, LPM filtration processes have reasonable energy consumption and in general, produce excellent hygienic quality treated water with a rather controllable membrane fouling at moderate capital costs (Katsoyiannis et al. 2013). A study of Drouiche et al. (2001) on the economic performance of ultrafiltration membrane process indicated that a drinking water system (480 m^3 /day) treating surface water in the Kabylia region of Algeria incurred a total cost of 0.235 $/$m^3$ including the capital, energy (0.01 $/$m^3$), membrane cleaning and replacement costs. Because of this, LPMs are increasingly being considered as alternatives to granular media filtration. As of 2000, out of the LPM full-scale plants identified worldwide, UF applications represent about 74% of the total installed capacity on the water industry (Laîné et al. 2000).

LPMs are historically operated in a dead-end mode in small volume applications due to higher water conversion factor. In dead-end filtration, the feed solution flows perpendicular to the membrane surface (Figure 2.12). The permeate drags all the solids in the feed solution to the membrane surface and causing membrane fouling (build-up of cake layer when particle deposit on top of the membrane or in the pores of membranes (Singh 2015). Cake layers can also be beneficial in some cases. For instance, a cake layer can act as an additional filter depending on its composition and rejection characteristics. This cake layer filtration is referred to as a secondary membrane or dynamic membrane and has been discussed in chapter 2.7.

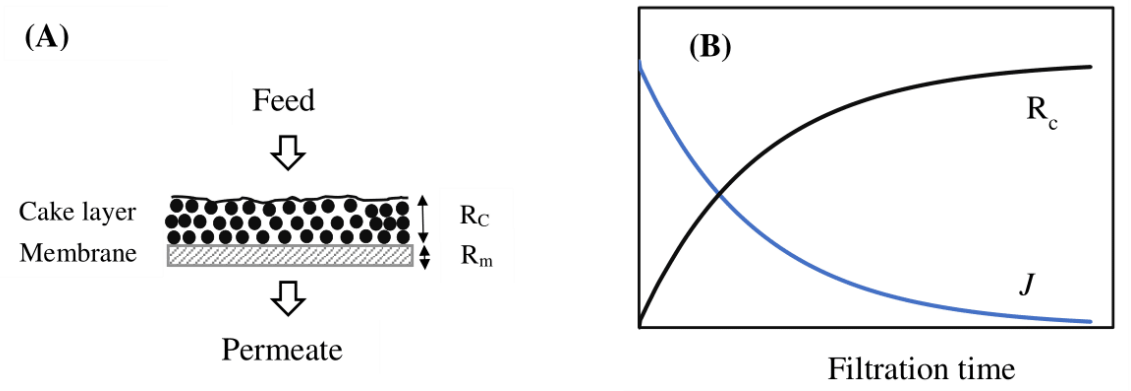

Figure 2.12. (A) Schematic representation of dead-end membrane filtration; **(B)** Evolution of flux decline and cake resistance (adapted from Singh 2015). R_c and R_m are the resistance of cake formed on the membrane and virgin membrane respectively, and *J* is the membrane water flux.

Fouling mechanisms include adsorption, pore blockage, precipitation, and cake formation. In particular, LPMs are highly susceptible to fouling. When the permeate flux drops below a critical flux value, physical cleaning or chemical cleaning is necessary to restore the permeability of the membrane. Physical cleaning of the membrane by means of hydraulic pressure is one of the solutions to mitigate membrane fouling. The backwash of the membrane is performed via a reversed flow, from the permeate side to the feed side of a membrane using a given type of medium (i.e. water or air), causing the foulants to detach and remove from the surface of the membrane (Chang et al. 2017). In general, the more intensive the backwash, in terms of high transmembrane

pressure, shortened frequency, and extended duration, the more effective it is at separating the foulants from the membrane surface. However, all the materials accumulated on the membrane surface cannot be flushed out by any physical cleaning procedure (termed irreversible fouling). This fouling lead to leads to a long-term increase in the resistance (with the subsequent increase in the operational costs) and to a progressive deterioration of the membrane (Ferrer et al. 2015).

The membrane flux is determined using the following expression

$$J = \frac{\Delta V}{A_m . \Delta t} \tag{2-31}$$

The membrane permeability is calculated according to:

$$k_o = \frac{J}{TMP} \tag{2-32}$$

where J is the membrane flux, ΔV is the produced permeate for a given time interval, Δt is the time interval between measurement, A_m is the membrane area, k_o is the pure water permeability of membrane, TMP is the trans-membrane pressure.

2.6.1 Hybrid membrane processes

More stringent regulations on drinking water quality as well as an increased focus on emerging contaminants have favored the development of alternative technologies to the conventional processes (clarification, coagulation/flocculation and filtration). Over the last two decades, low-pressure membrane filtration coupled with activated carbon has been emerged as a promising solution, often referred to as the hybrid membrane processes (HMPs), to create an innovative water treatment system. Such HMPs with adsorption can simultaneously enhance the reactivity and selectivity of pollutant removal in water engineering. As a result, the hybrid process concept has been employed in water and wastewater treatment to effectively remove both organic and inorganic pollutants from polluted natural water (Hashlamon et al. 2017; Jia et al. 2009b; Kalaruban et al. 2018b; Vigneswaran et al. 2003). It is a well-known fact that the application of the adsorbents in form of "powdered or micro-sized" is not possible in fixed-bed adsorption filters, because of high clogging potential in filter-bed, rapidly causing an increased pressure drop and thereby increasing pumping costs of the fluid through the adsorption filter and maintenance.

The main advantage of HMPs with adsorption over fixed-bed adsorption filters is the opportunity of employing very fine fractions of the granular adsorbents, which results in better and adsorption kinetics (Koltuniewicz et al. 2004). The hybrid process requires, especially the SMAHS requires a large adsorption reactor for adequate hydraulic residence time to achieve high removal efficiencies of dissolved contaminants, and consequently, the space requirement of HMPs is large. HMPs with adsorption can offset the disadvantage of the large equipment size when very fine fractions of the applied adsorbents are cheaper than the granular fractions. For instance, the current costs (on dry basis) for GFH and µGFH materials are estimated to 9 €/kg and 1.6 €/kg, respectively. Another synergistic advantage of low-pressure driven HMPs with adsorption (in contrary to fixe-

bed adsorption filters) is achieving simultaneous removal of colloids, microorganisms, and suspended solids by LPMs (Lebeau et al. 1998).

Combining adsorbents (e.g., PAC, micro-sized iron oxyhydroxides) with either MF or UF membranes presents numerous challenges including membrane abrasion, membrane fouling, optimization of operating conditions, prediction of process performances and selection of the process configuration (Stoquart et al. 2012).

***Configurations for hybrid membrane processes*:** The different configurations of HMP is generally classified into three categories:

I. HMP with adsorption prior to LPMs filtration (pre-treatment configuration, Figure 2.13(A)).
II. HMP with an integrated adsorption and LPMs filtration (integrated treatment configuration, Figure 2.13 (B)).
III. HMP with fixed-bed adsorption after LPMs filtration (post-treatment configuration, Figure 2.13 (C)).

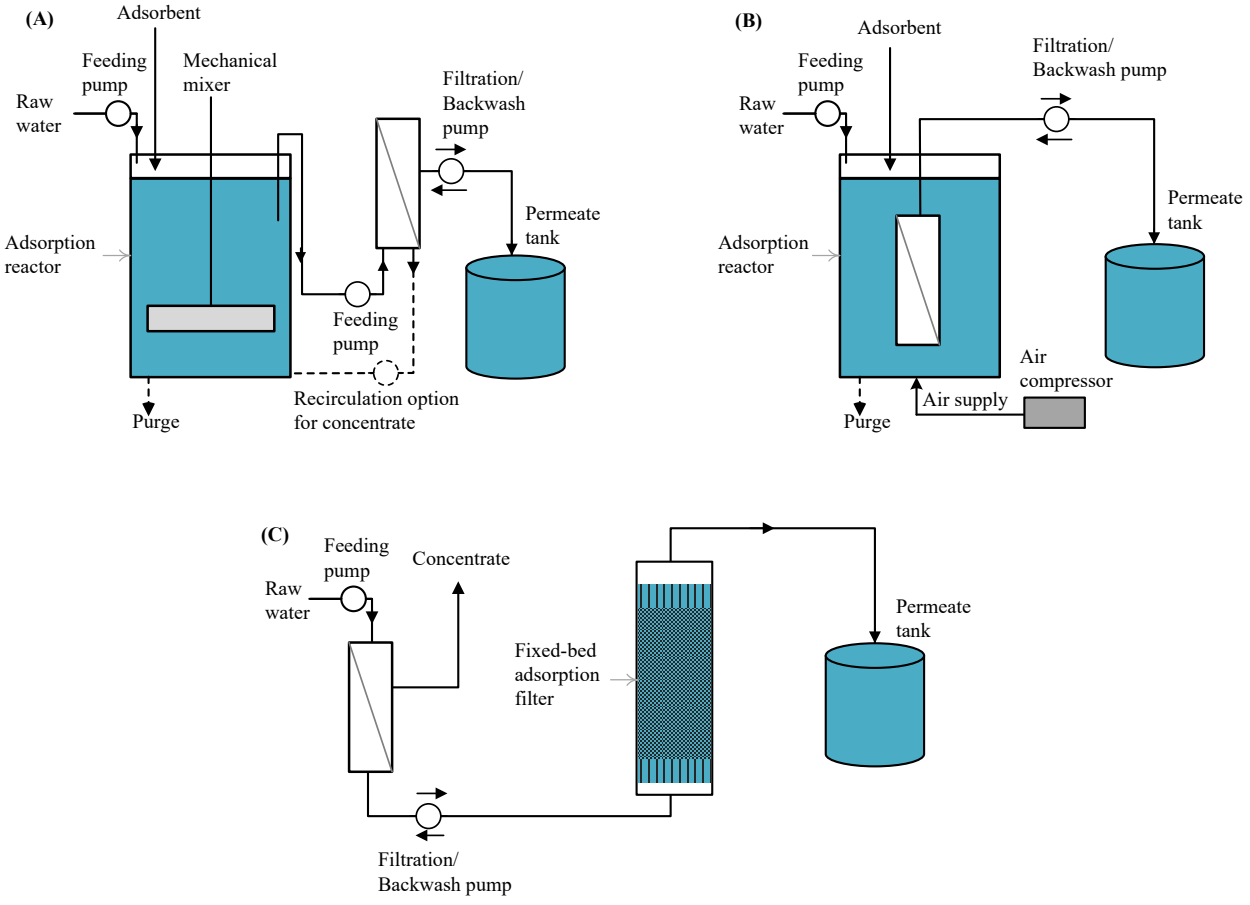

Figure 2.13. Schematic representation of the HMP with; **(A)** adsorption pre-treatment. When PAC is used, the concentrate can be recirculated in the adsorption reactor; **(B)** integrated adsorption treatment (termed as SMAHS in this thesis); **(C)** adsorption post-treatment.

For each category, dissolved contaminants and/or pollutants are predominantly removed by the activated adsorbent either by adsorption or biodegradation (biological mode) (Stoquart et al. 2012). The current thesis work focusses on the application of an HMP with adsorption of arsenic onto micro-sized iron oxyhydroxides.

HMP with integrated adsorption process: In the integrated configuration (referred to as SMAHS in this thesis), adsorbent such as PAC is added directly to the adsorption reactor containing polluted water and a submerged LPM unit. The membrane in this configuration enables relatively a higher adsorbent dose to be maintained in the system (Stoquart et al. 2012).

Recent studies show that the removal of organic and inorganic pollutants from drinking water by a SMAHS using micro-sized adsorbents is a promising technology (Akhondi et al. 2017; Shanmuganathan et al. 2015). The performance of SMAHS depends on the adsorption capacity of the applied adsorbent media to remove specific pollutants, mode of adsorbent dosage (initially or continuously dosed to adsorption reactor), adsorption reactor configuration and operating conditions including water matrix, hydrodynamic conditions such as air bubbling rate, water flux, feedwater pH, temperature, etc. (Campos et al. 2000; Jia et al. 2009a; Kalaruban et al. 2018b; Vigneswaran et al. 2003). High membrane water fluxes reduce costs due to large amounts of water being treated by small footprint installations. However, if due to increasing membrane water fluxes the hydraulic retention time in the adsorption reactor is rather short, the pollutant removal efficiency may decrease. Also, high fluxes may increase the rate of fouling on the membrane (critical flux phenomena). Nevertheless, applying aeration to the adsorbent suspension keeps the adsorbent particles completely dispersed in the reactor and helps to reduce the solid deposition on the membrane surface by the air scouring effect (Choi et al. 2009; Kalaruban et al. 2018b; Stylianou et al. 2018). For example, in PAC adsorption-membrane filtration systems, PAC might be initially or continuously dosed into the adsorption reactor. For the “PAC initially dosed” mode, the required PAC is added into the reactor at the start of each filtration cycle. For the “PAC continuously dosed” mode, the PAC is continuously dosed into the adsorption reactor during the filtration cycle. The mathematical modeling using different adsorption kinetic models has shown that higher removal efficiency can be acquired with the "adsorbent initially dosed mode" due to higher adsorbent use efficiency with this approach (Campos et al. 2000; Chang et al. 2003).

Further, the design of the submerged membrane module usually allows operation under conditions of relatively high solids concentration. This could considerably benefit its combination with adsorption by offering more flexibility for optimization of the use of PAC (from Chang et al. 2003). Moreover, the entire treatment activity (such as adsorption/biodegradation, liquid-solid separation, sludge accumulation and withdrawal) can be carried out in a single unit. In this system, dissolved organic compounds that normally can pass through the MF are pre-adsorbed onto PAC particles. The PAC together with adsorbed organics is then separated by the membrane filtration process (Guo et al. 2015).

2.7 Dynamic membrane

Dynamic membranes were first reported in 1965 by a study of the Oak Ridge National Laboratories (Marcinkowsky et al. 1966). Differing from the membrane formed through a casting membrane solution or melting spinning technique, a dynamic membrane (DM), which is also called "secondary membrane", the DM, can be formed *in-situ.* The DM builds up as a layer of particles such as metal oxides, soil-based compounds or powdered activated carbon deposited via permeation drag onto surfaces of the meshes, nylon, PES and ceramic-based MF and UF (Anantharaman et al. 2020; Ersahin et al. 2012; Matsuyama et al. 1994). This suggests that a DM filtration technology predominantly involves two layers namely the primary membrane/membrane support material as a supporting layer and the deposited layer of microparticles as the secondary membrane. The primary membrane or membrane support layer provides the foundation to the deposited layer, while the deposited layer of the coating agent acts as the main functional part (Li et al. 2018). The deposited layer of particles then determines removal rates of DM filtration system towards a target pollutant (Ersahin et al. 2012; Zhang et al. 2010), since the primary membrane does not have rejection behavior towards the target pollutant (Ersahin et al. 2012). DM may minimize fouling of the primary membrane to lower transmembrane pressures (TMP) and enables higher permeate fluxes (Anantharaman et al. 2020; Nyobe et al. 2019).

The DMs with different separating functions can be prepared through choosing suitable materials and DM-making techniques. DMs formed on the loose support materials such as MF and mesh have an advantage over traditional membranes to be operated under gravity driving mode (Li et al. 2018). A driving force by means of a 10 cm water head was sufficient during DM filtration of secondary wastewater effluent to achieve 200 L/(m^2·h) when a nylon mesh with an equivalent aperture of 25 µm was adopted as support material for the DM filtration (Hu et al. 2016). Further, once the membrane is fouled or utilized, the deposited layer of particles can be easily removed by either water or air backwash (Chu et al. 2008) and a new layer can be easily redeposited. The use of water has proven to be effective in cleaning fouled DMs. More than 90% of the original membrane permeability could be regained after four filtration cycles (Aghili et al. 2017; Lu et al. 2016). Similarly, bottom aeration (120 m^3/(m^2·h)) was adequate for removing all clogs of the dynamic membrane (Fan and Huang 2002).

DMs are categorized into two main classes, namely, self-forming DMs and pre-coated DMs. Whereby the feed constituents form the DM is referred to as self-forming DM, whereas a pre-coated/pre-deposited DM is formed by a layer of particles other than the feed over the surface of the conventional primary membrane prior to the introduction of the feed (Anantharaman et al. 2020; Ersahin et al. 2012; Li et al. 2018). Pre-coated DM systems have the flexibility of choice of appropriate inexpensive and affordable materials having the relevant properties with which to form the DM. Irrespective of DM type, the DM either: (a) enhances the overall performance of the conventional primary membrane; (b) expands the capability of the primary membrane to remove contaminants that otherwise would not be removed; or (c) protects the primary membrane from fouling (Anantharaman et al. 2020).

According to the formation mechanism, the DMs can be classified into two classes. When the pore size of the primary membrane is small enough to entirely retain the particles of the pre-coating agent (class I DMs). In this case, the dominant mechanism that governs DM formation is the concentration polarization (Tanny and Johnson 1978). Class II DMs are those whereby the diameter of the primary membrane is much larger (up to three orders-of-magnitude) than the diameter of the depositing particles (for example, dust or bacteria the feed solution). The depositing materials can bridge pores and create flocculation centers. Class II DMs are formed via the mechanisms of pore constriction and cake filtration (Anantharaman et al. 2020). Generally, in DM filtration technology a cake layer of particular thickness is explicitly formed as more and more particles are deposited over the surface of the primary membrane. Due to which the resistance might not be as severely affected during the formation of class I DMs compared to class II DMs (Anantharaman et al. 2020; Tanny and Johnson 1978). Therefore, class I DMs have recently gained popularity in water treatment for organics removal (Cai and Benjamin 2011; Huang et al. 2009).

Apart from the properties of the support and membrane materials, formation parameters including pressure, cross-flow velocity, and concentration of the feed may also have an impact on the performance of dynamic membranes. For MF and UF applications, DMs are formed at low pressures up to 1 bar (Zhao et al. 2006) and the pore size in the porous supports varied from 2.0 to 7.0 μm (Wilde et al. 1988).

2.7.1 Dynamic membrane forming materials

The most popular material used for the dynamic membranes is zirconium oxide from hydrated zirconium oxide. Other inorganic hydrous oxides and organic polyelectrolytes have also been tested, such as titanium dioxide for oil separation (Pan et al. 2012), PAC for COD removal (Ye et al. 2006), MnO_2 for turbidity removal (Cai et al. 2000), clay in treating domestic wastewater (Noor et al. 2002) clay for color removal (Wang et al. 1998) and arsenic removal (O'Day et al. 2005) through adsorption. O'Day et al. (2005) observed arsenic removal of 58.9% for the first 500 mL effluent at a flow rate of 0.15 mL/min with an influent arsenic concentration of 100 μg/L. The removal increased to 94.9% in the same volume of effluent when the flow rate was decreased to 0.08 mL/min. In this thesis, powdered-sized fractions of iron oxyhydroxide-based adsorbents are tested to determine their potential as a DM forming material.

3 Material and methods

3.1 Chemical, solutions and materials

3.1.1 Chemicals, reagents and glassware

Acid and bases: For pH adjustments and titrations, reagent grade (≥ 99 %, p.a., ISO) sodium hydroxide (NaOH), potassium hydroxide (KOH) and hydrochloric acid (HCl) supplied by Carl Roth GmbH + Co KG, Germany in liquid form were used and diluted in ultrapure water.

Reagents: For preparation of National Sanitation Foundation (NSF) challenge water (described in section 3.1.2), stock solutions were prepared by dissolving sodium dihydrogen phosphate ($NaH_2PO_4 \cdot H_2O$ 99.99%, Merck), sodium hydrogen carbonate ($NaHCO_3$ ≥ 99.5% p.a., Carl Roth GmbH + Co. KG, Germany), calcium chloride-2-hydrate ($CaCl_2 \cdot 2H_2O$ ≥ 99%, Riedel-de Haën, Germany), magnesium sulfate-6-hydrate ($MgSO_4 \cdot 6H_2O$ ≥ 99%, Riedel-de Haën, Germany), sodium fluoride (NaF, PanReac AppliChem, Germany), sodium nitrate ($NaNO_3$ ≥ 99%, Carl Roth GmbH + Co. KG, Germany) and sodium metasilicate pentahydrate ($Na_2SiO_3 \cdot 5H_2O$ ≥ 95%, Aldrich) in deionized (DI) water. The standard solution of As(V) was H_3AsO_4 (Certipur®) in HNO_3 (0.05 mol/L) with a concentration of 1 g/L. It was obtained from Merck chemical GmbH (Darmstadt, Germany), whereas the standard solution of As(III) was As_2O_3 in (2%) HNO_3 with a concentration of 1 g/L. It was delivered by Carl Roth GmbH + Co. KG (Darmstadt, Germany). Magnesium oxide (MgO, CAS: 1309-48-4) was purchased from Fisher Scientific GmbH, Germany.

Ultrapure water: Ultrapure water was provided by a 'Synergy®' water purification system supplied by Merck Chemicals GmbH, Germany. Purification cartridges were replaced as recommended by the manufacturer. Electrical resistivity at 25 °C was 18.2 MΩ·cm and total organic carbon (TOC) concentration ≤ 5 µg/L (manufacturer's specifications). For cleaning and rinsing procedures, DI water with an electrical conductivity ≤ 0.20 µS/cm was used.

Cleaning procedure of glassware: Glassware was cleaned in laboratory dishwashers operated with deionized water and intensive cleaning powder ('Roti®-Splish P', Carl Roth GmbH + Co KG, Germany) and subsequently dried at 65 °C. Prior to usage, glassware was rinsed with ultrapure water. Any glassware that was used for sampling, sample storage and measurement of TOC and DOC was burned at 550 °C or soaked in sodium persulfate solution for 1 h at 60 °C and afterward thoroughly rinsed with ultrapure water.

3.1.2 Test solutions

The test solution was initially prepared using DI water spiked with either As(III) or As(V) species, at an initial concentration of 190 µg/L. For experiments carried out in DI water, 2 mM of *N*,*N*-Bis(2-hydroxyethyl)-2-aminoethanesulfonic acid (BES) was added to the test solution for pH control at pH 8 ± 0.1. In addition to DI water, As(V) and As(III) test solutions were prepared in Hamburg (HH) tap water and NSF water with the same initial arsenic concentration, as used in the case of DI water, in order to study the effect of different water matrices on the arsenic adsorption

capacity. The major physicochemical parameters of the HH tap water and of NSF challenge water are listed in Table 3.1.

Table 3.1. Water quality parameters of Hamburg (HH) tap water (*data obtained from Hamburgwasser) and NSF challenge water.

Parameter	Water matrices	
	HH tap water*	NSF challenge water
Na^+ (mg/L)	14	73.7
Ca^{2+} (mg/L)	42	40.1
Mg^{2+} (mg/L)	4	12.6
HCO_3^- (mg/L)	150-300	183.0
Cl^- (mg/L)	19	71.0
SO_4^{2-} (mg/L)	23	50.0
NO_3^- (mg/L)	0.62	2.0
F^- (mg/L)	0.13	1.0
PO_4^{3-} (mg/L)	0.05-0.15	0.123
SiO_2 (mg/L)	16.6-18.5	20
DOC (mg/L)	0.8 ± 0.2	-

The NSF challenge water was prepared according to the National Sanitation Foundation (NSF) international and contains the following: 252 mg $NaHCO_3$, 12.14 mg $NaNO_3$, 0.178 mg $NaH_2PO_4 \cdot H_2O$, 2.21 mg NaF, 70.6 mg $NaSiO_3 \cdot 5H_2O$, 147 mg $CaCl_2 \cdot 2H_2O$ and 128.3 mg $MgSO_4 \cdot 7H_2O$ in 1 L of DI water. Prior to adsorption experiments, pH was adjusted to 8 ± 0.1 by adding either NaOH or HCl standard solutions (1.0 M).

3.1.3 Materials

µGFH was delievered by GEH Wasserchemie GmbH & Co, Osnabrück, Germany, and TMF was supplied by professor Manassis Mitrakas from Aristotle University of Thessaloniki (Tresintsi et al. 2013b). µGFH is a by-product generated during the industrial production of GFH, which is produced from a ferric chloride solution by neutralization and precipitation with sodium hydroxide. The ferric hydroxide precipitate is centrifuged and granulated by a high-pressure process (Thirunavukkarasu et al. 2003), while the preparation of TMF involves the co-precipitation of $FeSO_4$ and $KMnO_4$ in a kilogram-scale continuous process. The kilogram-scale production in a laboratory two-stage continuous flow reactor includes the coprecipitation into the water of the iron source ($FeSO_4 \cdot H_2O$) at pH 4 and the manganese source ($KMnO_4$), which is an oxidant for the process and also used to adjust the reaction's redox to 850 mV (Tresintsi et al. 2013b). The generated fraction of µTMF during a laboratory-scale production of TMF is ca. 10%. Therefore,

granular TMF (0.3 - 2 mm) was grounded to achieve an abundant quantity of µTMF to apply in current research work.

TMF (as received) was sieved, in order to obtain two size fractions, for application in the bench-scale experiments. The smaller fraction of TMF (1 – 63 µm) was obtained by passing through a 230-mesh sieve (= 63 µm), while the larger fraction of TMF (1 – 250 µm) was separated by a 60-mesh sieve (= 250 µm). The smaller and larger particle fractions of TMF are termed as µTMF (1 – 63 µm) and µTMF (1 – 250 µm), respectively. The grain size of the µGFH obtained from the manufacturer ranged between 1 and 250 µm, termed as µGFH (1- 250 µm). A smaller fraction of µGFH (1 - 63 µm) was separated from air-dried µGFH by passing a sieve with mesh size 63 µm. Note that henceforth in this thesis, the abbreviation 'fine-grained/micro-sized' will refer to particle diameter in the range of 1-250 µm, whereas the abbreviation 'powdered-sized' will refer to particle diameter in the range of 1-63 µm. All results presented on a dry mass basis of both iron oxyhydroxides after drying at 105°C for 24 h and subsequent cooling in a desiccator.

3.1.4 Characterization of adsorbent media

Particle size determination: Particle size distribution was determined by laser obscuration time measurement using an EyeTech device and corresponding analysis software supplied by Ankersmid (The Netherlands). For each analysis, the average of three individuals' measurements was determined by the software, each lasting until a confidence level of 98 % was reached. Each sample was analyzed at least two times. Prior to measurement of a set of samples, the system proper operation and setting were confirmed by measurement of 10 µm particles standards supplied by BS-Partikel GmbH, Germany.

It was observed during adsorbent particles of larger than 10 µm are susceptible to breakage due to suspension of particle by magnetic stir in optical cell. In this case, fine grain absorbents (particle size ranging between 1 and 250 µm) the liquid flow cell of EyeTech was filled with 1 L of DI water, and approximately 100 mg of adsorbent material was added. Mechanical shaking was provided in the liquid flow cell, which keeps the material particles in suspension. The suspension was then supplied to the optical cell and circulated through it for 5 min at a pump speed of 0.674 L/min. Three cycles of the suspension were performed each lasting until a confidence level of 98 % was reached.

Surface characterization: The surface area of the media was determined by nitrogen gas adsorption at liquid N_2 temperature (77 K) using a surface area analyzer (Nova 4200, Quantachrome Instruments, USA) according to Brunauer Emmette Teller (BET) model. Six-point surface area measurements are employed to determine the surface area of the samples. The pore-size distributions were obtained using the standard Dubinine-Radushkevic and the Barrette-Joynere-Halenda (BJH) method (Barrett et al. 1951). Scanning electron microscopy (SEM) imaging was conducted at the electron microscopy unit (BEEM) of Hamburg University of Technology with Zeiss Leo Gemini 1530 (Carl Zeiss AG, Oberkochen, Germany).

Iron content determination of adsorbent media: The iron content of the adsorptive media was determined by acid digestion. Briefly, one gram of media (on dry basis) was added to 50 mL of 10% HNO_3 in a glass beaker and the suspension was heated using a hot plate to boiling point. After 2 h, the iron oxide in the suspension was completely dissolved and the acid solution turned yellow (AWWARF 1993). At this point, heating was ceased, the suspension after cooling was made up to 1 L with DI water, filtered through 0.45 µm filter, and the iron content determined by DIN 38406 method using a photometer (model UV-1700, Shimadzu, Germany).

3.2 Experimental setups and procedures /methods

3.2.1 Batch adsorption kinetic procedure

The slurry reactor was applied for kinetic tests to determine the mass transfer coefficients for the adsorption process (Dotto et al. 2017; Worch 2012). To ensure that film mass diffusion mass would not be the rate-limiting step for the overall adsorption process (Bi > 30), high mixing at 150 rpm using an electrical stirrer (Heidolph Instruments GmbH & Co. KG) in the batch slurry reactor setup was provided. The known amount of adsorbent media mass was brought in contact with the test solution. For experiments focusing on the determination of kinetic data for mass transfer coefficients, an adsorbent mass of 40 mg/L was calculated from the batch adsorption isotherm data to ensure that batch kinetic tests were carried out in the presence of limited adsorption sites for accurate determination of adsorption mass transfer rates through kinetic data. In the slurry reactor setup, the aforementioned amount of adsorbent media was carefully added into a 2 L glass beaker containing DI water spiked with As(V). The stirrer did not impact the particle size distribution of the media, which was proofed by measurements (Figure A.7).

The mixing was continuously maintained during sampling in order to avoid changes in adsorbent media concentration. The pH value of the test solutions in the slurry reactor was monitored intermittently. Sample aliquots of ~ 5 mL were collected at predefined time intervals in each test. The same volume of test solution without As(V) was then injected back into the flask. The collected sample aliquots were stored for further analysis.

3.2.2 Batch adsorption isotherm procedure

Batch equilibrium and kinetic adsorption tests were performed to study the adsorption potential of fine-grained iron oxyhydroxides for removing arsenic species from the different examined test solutions/water matrixes. To derive the adsorption isotherms, the method of adding various quantities of adsorbent to a constant solution volume (500 mL), having the same initial concentration of As(V) or As(III) species, was adopted. Additionally, As(III) test solutions were preliminary bubbled for 30 min with pure N_2 gas at 0.1 bar (flow rate 11.25 mL/min) to minimize the influence of dissolved oxygen on As(III) potential oxidation and adsorption. The flasks were immediately closed and placed on the platform shaker in darkness in the thermostat cabinet (Temperature (T)= 20 ± 0.5 °C) to ensure the stability of As(III) species during and after adsorption onto the examined adsorbent.

For batch adsorption experiments, different adsorbent dosages in the range of 2-100 mg were placed in 1 L flasks and equilibrated with 500 mL of the arsenic species in three different water matrixes. Only the adsorbent doses that provided the arsenic concentration between 1 and 100 µg/L were considered for adsorption isotherms. Different adsorbent doses were found to provide the arsenic concentration between 1 and 100 µg/L focusing on the removal of As(III) in DI water, HH tap water, and NSF water, respectively. For each set of tests, a reference blank sample (i.e., without the presence of an adsorbent) was filled. The flasks were stirred using a platform shaker for 96 h at 20 ± 0.5 °C. The equilibration time was determined from the corresponding kinetic experiments. At the end of the equilibration time, the suspensions were immediately filtered through a 0.45 µm membrane syringe filter (PVDF, Carl Roth GmbH + Co. KG), and the filtrates were collected and stored for the subsequent analytical determination of residual (still dissolved and removed) arsenic.

3.2.3 Batch adsorption tests to investigate the influence of equilibrium pH

Batch adsorption experiments focusing on equilibrium pH were carried out in 1 L reagent flasks, and 5 mg of adsorbent dose (on dry basis) was carefully placed into each flask. The influence of pH was evaluated by taking the 500 ml test solution with initial concentration of either As(V) or As(III) in the pH range of 3-9. Like adsorption isotherm tests, the flasks were placed on platform shaker and mixing was provided for 96 h. All experiments were carried in duplicate. At the end of the equilibration time, the suspensions were immediately filtered through a 0.45 µm membrane syringe filter (PVDF, Carl Roth GmbH + Co. KG), and the filtrates were collected and stored. The concentrations of residual arsenic in the resulting filtrates were determined by graphite furnace atomic absorptions spectrometry.

3.2.4 Spent iron oxyhydroxides regeneration procedure

Most of the applied arsenic adsorbents such as GFH, Bayoxide, and titanium dioxide appear to have a very low removal efficiency for As(III) compared to As(V), due to the predomination of uncharged As(III) species (H_3AsO_3) at pH range encountered in natural waters (Guan et al. 2012; Lakshmipathiraj et al. 2006). In practice, when As(III) is present, a chemical or biological pre-oxidation step is embodied (Sorlini and Gialdini 2010) followed by the removal of arsenic in the form of As(V). Therefore, the spent adsorbents of full-scale arsenic treatment plants contain almost exclusively As(V), which in turn implies that the alkaline regeneration stream will contain only the leached As(V). For this reason, regeneration experiments were carried out through batch adsorption tests with As(V).

Spent adsorbent was regenerated using NaOH through batch and continuous mode method. To gain preliminary information on optimization of alkaline conditions, a series of batch adsorption tests were carried out with spent adsorbent of 50 mg (on dry basis) containing 10 ± 0.2 mg As(V)/g using NaOH solution in the concentration range between 0.01 and 0.1 M. In addition, the contact time was varied in the time between 6 h and 96 h to determine the optimal contact time. The mixing was provided by placing the flasks on the platform shaker. Then, NaOH solutions were immediately filtered through a 0.45 µm membrane syringe filter (PVDF, Carl Roth GmbH + Co.

KG, Germany), and the filtrates were collected and stored for the subsequent analytical determination of arsenic.

3.2.5 Submerged membrane adsorption hybrid system experiments

A self-assembled MF membrane module made with hollow fiber outside-in PVDF-type membrane (Microza microfilter, Pall membrane) with specifications of 0.1 µm nominal pore size and 0.018 m^2 was used in the slurry reactor of the SMAHS to separate the loaded adsorbent particles (Figure 3.1). The inner and outer diameter of hollow MF fiber was 0.7 and 1.3 mm, respectively. The feed solution was prepared using either DI or NSF water matrix spiked with As(V) to adjust a concentration of either 190 µg/L or 380 µg/L, and the pH of the solution was maintained at 8 ± 0.1.

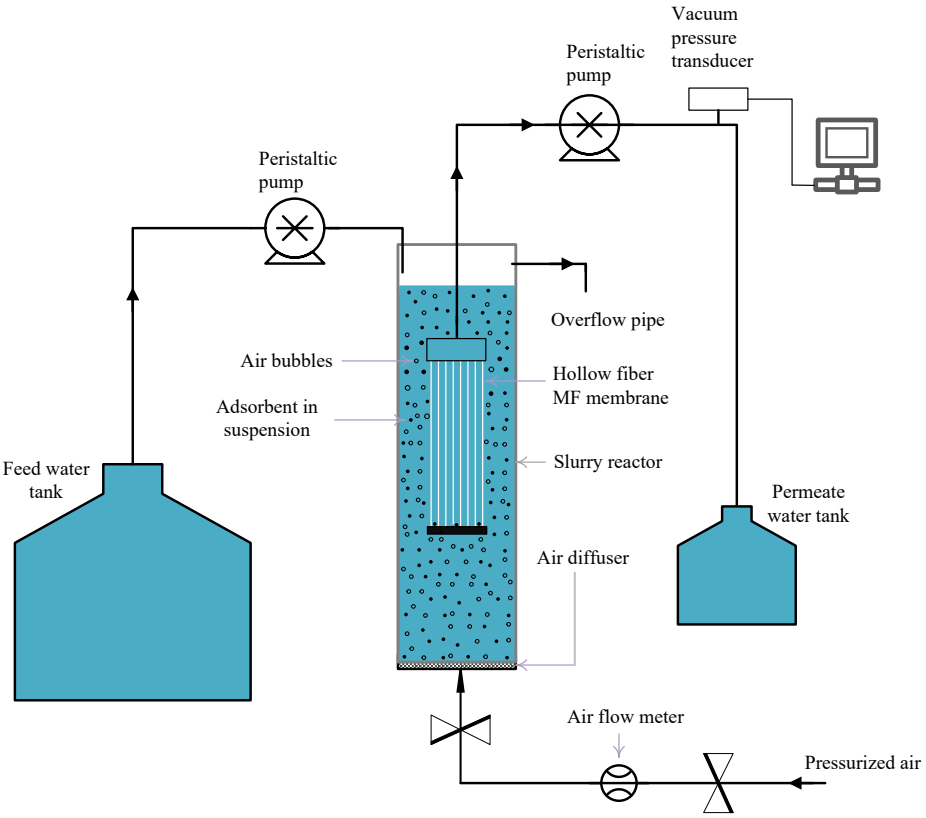

Figure 3.1. Schematic diagram of the submerged membrane adsorption hybrid system (SMAHS)

A transparent cylinder (6 cm in diameter) made of polyvinylchloride (PVC) was used as a slurry reactor. A sintered glass diffuser (VitraPOR® ROBU Glasfilter Geräte GmbH) with a pore diameter of 10-16 µm was fixed at the bottom of the slurry reactor. The slurry reactor was filled with I L of arsenic-contaminated water. The MF membrane module was positioned in the middle of the reactor. The permeate port was located on the top side of the MF module. Air was transported from a purified air cylinder by PVC tubing to a sintered glass diffuser to generate fine air bubbles.

The SMAHS experiments were carried out in a continuous flow operation with adsorbent initially adsorbent dosed mode. In this mode of operation, the total amount of adsorbent was added into the reactor at the beginning of the experiment. A multi-channel peristaltic pump was employed, and it was operated in such a way that the feed solution was pumped into the reactor at the same volumetric flow rate as the permeate. The system was operated at constant membrane flux in a dead-end mode. Prior to the adsorbent addition, the peristaltic pump for feed and permeate was operated for at least 5 min to precondition the system. The adsorbents (1, 2, 3, and 5 g each) were then added to As(V) contaminated water (1 L) in the slurry reactor. Air was entered continuously from the bottom to keep the adsorbent particles in suspension and to generate scoring on the MF membrane surface. In the absence of air, adsorbent particles could settle at the bottom of the slurry reactor and thus circumventing close contact between adsorbent and As(V) species. The transmembrane pressure was measured by a signal conditioned precision vacuum pressure transducer (423SC15D-PCB, Sensortechnics). The data were collected automatically by a data logger.

3.2.6 Experimental procedure for regeneration of spent adsorbent in SMAHS

The operational expenses can be significantly decreased if the spent media can be regenerated *in-situ* and subsequently, be used for As(V) removal. Therefore, an integrated procedure proposed by Tresintsi et al. (2014a) was adopted to regenerate the spent media by MgO in the SMAHS. This approach combines the As(V) leaching (desorption step) in the slurry reactor and adsorption of leached As(V) in the MgO filter (adsorption step) under a strong alkaline environment in a continuous recirculation configuration. It is relevant to mention that fine-grained adsorbent was considered to be spent/exhausted when the As(V) concentration in permeate of a SMAHS has reached the WHO guideline value of 10 µg/L. This approach was followed as in real arsenic water treatment systems, the exhausted adsorbent material is generally removed and replaced by fresh/virgin adsorbent material. Only µGFH was evaluated for its regenerability in the SMAHS as a representative of iron oxyhydroxide-based adsorbents.

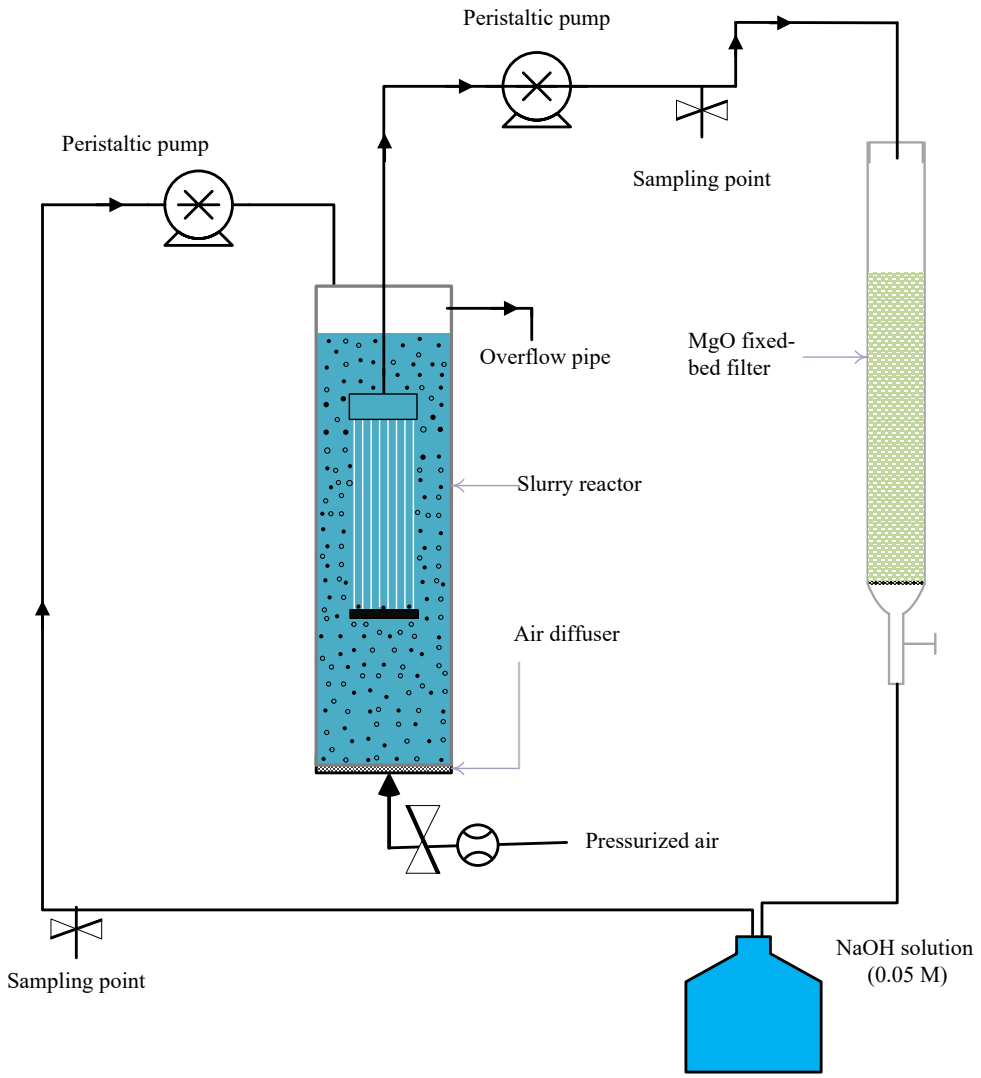

Figure 3.2. Schematic diagram of the *in-situ* regeneration process using MgO filter in the SMAHS.

The fixed-bed adsorption filter containing 65 g granular MgO (particle size ranging between from 0.25 to 1 mm) was serially attached with a slurry reactor which contained the spent adsorbent (Figure 3.2). The MgO filter consists of a cylindrical glass column and has 2 cm inner diameter. The column has a height of 40 cm and was equipped with PTFE valves, caps, and glass frit in the bottom to retain MgO particles. The arsenic polluted water drawn from the slurry reactor by the peristaltic pump was fed to MgO filter. Prior to pump the arsenic polluted water to MgO filter, 200 mL of 0.05 M NaoH was first added via a peristaltic pump on the feed side to raise the slurry pH to > 12. The MgO filter operated at a flow rate of 30 mL/min and employing an empty bed contact time of 3 min. A second peristaltic pump on the permeate side of the submerged MF unit was used to continuously recirculate the 0.05 M NaOH solution through the slurry reactor. Optimum As(V) desorption was obtained by a 0.05 N NaOH solution (determined from the results of the batch

desorption experiments, which results in a pH range 12.5-12.7. Samples were collected at reguar time intervals before and after the MgO filter to monitor the arsenic concentration in the slurry reactor and in effluent of the MgO filter.

The regeneration process was considered to conclude when the arsenic concentration in the slurry reactor was below < 10 µg/L. Ultrapure water with pH 2.0 was then pumped for 1 h through the slurry reactor of the SMAHS to neutralize the µGFH. The influent was then replaced with product water of the SMAHS (arsenic concentration < 10 µg/L) from the proceeding operation cycle and operated for 1 h. Afterward, arsenic polluted NSF water with pH 8 ± 0.1 (as in the first operation cycle) was then continuously passed through the slurry reactor to evaluate the regenerability of the spent µGFH. The success of the regeneration was evaluated by the reapplication of regenerated media in SMAHS and determining the adsorption efficiency of regenerated µGFH for As(V) remediation from water.

3.2.7 Experimental procedure of dynamic membrane filtration

The pre-coated dynamic formed iron oxyhydroxide DM was formed according to the following procedure. The primary MF membrane was first rinsed with at least 1 L of ultrapure water. 0.5 L of ultrapure water was then filtered through each membrane to determine the pure water permeability. The top-end piece of filtration cell contains the feed inlet, while the bottom of the cell contains a porous insert that holds a 28.7 cm² membrane.

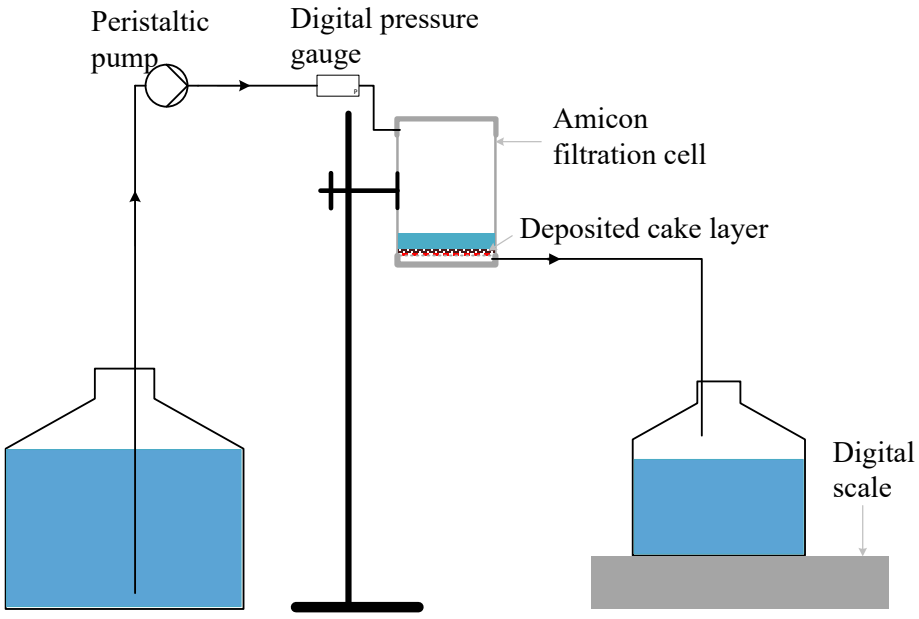

Figure 3.3. Laboratory installations for dead-end filtration.

The suspension formed by mixing microparticles of iron oxyhydroxides (300 or 400 mg in 150 mL DI water) was transferred to an Amicon filtration cell housing the primary membrane. The cell was then sealed with the upper cap and O-ring. 0.5 L of ultrapure water was filtered at 0.5 bar applied pressure through each membrane. A uniform thin layer of adsorbent particles was

deposited over the surface of the support membrane by permeation drag, which is the convective force dragging the particles towards the primary membrane. The pure water permeability of iron oxyhydroxide dynamic membrane was also determined by filtering at least 0.5 L DI water at 0.5 bar.

Once the DM was formed by pre-deposition of powderêd-sized adsorbent (0-63 µm), feed solution containing As(V) concentration of either 190 or 380 µg/L was pumped using a peristaltic pump from a solution reservoir through the membrane filtration cell (Figure 3.3). The TMP was measured by a signal conditioned precision vacuum pressure transducer (423SC15D-PCB, Sensortechnics). The data were collected automatically by a data logger. The permeate quality was monitored by taking samples at different time intervals to measure the As(V) concentration. The performance of dynamically formed iron oxyhydroxide membrane was evaluated under different operating conditions. The recorded As(V) removal rates were then modeled using a mathematical model based on the HSDM.

3.3 Analysis

3.3.1 Electrical conductivity, pH and temperature

Electrical conductivity (EC), pH and T were determined using handheld meters supplied by Xylem Analytics Germany Sales GmbH & Co. KG. (Germany). Adjustment of the EC probe's cell constant was performed monthly using a 0.01 mol/L KCl standard of 1,413 µS/cm supplied by Carl Roth GmbH + Co KG, Germany. Calibration of pH probes was carried out at least weekly by a two- or three- point calibration using pH standards of pH = 4.0, 7.0 and 10.0 supplied by Carl Roth GmbH + Co KG,Germany.

3.3.2 Chemical analysis

The adsorbent particles free samples analyzed at pH 2 using HCl for total arsenic. A atomic absorption spectrometer instrument (Model: 4100 ZL, Perkin-Elmer, Germany) with a Perkin-Elmer Graphite Furnace Tube atomizer was used to measure the arsenic concentrations. Argon gas was applied to atomize the samples. The instrument setup parameters were: 380 mA lamp current, detection at a wavelength of 193.7 nm, 0.7 nm silt width and peak area as measurement mode.

The limit of detection was 0.5 µg/L. Prior to analysis, As(III) water samples from the isotherm experiments were acidified ($2 < pH < 4$) and passed through a 30 mL column (with ID = 1 cm), containing an anion exchange resin (Dowex® 1 × 8–100, mesh size 50–100, Sigma-aldrich Chemie GmbH, Germany), which retained As(V), whereas the total arsenic concentration of water samples from the adsorption kinetics experiments were analyzed. This method of arsenic speciation needs approx. 50 mL of water sample. Therefore, only the total arsenic concentration of the water samples from adsorption kinetics was analyzed, presenting the concentration of individual arsenic species in the water samples. The initial concentration of phosphate in HH tap water was measured using ICP-MS (available at central chemical laboratory of TUHH, Model: NexION 300D, PerkinElmer, Germany).

4 Characterization and arsenic adsorption efficiency of fine-grained iron oxyhydroxides

Adsorbent physicochemical properties have been reported to greatly affect its adsorption efficiency. Accordingly, this chapter first investigates characterization of the applied adsorbents in terms of particle size distribution, moisture content, iron content, specific surface area, and surface morphology via SEM (Chapter 4.1). The effect of solution pH on the adsorption efficiency of the adsorbents were evaluated in chapter 4.2. The fine-grained iron oxyhydroxides were then tested as arsenic adsorbent through batch adsorption tests in three different water matrices. The adsorption isotherms were applied to describe the adsorption isotherm data and to investigate the adsorption mechanism (Chapters 4.3 and 4.4). Finally, the regenerability of the spent applied adsorbents were investigated through batch desorption tests (Chapter 4.5).

Selected contents of this chapter have been published in collaboration with I.A. Katsoyiannis, M. Mitrakas, A.Zouboulis and M. Ernst: Water 2018, 10(7), 957.
Usman et al. (2018b): https://doi.org/10.3390/w10070957

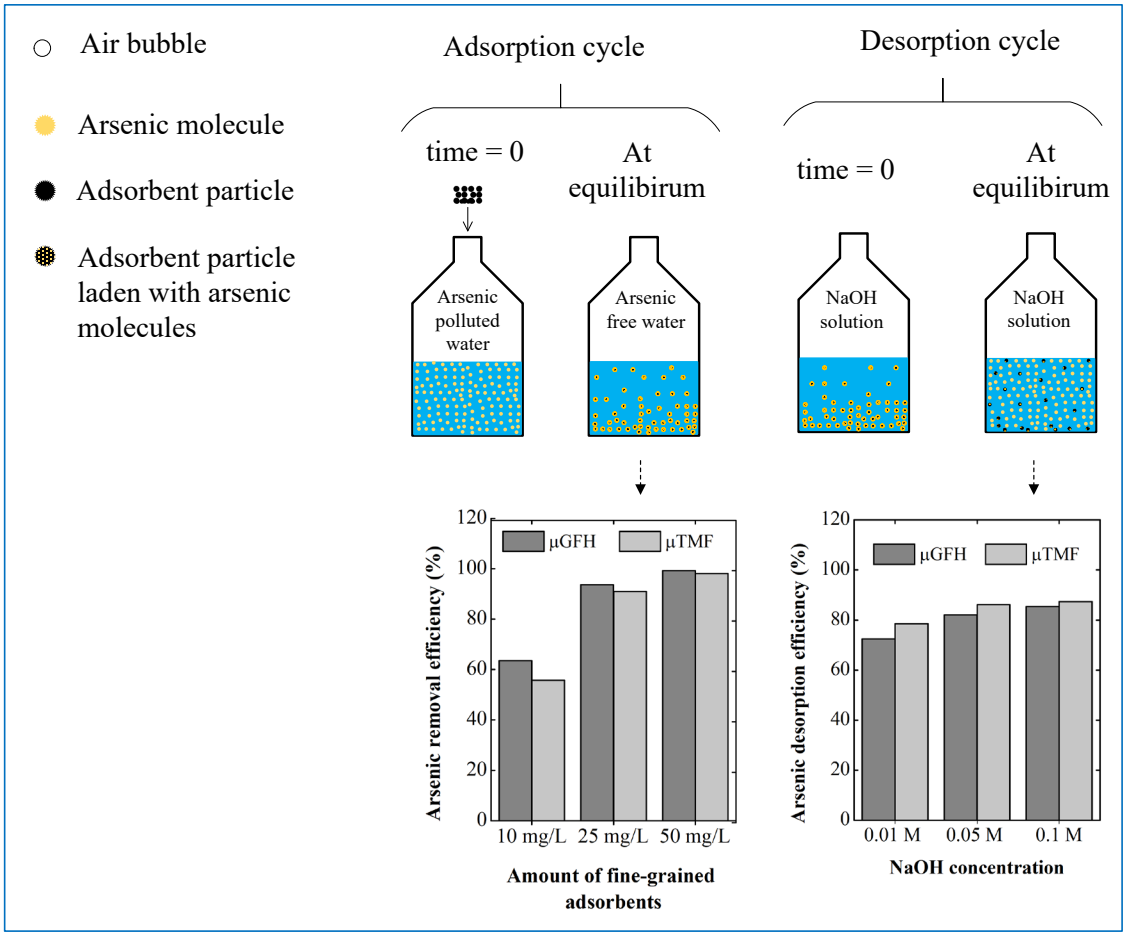

4.1 Characterization of fine-grained iron oxyhydroxides

4.1.1 Particle size distribution of µGFH and µTMF

The particle size has a strong effect on the removal kinetics of adsorbate. Banerjee et al. (2003) observed that the removal of As(III) by the pulverized/micro-sized powdered µGFH (with particle size < 63 µm) was faster than that of GFH (0.320 mm < mean particle size < 2 mm) at same experimental conditions. A similar trend was also recorded by Tresintsi et al. (2015) during the adsorption of arsenic species onto TMF. The length-based particle size distributions of µGFH and µTMF are shown in Figure 4.1.

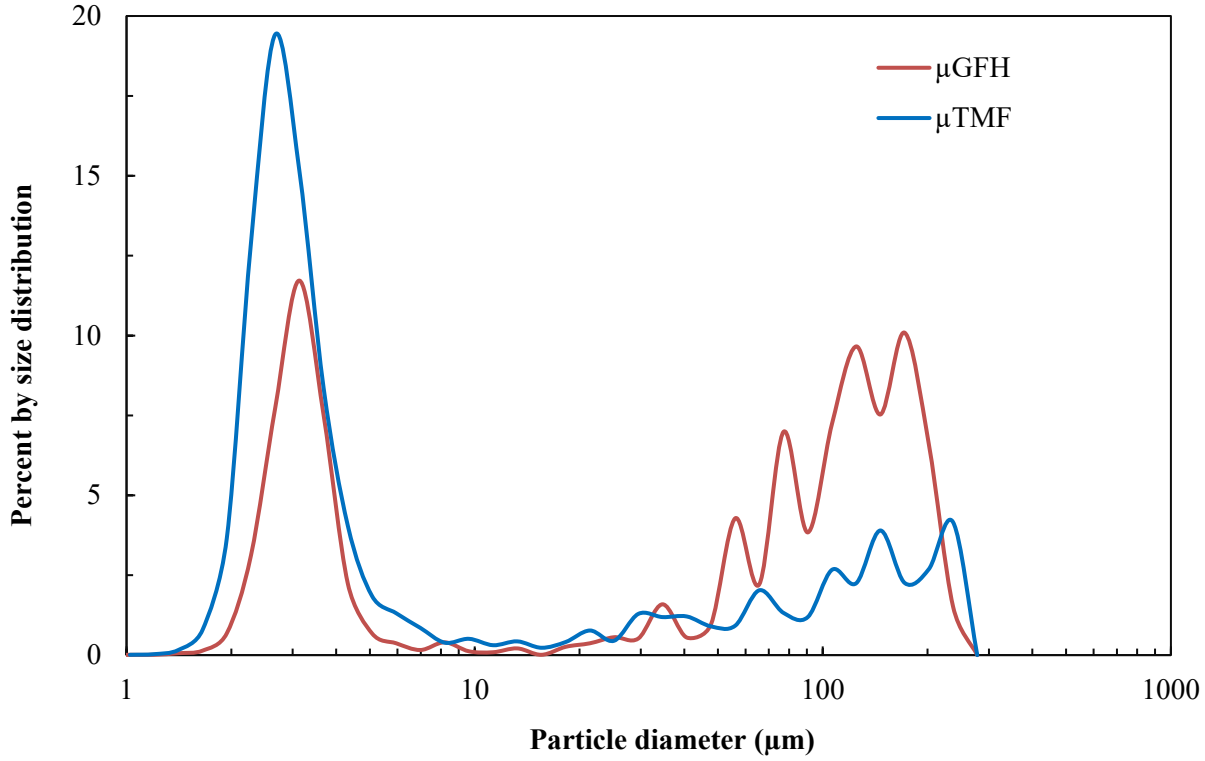

Figure 4.1. Particle size distribution of µGFH and µTMF particles as measured by the EyeTech instrument.

It can be seen from Figure 4.1 that all the particles of µGFH and µTMF range from 1 to less than 250 µm. There is no single grouping of particles in length-based size distribution and many peaks are observed in the size distribution of fine-grained iron oxyhydroxide. However, µGFH and µTMF have one peak at ~3 µm and ~2.5 µm with 12 and 19 % of total particles, respectively. The mean length-based particle size of µGFH and µTMF as determined by the EyeTech instrument is 78.4 and 40 µm, respectively.

4.1.2 Surface characterization of applied iron oxyhydroxides

The surface properties of adsorbent particles were investigated using the Brunauer-Emmett-Teller (BET) method, which allows to determine parameters such as specific surface area, pore volume and mean pore diameter. Because specific surface areas are generally positively correlated with adsorption efficiency, specific surface areas of applied iron oxyhydroxides are first evaluated. Table 4.1 summarizes the physicochemical data derived for both applied adsorbents. The determination of surface morphological characteristics of the applied iron oxyhydroxides shows a specific surface area of 283 ± 3 m^2/g, a pore volume 0.28 mL/g and a mean pore diameter 2.6 nm for µGFH, whereas for µTMF, the specific surface area of 178 ± 8 m^2/g, pore volume 0.35 mL/g and a mean pore diameter 3.4 nm. Since, the mean pore size of applied iron oxyhydroxides ranges between 2 and 50 nm, which is characteristic of the mesoporous materials (Badruzzaman et al. 2004). These results are in agreement with results of Badruzzaman et al. (2004) for GFH, as well with other studies for TMF (Tresintsi et al. 2014b). The large pore size of either adsorbent allows arsenic ions to diffuse into the pore channel of the mesoporous material with relevant convenience, since arsenic ionic radius is significantly small ($H_2AsO_4^-$ = 0.416 nm and $HAsO4_2^-$ =0.397 nm) (Kim et al. 2004). Therefore, it is apparent that arsenic oxyanions will initially be adsorbed onto the surface of the adsorbent and when the exterior surface reached is near to saturation it can diffuse into the pores and bind to the inner surfaces of the adsorbent particles. It is relevant to mention that the pore volume as well as mean pore diameter is negatively correlated with specific surface area of the µGFH and µTMF.

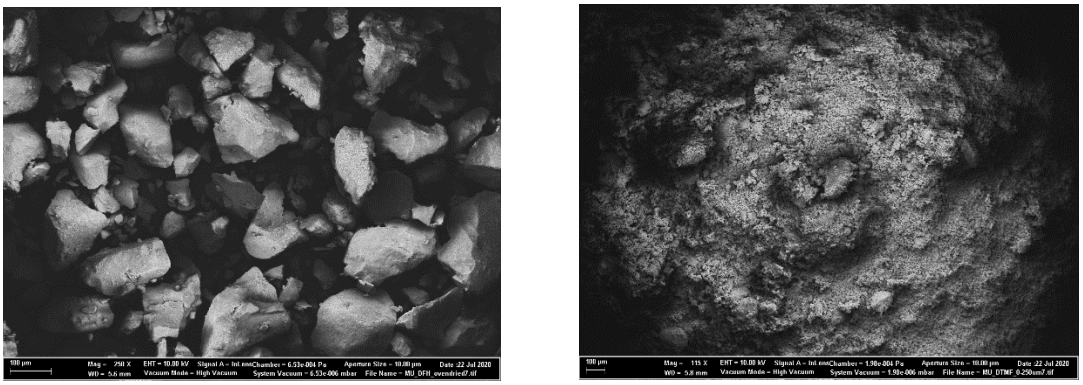

Figure 4.2. SEM images of (left) µGEH and (right) µTMF particles at resolution of 100 µm.

The surface morphology of applied adsorbents was determined by SEM and captured images are shown in Figure 4.2. Both adsorbents have regular distribution. Moreover, the images show that the µTMF has higher quantity of fine particles than µGFH, which is in agreement with the particle size distribution (Figure 4.1).

Table 4.1. Main characteristics of applied fine-grained arsenic adsorbents.

Properties	µGFH	µTMF
Moisture content (%)	~ 50 ± 2	~ 5
Iron (Fe) content (wt %)	59.8	44.5
BET surface area (m^2/g)	283 ± 3	178 ± 8
Pore volume (mL/g)	0.28	0.35
Mean pore diameter (nm)	2.6	3.2
Isoelectric point (pH_{IEP})	8[a]	7.2 ± 0.1[b]

Note: Data from [a] Naeem et al. (2007), [b] Tresintsi et al. (2013b).

As it can be seen in Table 4.1, both iron oxyhydroxides present a quite high Fe content and specific surface area. The specific (BET) surface area of an adsorbent is an important parameter as it determines the number of adsorption energy sites and the accessibility of the contaminant to the adsorbent (Crittenden et al. 2012). The results are comparable to results of other studies. According to Tresintsi et al. (2013b), the determined specific surface area and Fe content of TMF are 187 m^2/g and 38.1 wt%, respectively, while the specific surface area of µGFH reported by Hilbrandt et al. (2018) is 304 ± 5 m^2/g. Both adsorbents have quite high Fe content, which is important regarding their adsorptive capacity since the adsorption of arsenic takes place mainly because of the iron-based adsorption sites. In particular, the adsorption of As(V) is believed to be dominated by (monodentate and bidentate) inner-sphere complexation between media surface groups and adsorbing molecules. These types of surface complexes are restricted to ions such as arsenic that have a high affinity for surface sites and can bind to the media surface through covalent bonding (Essington 2015).

Regarding the specific surface area of the adsorbents, µGFH has a considerably higher BET surface area than µTMF. This might play an important role in the adsorption efficiency of arsenic, acting synergistically to the very high Fe content. Both adsorbents have a pH_{IEP} at values above 7, specifically at 7.2 for µTMF and 8 for µGFH. pH_{IEP} of the solid adsorbents plays a critical role as at solution pH values lower than the pH_{IEP}, the overall surface charge of the adsorbent is positive.

4.2 Arsenic adsorption at varying pH

The solution pH of the aqueous solution is an important variable which controls the adsorption at the water–adsorbent interfaces. Therefore, the adsorption of arsenic onto µGFH and µTMF was examined at different pH-values ranging from 3.5 to 9 and has been graphically presented in Figure 4.3. The plots indicate that the adsorption capacity of µGFH for As(V) depends strongly on the solution pH. It can be seen from Figure 4.3 that As(V) adsorption capacity of the µGFH decreases with increasing pH, and the removal of As(V) is maximum (29.5 µg/mg) at pH 3.5 and is minimum

(6.5 µg/mg) at pH 8.7. For As(III), the adsorption capacity of the µGFH is not a strong function of pH. Similar pattern is obtained for As(III) and As(V) adsorption onto µTMF. In case of As(V), a slight decrease in adsorption capacity at pH values from 3.5 to 6 is observed, however, adsorption capacity diminishes more rapidly as the solution pH increases from 6 to 8.5. This can be attributed both to arsenic speciation and the surface characteristics of the adsorbent. pH_{IEP} of µGFH - the pH at which the solid surface has a net zero charge - is 8 and in highly acidic medium, the surface of adsorbent is highly protonated. With increasing pH, the net surface charge on the adsorbent becomes less positive. At equilibrium pH > pH_{IEP}, the net surface charge becomes negative, resulting in repulsive forces between adsorbent and anionic adsorbate. µGFH with positive surface charge shows greater tendency to adsorb anions.

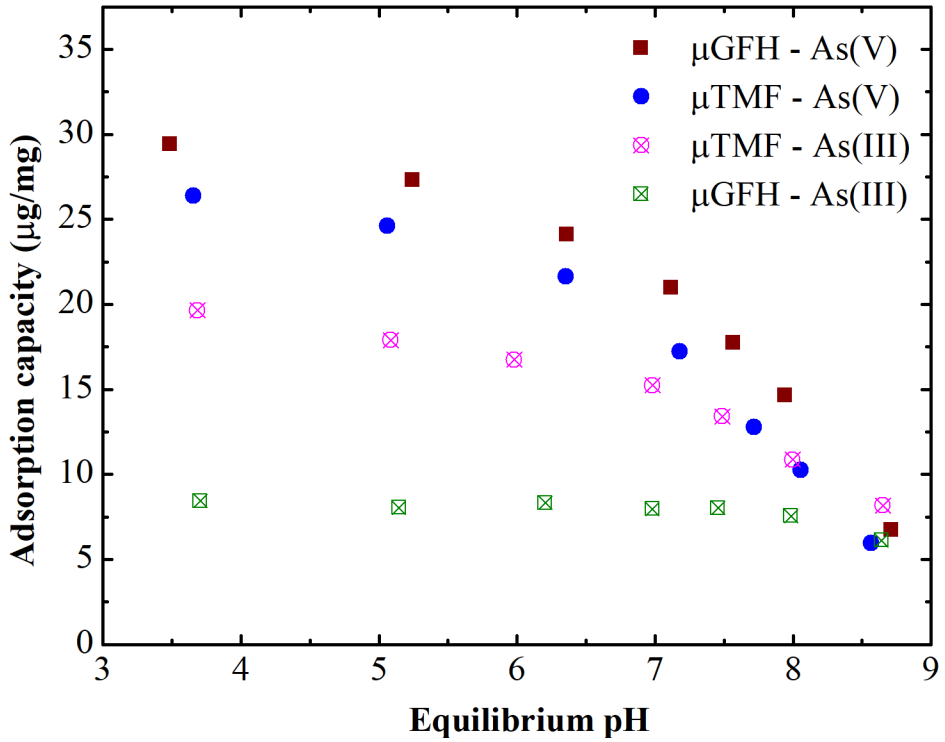

Figure 4.3. Effect of equilibrium pH on arsenic adsorption onto iron oxyhydroxides (n=2). Experimental conditions: Initial arsenic concentration= 190 µg/L in DI water, adsorbent dose= 10 mg/L and T= 20 + 1 °C.

Further, arsenic speciation are strongly influenced by the equilibrium pH. As the pH increases from 5 to 9, a gradual predomination of $HAsO_4^{2-}$ in the equilibrium solution relative to the monovalent $H_2AsO_4^-$, with the former one demanding two active sites to be adsorbed on oxy-hydroxides surface. In addition to that, concentrations of OH^- increases in alkaline solutions, which strongly compete with As(V) for adsorption sites. Different research groups have reported that iron hydroxide-based adsorbents adsorb As(V) mainly via electrostatic (Coulombic interaction) forces as well as ligand exchange reactions (Lewis acid-base interactions) to form monodentate and bidentate inner-sphere complexes (Banerjee et al. 2008; Manning et al. 1998).

In case of As(III) arsenic speciation, it is electrically neural at pH values form 3 to ≈ 9. Therefore, the role of electrostatic interactions is practically insignificant in the adsorption mechanism of the non-ionized As(III) species, which mainly occurs through a Lewis acid-base ligand-exchange reaction preferably onto non-ionized surface functional groups (Manning et al. 1998).

4.3 Adsorption equilibrium isotherms for arsenic adsorption onto µGFH and µTMF

The most widely used isotherm models, the Freundlich, Langmuir and D-R isotherms were adopted to describe the arsenic isotherm experimental data. The goodness-of-fit parameters for each isotherm model include determination of chi-squared value (χ^2, Eq. 4-1) and correlation coefficient to ensure that the chosen model is scientifically sound, robust and acceptable.

According to Tran et al. (2017), a chi-squared value (χ^2) must be taken into account in addition to the calculation of correlation coefficient (R^2) for the non-linear form of the isotherm model. χ^2 indicates the bias in the experimental and model results. Its value is close to zero, if the data obtained using a model is similar to the experimental data, whereas its high value indicates the high bias between the experimental data and the model output.

$$\chi^2 = \sum \left(\frac{Q_{e,exp} - Q_{e,cal}}{Q_{e,cal}} \right)^2 \tag{4-1}$$

Where $Q_{e,exp}$ represents the experimental solid-phase equilibirum concentration, and $Q_{e,cal}$ represents the solid-phase equilibrium concentration predicted by the model. The goodness of fit was evaluated through standardized residuals defined as the ratio of the residuals over the estimated variance and the lack of fit test. The standardized residuals for the regression model used in the isotherms are shown in Figures A.1-A.4. As observed, standardized residuals ranges from -2 to 2 and are randomly distributed around the x-axis. This suggests that predicted values by the model were closed to measured values with not over or under estimation of overall prediction and there is no pattern suggesting an error due to the chosen models. Thus, it is concluded that the chosen models fits reasonably well to the observed values.

The Freundlich and Langmuir isotherms for adsorption of As(V) and As(III) on µGFH and µTMF in DI water are shown in Figures 4.4 and 4.5.

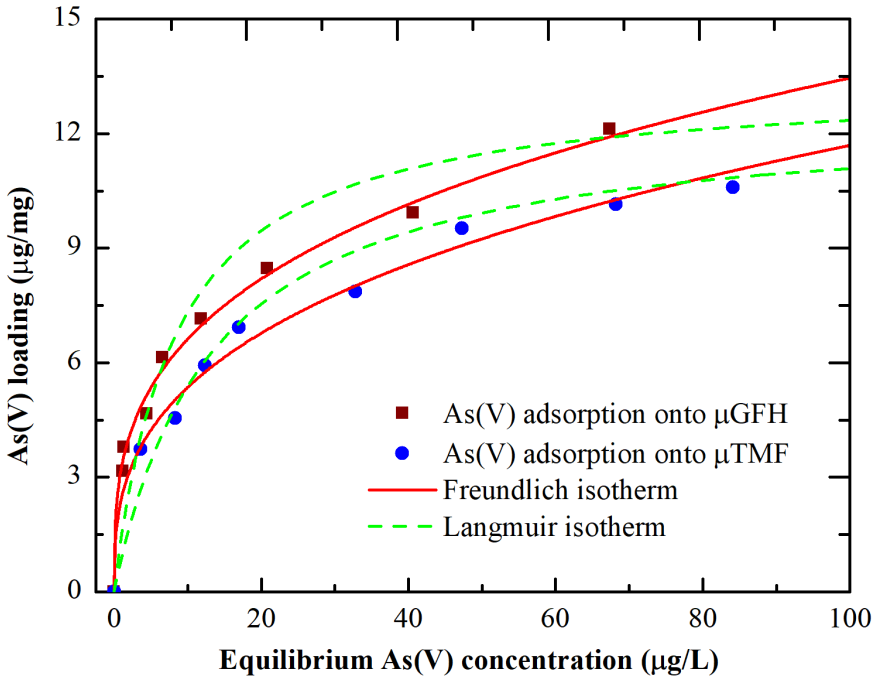

Figure 4.4. Freundlich and Langmuir isotherms for adsorption of As(V) onto µGFH and µTMF at initial As(V) concentration= 190 µg/L in DI water and pH 8 (n=2).

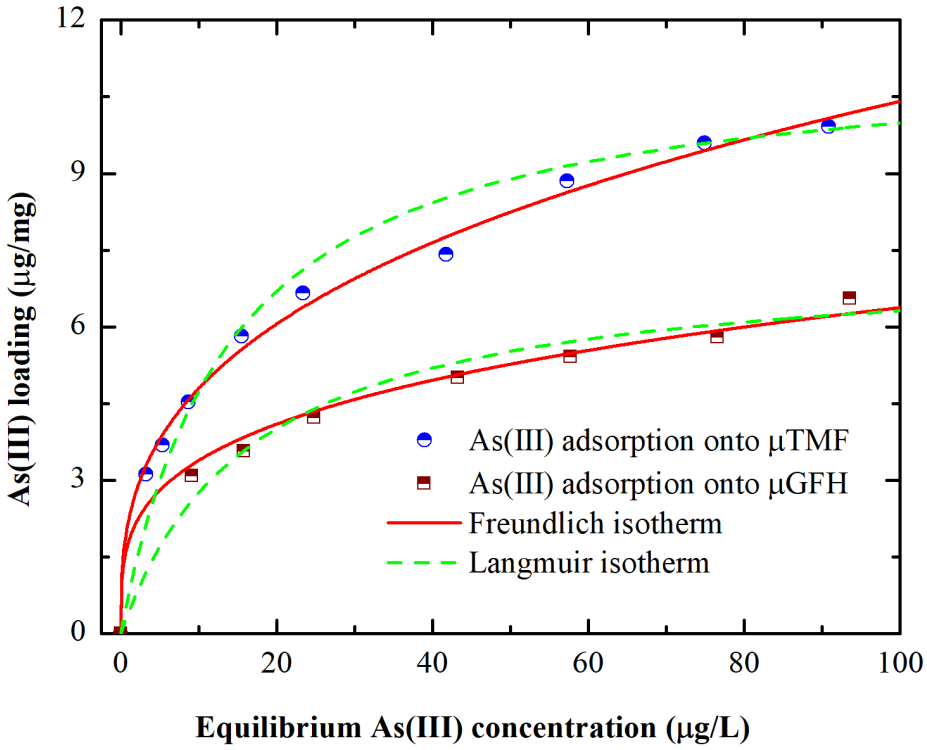

Figure 4.5. Freundlich and Langmuir isotherms for adsorption of As(III) onto µGFH and µTMF at initial As(III) concentration= 190 µg/L in DI water and pH 8 (n=2).

The major parameters of the Freundlich and Langmuir at 20 °C and pH 8 in the case of As(V) and As(III) species, along with the correlation coefficients and the respective chi-squared values, are summarized in Table 4.2. The correlation coefficients and the chi-squared values indicated that the Freundlich model describes the isothermal adsorption behavior of arsenic species notably well. The Q_{10} value is calculated by the Freundlich isotherm model, setting K_F and n values at the equilibrium arsenic liquid phase concentration of 10 µg/L.

Table 4.2. Key parameters of adsorption isotherms along with the correlation coefficients and the respective chi-squared values.

Freundlich isotherm model						
Adsorbent media	Arsenic specie	K_F (µg/mg) $(L/\mu g)^n$	n	Q_{10} (µg/mg) at C_e = 10 µg/L	R^2	Chi-squared ($\chi^{2)}$
µGFH	As(V)	3.3	0.30	6.9	0.995	0.085
µGFH	As(III)	1.8	0.27	3.5	0.992	0.032
µTMF	As(V)	2.5	0.35	5.5	0.992	0.108
µTMF	As(III)	2.2	0.34	4.8	0.995	0.047
Langmuir isotherm model						
Adsorbent media	Arsenic species	b (L/mg)	Q_{max} (µg/mg)	R_L (-)	R^2	Chi-squared
µGFH	As(V)	0.120	13.4	4×10^{-5}	0.922	1.45
µGFH	As(III)	0.059	7.4	8×10^{-5}	0.975	0.108
µTMF	As(V)	0.075	12.6	7×10^{-5}	0.954	0.645
µTMF	As(III)	0.071	11.4	7×10^{-5}	0.961	0.453

The R^2 of the Freundlich isotherm model is greater than 0.98 and χ^2 is less than 1 for arsenic adsorption, whereas the R^2 of the Langmuir isotherm is greater than 0.92, but χ^2 values are close to 1, respectively for µGFH. Therefore, the Freundlich isotherm fits better than the Langmuir isotherm for As(V) and As(III) adsorption onto two different applied iron oxyhydroxides. Similar observations were made in the past during adsorption of As(V) onto small fractions of GFH with

R^2 of greater than 0.92 (Badruzzaman et al. 2004) and As(III) and As(V) adsorption onto TMF (Tresintsi et al. 2013b).

Moreover, the Freundlich energy intensity constant (n) and Langmuir constant related to energy of adsorption can be used to determine the adsorption efficiency of applied fine-grained iron oxyhydroxides towards arsenic. As the value of n is less than 1, and R_L value, calculated using Eq. 2-12, is between 0 and 1. The values of these two constant indicate arsenic adsorption onto two applied fine-grained iron oxyhydroxides is favorable. Therefore, it can be concluded that the applied iron oxyhydroxides exhibit greater affinity towards As(V) and As(III) adsorption.

Using the values of Langmuir energy constant (b) as summarized in Table 4.2, it is possible to calculate the Gibbs free energy (ΔG^o) using the following expression (Saldaña-Robles et al. 2017):

$$\Delta G^o = R\ T\ \ln(\frac{1}{b}) \tag{4-2}$$

where R denotes the universal gas constant and its value is 8.314 J mol^{-1} K^{-1}, and T is the absolute temperature. The negative values of ΔG^o for As(V) adsorption onto µGFH (-11.7 kJ mol^{-1}) and µTMF (-10.5 kJ mol^{-1}) have been calculated, which indicates the arsenic adsorption onto applied iron oxyhydroxides is spontaneous and exothermic. Similar results were reported during adsorption of As(V) onto GFH at 25 °C and pH 7.4 in single solute system (Saldaña-Robles et al. 2017). It is generally believed that the adsorption is exothermic. When the adsorbate accumulates onto the surface of the adsorbent, this leads to a decrease in the residual forces on the surface of the adsorbent. This causes a decrease in the surface energy of the adsorbent and therefore, adsorption process is exothermic. The negative values of ΔG^o are also calculated for the case of As(III) adsorption onto µGFH and µTMF.

Comparing the adsorption capacity (Q_{10}) of fine-grained iron oxyhydroxides for As(V), the calculated Q_{10} value for µGFH is 6.9 µg/mg compared to 5.5 µg/mg for µTMF. The higher calculated Q_{10} value is mostly likely linked to large specific surface area, large pH_{IEP} and Fe content of µGFH. It is concluded that specific surface area along with pH_{IEP} and iron content play notable role in the adsorptive removal of As(V) by iron oxyhydroxide-based adsorbents.

When the Q_{10} values for As(III) adsorption onto µGFH and µTMF are compared, µTMF exhibit much higher adsorption efficiency towards As(III) despite fact that it has lower pH_{IEP}, specific surface area and Fe content. µTMF is an iron oxyhydroxide-based adsorbent in which Mn(IV) is homogeneously distributed into the crystal structure (Tresintsi et al. 2013b), whereas µGFH is a single iron oxyhydroxide-based adsorbent. The primary benefit of Mn(IV) in µTMF that it combines the oxidation property of Mn and increases removal capacity for this species by simulation of Fe(III)-Mn(IV) binary adsorbent. As reported by Gude et al. (2017), MnO_2 is the electron acceptor for As(III) oxidation, resulting in the reduction of MnO_2 to Mn(II). The reduction of MnO_2 by As(III) entails a two-step reaction where both the initial MnO_2 and the intermediate product, MnOOH, can oxidize As(III).

$$2MnO_2 + H_3AsO_3 + H_2O = 2MnOOH^* + H_3AsO_4 \tag{4-3}$$

$$2MnOOH^{*} + H_3AsO_4 + 4H^{+} = 2Mn^{2+} + H_3AsO_4 + 3H_2O \quad (4\text{-}4)$$

Because of oxidizing mediation of Mn(IV), µTMF has shown an enhanced As(III) adsorption in comparison to µGFH. The Q_{10} values for µTMF and µGFH are 4.8 µg/mg and 3.5 µg/mg respectively (Table 4.2). Enhanced As(III) adsorption by Mn(II)/Mn(IV) modified forms of iron (oxy)hydroxide adsorbents was reported in the past by different research groups (Huang et al. 2011; Zhang et al. 2007; Zhang et al. 2009). Based on these results, it can be concluded that the high uptake capability of the µTMF, a Fe(III)–Mn(IV) composite adsorbent makes it potentially attractive material for applications in water treatment for the adsorptive removal of As(III).

Comparing the adsorption capacities of µGFH and µTMF for As(III) and As(V) obtained in the present study with those included in Table 4.3.

Table 4.3. Adsorption capacities of some adsorbents reported in literature (pH is shown in parenthesis where reported).

Adsorbent media	Particle fraction (µm)	Initial arsenic concentration (µg/L)	Q_{10} (µg/mg) at C_e = 10 µg/L		Data source
			As(III)	As(V)	
GFH	500 – 1000	800	-	4.3 (7.4)	Saldaña-Robles et al. (2017)
GFH	105 – 250	100	-	8.5 (7)	Badruzzaman et al. (2004)
GFH	320 - 2000	100	-	1.1 (6.5)	Banerjee et al. (2008)
µGFH	1 – 250	190	3.5 (8)	6.9 (8)	This work
µTMF	1 – 250	190	4.8 (8)	5.5 (8)	This work
µTMF	1 – 63	200 - 2000	10.9 (8)	10.3 (8)	Tresintsi et al. (2013b)

Table 4.3 exhibits differences in Q_{10} values for GFH even though it is a commercial adsorbent media and has constant BET surface area of ~ 300 m^2/g. The adsorption capacities in a similar magnitude are generally expected at equilibrium for different grain sizes of adsorbent media. Saldaña-Robles et al. (2017) obtained Q_{10} value for GFH is lower than this study after an equilibration time of 1 day, even though the former study was conducted at lower pH. This divergence in results might be attributed to the fact that equilibrium for As(V) onto GFH was not fully reached after a contact time of 1 day due to large-sized grains of GFH. This was shown by Westerhoff et al. (2005) where equilibrium was not fully accomplished for GFH (grain size: 600 - 2000 µm) even after 7 days of contact time. Another study with equilibrium time of 1 day at pH 6.5 reported Q_{10} value lower than the Q_{10} value report in this work (Banerjee et al. 2008)

The work of Badruzzaman et al. (2004) reported a Q_{10} value of 8.5 µg As(V)/mg for GFH (grain size: 1 – 250 µm) during As(V) adsorption at the equilibrium pH value of 7 and 24 ± 0.5 °C after 18 days of contact time. The calculated Q_{10} value is higher than the recorded Q_{10} value in the current study. The divergence in Q_{10} value between the current study and Badruzzaman et al.

(2004) could be ascribed to the differences of experimental conditions (equilibrium pH value, temperature, water matrix and longer contact time). At pH 7, As(V) is present as an oxyanion in the form of $H_2AsO_4^-$, while it transforms into $HAsO_4^{2-}$ at pH 8. The latter requires two active adsorption sites to be adsorbed on the absorbent surface. In addition, Badruzzaman et al. (2004) used bicarbonate as a pH buffer. In the current study, BES was used as a pH buffer to facilitate the required constant pH condition, since no influence on arsenic adsorption was observed, which is in agreement with the results reported by Banerjee et al. (2003). These results can be considered to be in agreement, since the observed small differences are considered negligible and could be attributed to the respective difference in the initial material used.

It is known that either the Langmuir or the Freundlich isotherm constants can insignificantly contribute to elucidating adsorption mechanisms, they are less helpful in this regard than data on adsorption kinetics (Mahramanlioglu et al. 2002) . To understand the adsorption type, equilibrium data was tested with the D-R isotherm. The D-R isotherm plot for adsorption of arsenic is presented in Figure 4.6.

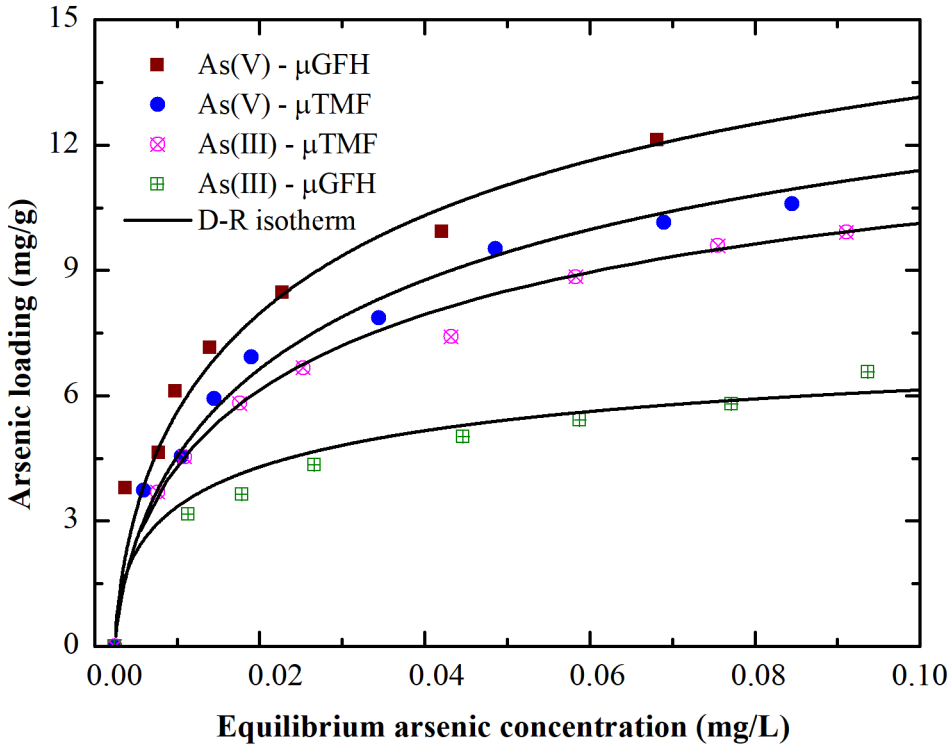

Figure 4.6. Dubinin-Radushkevich (D-R) isotherm for adsorption of As(V) and As(III) onto applied iron oxyhydroxides at initial arsenic concentration= 190 µg/L in DI water and pH 8 (n=2).

The calculated adsorption capacities (Q_{DR}) by the D-R isotherm for As(V) adsorption onto µGFH and µTMF are 18.2 and 15.3 µg/mg respectively, whereas the Q_{DR} values in case of As(III) adsorption are 7.5 and 13.3 µg/mg for µGFH and µTMF respectively. The energy of adsorption (E) is defined as the free energy change when 1 mol of the arsenic ion is transferred from infinity in the solution to the surface of the iron oxyhydroxide material. The E values are calculated by Eq.

2-14. Table 4.4 shows the E values of 7.9 and 7.6 kJ/mol for As(V) adsorption onto µGFH and µTMF respectively. It is known that magnitude of E is useful for estimating the type of adsorption and if this value is between 8 and 16 kJ/mol, the adsorption type is chemisorption and the E value of less than 8 kJ/mol suggest that predominant adsorption mechanism is physical in nature (weak van der Waals forces). The value of E found in this study is within the energy range of chemical adsorption for As(V) and As(III) onto µGFH and µTMF. It can be concluded that predominant adsorption mechanism is chemical adsorption in case of arsenic adsorption onto fine-grained iron oxyhydroxides.

Table 4.4. Key parameters of the Dubinin-Radushkevich (D-R) isotherm for arsenic adsorption at initial arsenic concentration = 190 µg/L in DI water and pH 8.

Adsorbent media	Arsenic specie	Q_{DR} (µg/mg)	E (kJ/mol)	R^2	Chi-squared (χ^2)
µGFH	As(V)	18.2	8.2	0.995	0.085
µGFH	As(III)	8.2	8.6	0.981	0.138
µTMF	As(V)	15.3	8.4	0.992	0.108
µTMF	As(III)	13.3	8.9	0.987	0.047

4.4 Effect of water matrix on arsenic adsorption

Batch adsorption tests were also conducted in HH tap water and NSF water to assess the real and practical adsorption potential for removing As(III) and As(V) from drinking water. The adsorption isotherms for As(V) and As(III) onto µGFH and µTMF at 20 °C and at the equilibrium pH value of 8 ± 0.1 in three different water matrixes are presented in Figures 4.7 and 4.8.

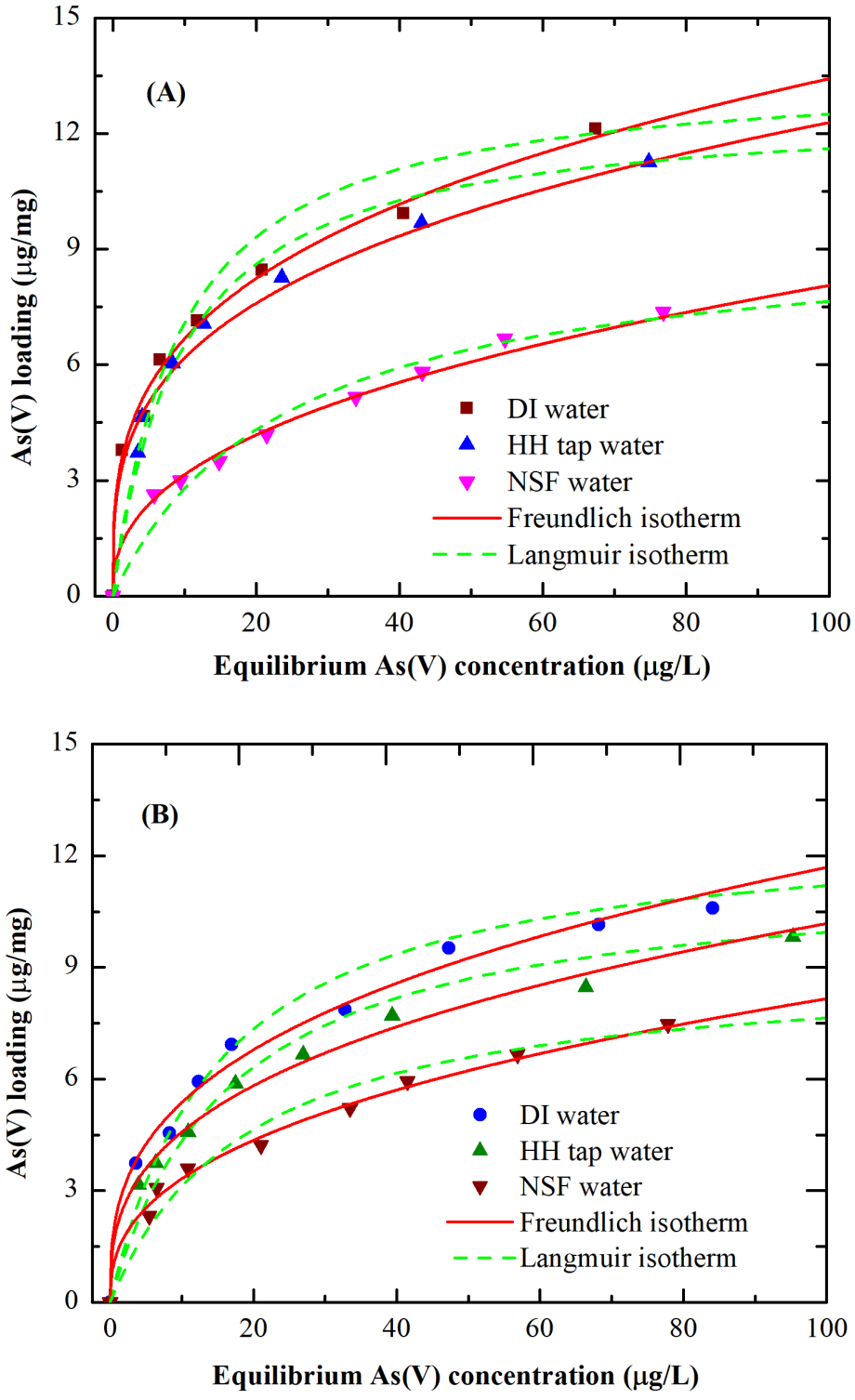

Figure 4.7. Freundlich and Langmuir isotherms for As(V) adsorption isotherms of **(A)** µGFH; **(B)** µTMF in three different water matrices (n=2). Solid lines represent the Freundlich isotherm, whereas dashed lines represent the Langmuir isotherm. Experimental conditions: Initial As(V)= 190 µg/L, equilibrium pH value= 8 and T= 20 °C.

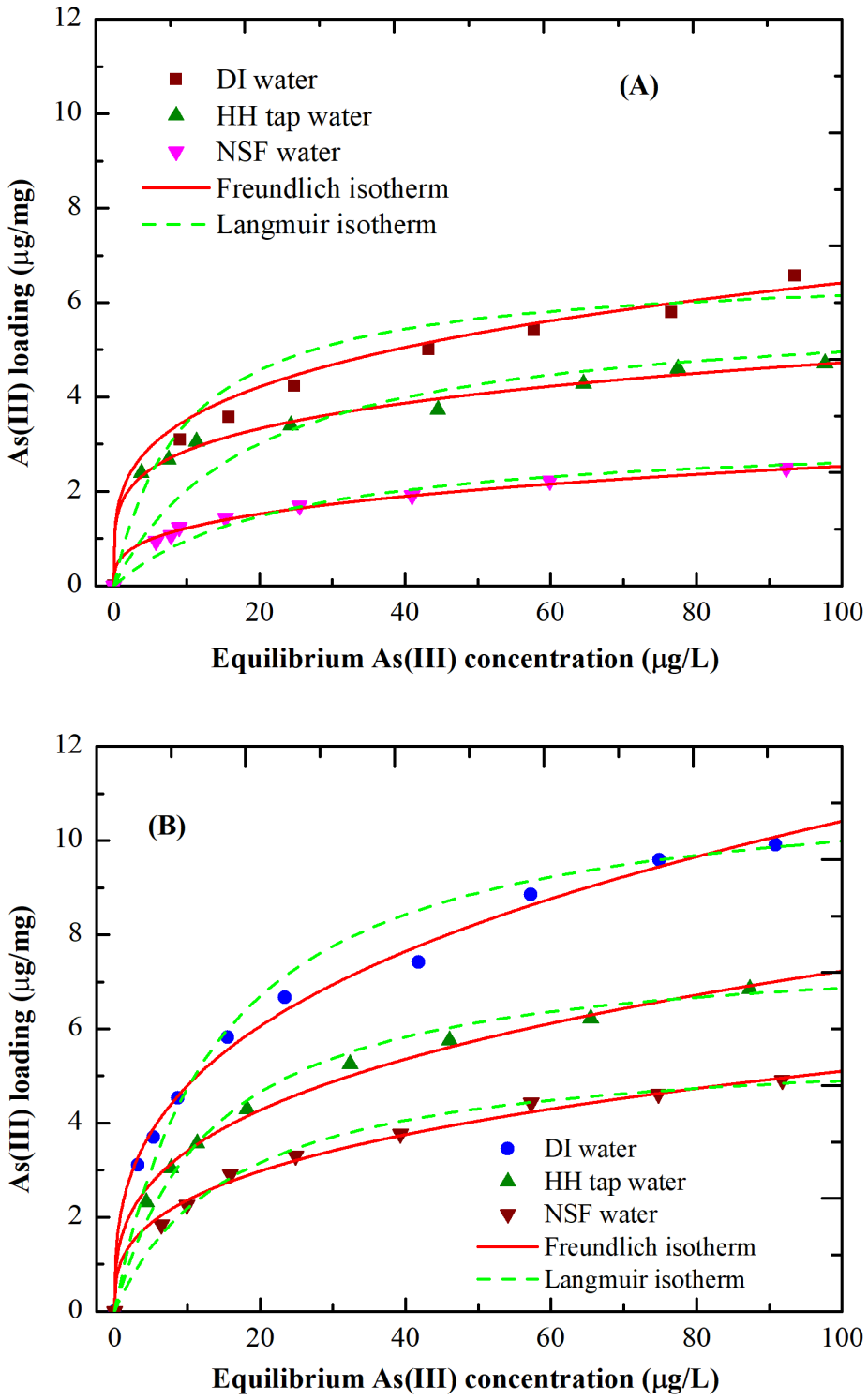

Figure 4.8. Freundlich and Langmuir isotherms for As(III) adsorption onto **(A)** µGFH; **(B)** µTMF in three different water matrices (n=2). Solid lines represent the Freundlich isotherm, whereas dashed lines represent the Langmuir isotherm. Experimental conditions: Initial As(III)= 190 µg/L, equilibrium pH value= 8 and T= 20 °C.

The key parameters of the Freundlich and Langmuir isotherms for adsorption of As(V) and As(III) on µGFH and µTMF along with the values of Q_{10}, R^2 and Chi-squared (χ^2) are summarized in Tables 4.5 and 4.6.

Table 4.5. Key parameters of the Freundlich isotherm along with the correlation coefficients and the respective chi-squared values.

Adsorbent media	Arsenic specie	Water matrix	K_F (µg/mg) $(L/\mu g)^n$	n	Q_{10} (µg/mg) at C_e = 10 µg/L	R^2	Chi-squared ($\chi^{2)}$
µGFH	As(V)	DI water	3.3	0.30	6.9	0.995	0.085
		HH tap water	3.1	0.31	6.3	0.990	0.148
		NSF water	1.2	0.40	3.2	0.993	0.038
µGFH	As(III)	DI water	1.8	0.27	3.5	0.992	0.032
		HH tap water	1.7	0.22	2.8	0.994	0.012
		NSF water	0.6	0.32	1.2	0.982	0.009
µTMF	As(V)	DI water	2.5	0.35	5.5	0.992	0.108
		HH tap water	2.1	0.35	4.6	0.995	0.064
		NSF water	1.4	0.39	3.3	0.994	0.038
µTMF	As(III)	DI water	2.2	0.34	4.8	0.995	0.047
		HH tap water	1.8	0.30	3.6	0.991	0.043
		NSF water	1.1	0.33	2.3	0.994	0.017

The As(V) adsorption capacity of µGFH and µTMF in HH tap water and in NSF water has been decreased as compared to in DI water over the entire range of equilibrium As(V) concentrations (Figures 4.7 and 4.8), the decrease of the adsorption capacity was found to be more significant in the case of NSF water. For example, the calculated Q_{10} value for As(V) adsorption onto µGFH in HH tap water and NSF water is 6.3 µg As(V)/mg and 3.2 µg As(V)/mg, respectively. Due to the presence of different competing interfering ions such as phosphate and silicate, a reduction of 8 % and 54 % in the Q_{10} values for As(V) was observed regarding in cases of HH tap water and NSF water, respectively. Similar trend in the Q10 values has been recorded for As(V) adsorption onto

µTMF in HH tap water and NSF water. However, a reduction of 40 % was calculated for As(V) adsorption onto µTMF, 14 % lower reduction in the Q_{10} value than µGFH.

Table 4.6. Key parameters of the Langmuir isotherm along with the correlation coefficients and the respective chi-squared values.

Adsorbent media	Arsenic specie	Water matrix	b (L/mg)	Q_{max} (µg/mg)	R_L (-)	R^2	Chi-squared
µGFH	As(V)	DI water	0.120	13.4	4×10^{-5}	0.922	1.45
		HH tap water	0.104	12.7	5×10^{-5}	0.973	0.415
		NSF water	0.048	9.1	0.1×10^{-5}	0.958	0.245
µGFH	As(III)	DI water	0.059	7.4	8×10^{-5}	0.975	0.108
		HH tap water	0.052	5.9	0.5×10^{-5}	0.793	0.451
		NSF water	0.042	3.2	0.1×10^{-5}	0.936	0.039
µTMF	As(V)	DI water	0.075	12.6	7×10^{-5}	0.954	0.645
		HH tap water	0.060	11.6	9×10^{-5}	0.963	0.430
		NSF water	0.052	9.1	0.1×10^{-5}	0.965	0.222
µTMF	As(III)	DI water	0.071	11.4	7×10^{-5}	0.961	0.453
		HH tap water	0.077	7.7	7×10^{-5}	0.977	0.076
		NSF water	0.062	5.7	8×10^{-5}	0.981	0.076

In the case of As(III) adsorption onto µGFH, the calculated Q_{10} value of 3.5 µg/mg in DI water has been reduced to 2.8 and 1.1 µg/mg in HH tap water and in NSF water, respectively. A reduction of 66 % in the Q_{10} value was calculated for As(III) adsorption onto µGFH in NSF water, which indicates a much stronger water matrix effect onto As(III) adsorption compared to As(V) adsorption onto µGFH (54 % reduction in NSF water). A similar trend in reduction in the Q_{10} values for µTMF can be seen in Table 4.5. The observed reduction in the Q_{10} values for HH tap water and NSF water can be attributed to As(III) speciation, because As(III) is electrically neutral at the set pH value of 8, resulting in nearly negligible electrostatic attraction, while the co-presence of their anions may have significant electrostatic attraction with the charged surface of µGFH. Therefore, reductions of 19 % and 66 % were recorded in the Q_{10} values for As(III) in HH tap

water and NSF water, respectively, indicating also that in NSF water, the concentration of competing and interfering ions is higher, as compared with HH tap water.

Especially, the presence of phosphates and silicates showed the most adverse effect on the arsenic adsorption capacity of iron oxide-based adsorbents (Genz et al. 2004; Nguyen et al. 2011). At pH 8.2, GFH has a strong affinity with phosphate, existing as HPO_4^{2-} (Genz et al. 2004) and therefore, strongly competes with arsenic species for similar adsorption sites. Amy (2005) reported a reduction of 3 % in the As(V) adsorption capacity of GFH in the presence of only 125 µg/L phosphate at pH 8 during batch tests. However, the reduction of the Q_{10} value increased to 36 % when the phosphate concentration was increased to 250 µg/L. In the case of silica competition under the same experimental conditions, Amy (2005) recorded a reduction of 25 % and 60 % in the Q_{10} values for As(V) when silica was present with 13.5 and 22 mg/L concentrations, respectively. Similar impact of co-anions has been reported elsewhere during the arsenic adsorption onto TMF in batch adsorption tests at the equilibrium pH of 8, the measured Q_{10} values of 10.3 µg As(V)/mg and 10.9 µg As(III)/mg in DI water were reduced to 5.4 µg As(V)/mg and 4.6 µg As(III)/mg in the case of NSF water, resulting in reductions of 48 % and 58 % for As(V) and As(III), respectively (Tresintsi et al. 2013b). In the case of arsenic adsorption onto Bayoxide in NSF water, reductions of 54.6 % and 96.9 % at the equilibrium pH of 7.5 has been observed for As(V) and As(III), respectively (Amy 2005). Silicate also presents strong competition with arsenic species for similar adsorption sites because it exists as $H_3SiO_4^-$ at pH 8, which requires one active site for adsorption (Tresintsi et al. 2012).

4.5 Regeneration of spent fine-grained iron oxyhydroxides

Figure 4.9 shows the influence of concentration of NaOH solution on As(V) desorption efficiency as a function of contact time.

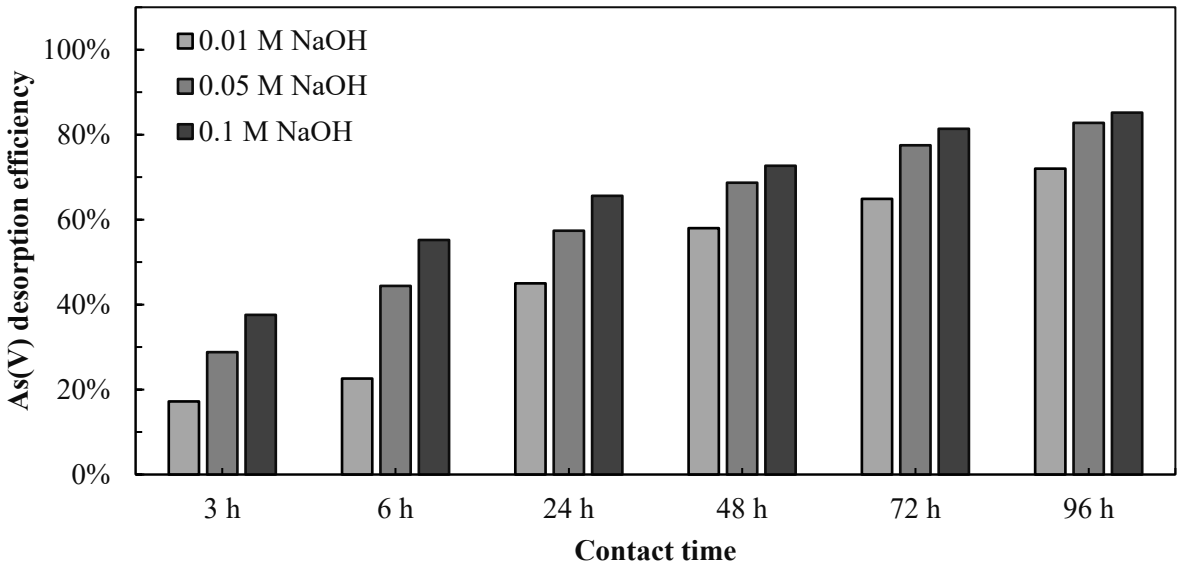

Figure 4.9. As(V) desorption from spent µGFH as a function of contact time at three different NaOH concentrations (n=2).

The experimental result shows that that NaOH concentrations of 0.05 and 0.1 M can effectively restore adsorption capacity of µGFH with a contact time of 96 h. However, the achieved desorption capacity using 0.01 M NaoH solution, which results in a pH range 11.9–12, at the end of 96 h contact time is 90 %. Figure 4.9 also exhibits the influence of contact time on As(V) desorption efficiency. The experimental result shows that 0.1 M of NaOH solution shows rapid desorption rates followed by 0.05 M and 0.01 M NaOH solutions, respectively. µTMF also exhibit the similar pattern As(V) desorption at different NaOH concentrations (Figure 4.10).

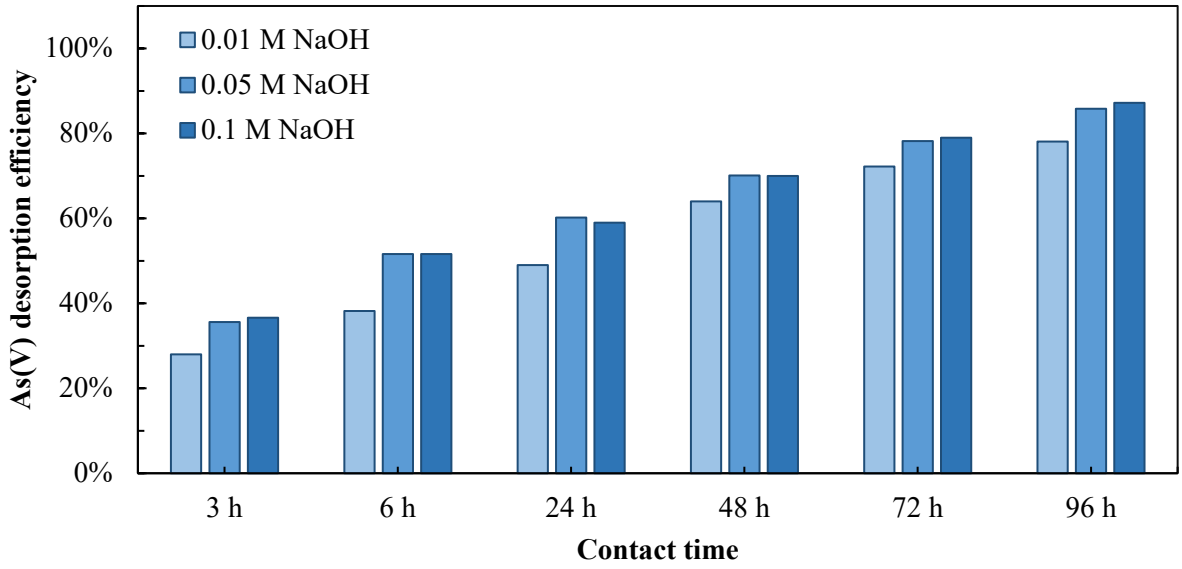

Figure 4.10. As(V) desorption from spent µTMF as a function of contact time at three different NaOH concentrations (n=2).

At higher (0.1M) NaOH concentrations/higher pH values (12.7 -13), 86 % desorption of adsorbed As(V) was observed. However, at higher pH values, disintegration of iron oxyhydroxides might lead to a major decrease in its mechanical strength, which is required for reuse of regenerated adsorbent (Tresintsi et al. 2014a). On the contrary, As(V) desorption has been significantly decreased at lower NaOH concentration (0.01 M), implying both longer regeneration time and lower desorption efficiency. 0.05 M NaOH solution was chosen in this work as the optimal conditions for continuous mode experiments using slurry-bed reactor in a SMAHS as dilute NaOH solution is more suitable and cost-effective in real arsenic treatment systems.

5 Application of fine-grained iron oxyhydroxide-based adsorbents in submerged membrane adsorption hybrid system

This chapter investigates the effect of contact time on As(V) adsorption from NSF water matrix by µGFH and µTMF in batch slurry reactor setup (Chapter 5.1). Moreover, in this chapter, the use of fine-grained fractions of applied iron oxyhydroxides was investigated and its application was proposed in an integrated water treatment concept (SMAHS) combing arsenic adsorption onto fine-grained adsorbents and submerged MF unit (Chapter 5.2). It is expected that the SMAHS could reduce the overall costs of treatment by using low-cost adsorbents such as µGFH and µTMF. The adsorbent efficiency was assessed in terms of volume of treated water until 10 µg As(V)/L (EU drinking water directives, US environmental protection agency (EPA) and world health organization (WHO) guideline value) was reached as well as the amount of arsenic adsorbed per unit mass of adsorbent. Further, two contact times of 3 h and 6 h were considered to investigate more insights into arsenic adsorption.

Selected contents of this chapter have been published in collaboration with Ioannis A. Katsoyiannis and M. Ernst: Environmental Science and Pollution Research 2020. Usman et al. (2020a): https://doi.org/10.1007/s11356-020-08327-w

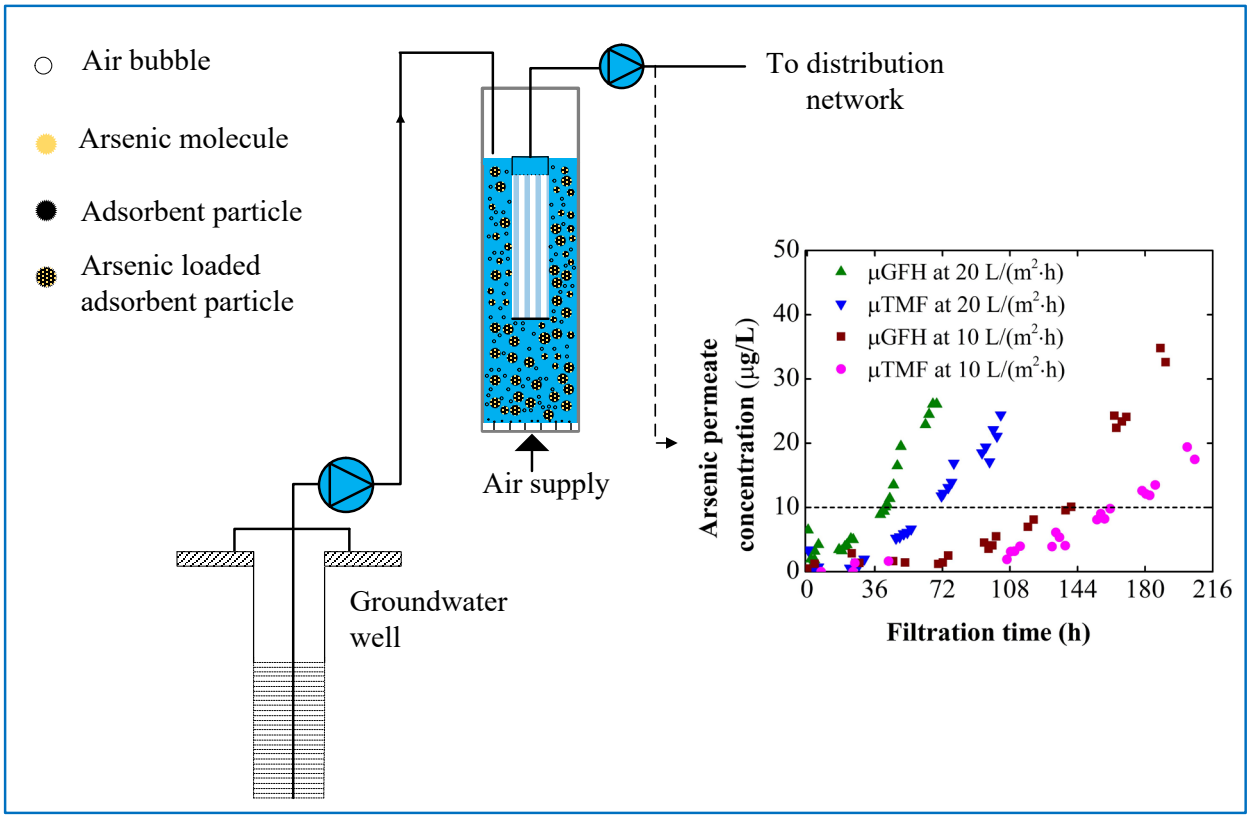

5.1 Effect of contact time

Batch adsorption kinetics experiments are conducted in NSF water to study the effect of contact time on the rate of adsorption of As(V) onto adsorbent media (Figure 5.1). The adsorption kinetic plots exhibit that initial rate of As(V) adsorption onto both adsorbents is rapid and removal rate increases with increasing contact time. At the end of the experiment (contact time of 6 h), about 95% of the As(V) was adsorbed onto µTMF relative to µGFH (93%). Due to the large concentration gradient between the bulk solution and media surface, the rapid initial removal rate of As(V) has been observed. This can be seen in Figure 5.1 that about 70-80% of As(V) is adsorbed within the first 1 h of contact and only 20-30% additional As(V) adsorption has occurred in the following 5 h. Banerjee et al. (2008) reported that similar pattern during adsorption of As(V) onto GFH (with particle sizes between 0.32 and 2 mm) in ultrapure deionized water, but at a much lower initial arsenic to media ratio of 0.4 µg As(V)/mg GFH. In the present study, initial arsenic to media ratio is 1.9 µg As(V)/mg. It can be concluded that small size of µGFH favors faster removal rate of As(V) compared to GFH even though the liquid/mass is high in this work.

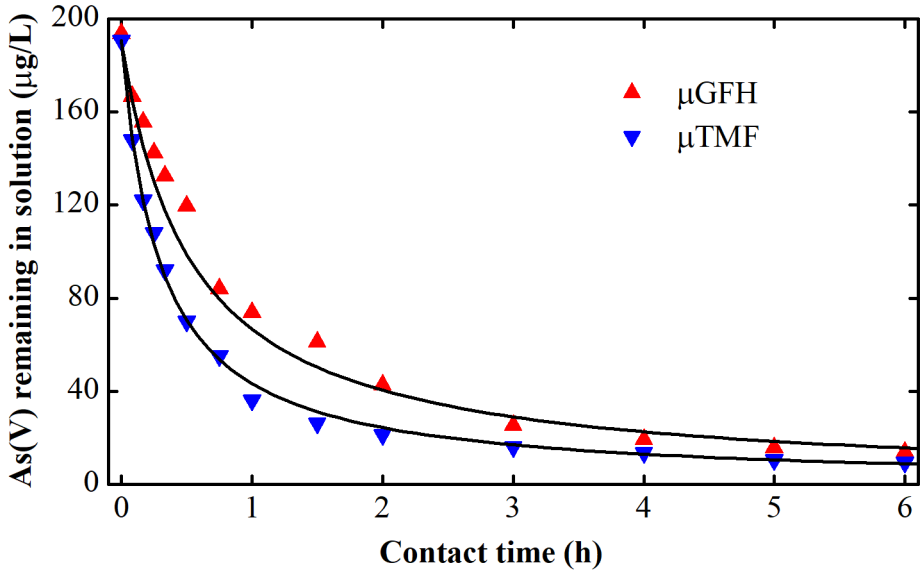

Figure 5.1. Effect of contact time on As(V) adsorption rate onto adsorbents in NSF water (n=2). Solid lines represent the fitting using second-order adsorption kinetic model. Experimental conditions: Adsorbent dosage = 100 mg/L, initial As(V)= 190 µg/L, pH = 8 ± 0.1 and T = 20 °C, residual As(V) concentration for µTMF and µGFH is 9.5 and 13.8 µg/L, respectively.

First- and second-order adsorption kinetic models are considered to analyze the removal rates of As(V) from aqueous solution. The first order model implicate that the adsorption rate is proportional to the concentration gradient, whereas the second order model indicates that the adsorption rate is proportional to the square of the concentration gradient. The linear forms of the first- and second-order kinetic models are expressed by Eqs. 2-29 and 2-30.

The second-order kinetic model shows better fit to the kinetic data of As(V) adsorption onto iron oxyhydroxides as indicated by the higher correlation coefficient (R^2) values in Table 5.1.

Table 5.1. The first and second-order rate constants (k_1 & k_2) for the two adsorbents with different contact times.

Media	First-order kinetic equation for				Second-order kinetic equation for			
	contact time (≤3 h)		contact time (≤ 6 h)		contact time (≤ 3 h)		contact time (≤ 6 h)	
	k_1 (L/mg·h)	R^2	k_1 (L/(mg·h))	R^2	k_2 (L/mg·h)	R^2	k_2 (L/mg·h))	R^2
µGFH	1.06	0.68	0.53	0.86	0.010	0.95	0.014	0.99
µTMF	0.74	0.95	0.65	0.50	0.020	0.99	0.018	0.99

The calculated k_2 values for the initial contact time of ≤ 3 h for µTMF and µGFH are 0.02 and 0.01 L/(mg·h), respectively (Table 5.1). The higher value of k_2 for µTMF indicates the faster adsorption rate. This shows that As(V) removal occurred more rapidly with the µTMF which has a smaller mean particle size (40 µm). Similarly, after a contact time of 6 h, µTMF removes 22 % more arsenic within this time compared to µGFH.

5.2 As(V) removal using submerged membrane adsorption hybrid system

The influence of various operating conditions on slurry reactor combining adsorption onto adsorbent media and a submerged MF membrane has been studied. In this unit, the added adsorbent media is used to remove pollutants, e.g., As(V) which is present in the source water and at a second step, the submerged membrane functions as a complete barrier to arsenic loaded media particles. In the following section, the influence of several operational parameters has been studied, in order to define the optimum conditions for efficient operation of the hybrid treatment system.

5.2.1 Hydrodynamic conditions / Influence of air bubbling rate

The influence of bubbling on the adsorption process has been studied at bubbling rates 1.2, 2 and 3 $L_{air}/(min \cdot L_{slurry})$. Air is transported from an air cylinder by PVC tubing to a ceramic bubble diffuser to generate fine air bubbles in the slurry-bed reactor to create CSTR conditions.

The adsorption process normally follows four consecutive steps (Jia et al. 2009a): (1) external diffusion from bulk solution to liquid film; (2) diffusion in the liquid film surrounding the particle surface; (3) surface diffusion along the adsorbent inner surface; (4) adsorption of pollutant onto the active sites in the micropores. Among these four steps, the air bubbling rate will have an effect on the first two steps. Jia et al. (2009a) reported during adsorption of Atrazine on PAC that mass transfer in the liquid film surrounding the adsorbent particle is very sensitive to air bubbling rate and therefore, optimum air bubbling rate should be achieved for better removal of pollutant via adsorption in slurry-bed reactor.

Figure 5.2 shows that at all three air bubbling rates, As(V) removal efficiency of about 80 % was achieved after approximately 5 min. At air bubbling rates of 2 and 3 $L_{air}/(min \cdot L_{slurry})$, an increase in the As(V) concentration with time was slow and As(V) removal efficiency of over 70 % was achieved in a 6 h long continuous flow experiment. However, in case of 1.2 $L_{air}/(min \cdot L_{slurry})$ the increase in As(V) concentration with time was comparatively faster than that of 2 and 3 $L_{air}/(min \cdot L_{slurry})$ and at the end of 6 h, the As(V) permeate concentration was approximately 70 µg/L (just over 60% removal efficiency) at air bubbling rate of 1.2 $L_{air}/(min \cdot L_{slurry})$, while at 2 $L_{air}/(min \cdot L_{slurry})$ the As(V) permeate concentration was around 1.5 times lower than that of at $L_{air}/(min \cdot L_{slurry})$ air bubbling rate. It is concluded that air bubbling rate affects the arsenic concentration profile over time and reveals positive effect on adsorption process with increasing air bubbling rate from 1.2 to 2 $L_{air}/(min \cdot L_{slurry})$. Further increase in bubbling to 3 $L_{air}/(min \cdot L_{slurry})$ did not noticeably enhance As(V) adsorption rate. According to Jia et al. (2005), there is a limit to bubble-induced mass transfer. This indicates that hydrodynamic conditions at ≥ 2 $L_{air}/(min \cdot L_{slurry})$ for As(V) mass transfer are optimized and a further increase in air bubbling rate will not promote the adsorption rate. It can also be concluded that air bubbles keeps the adsorbent in suspension therefore promotes the contact between adsorbent and adsorbate.

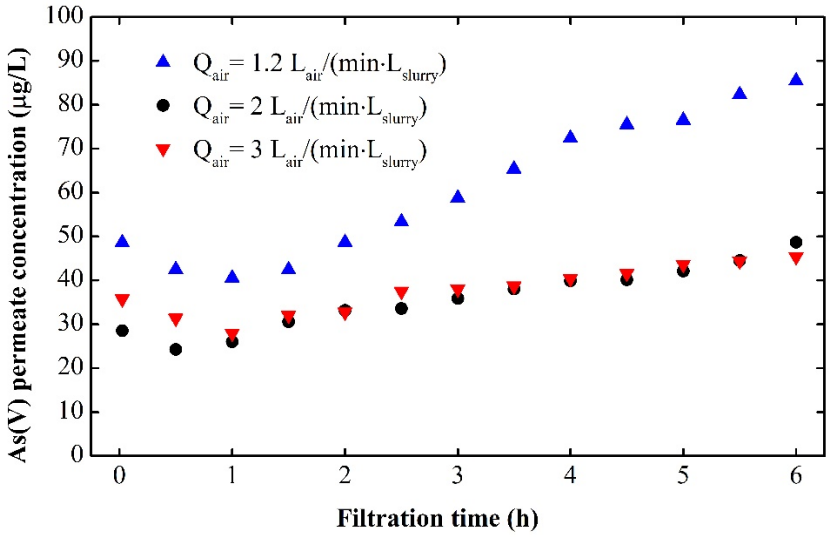

Figure 5.2. As(V) concentration in the permeate over time with µGFH for varying air bubbling rates (n=2) with As(V)= 190 µg/L, adsorbent dosage= 1 g/L, membrane water flux= 20 L/(m^2·h), feed solution pH =8.0 and permeate pH= 8.0 - 8.2.

5.2.2 Influence of adsorbent dosage

Once the effect of the air inflow rate has been quantified, the next important parameter in continuous operation units is the adsorbent dosage. In this section, the evaluation of the adsorption media in SMAHS is studied in terms of its ability to decrease the As(V) permeate concentration below the drinking water guideline value of 10 µg/L (termed $Q_{10,SMAHS}$ hereafter), rather than to enhance the maximum capacity (Q_{max}) and/or higher removal efficiencies, which provides

marginal information on ability of a specific adsorbent to reach guideline value set by EU drinking water directives, US environmental protection agency (EPA) and world health organization (WHO). At an adsorbent dosage of 1 g/L, over 80 % As(V) removal efficiency was obtained (Figure 5.3) but As(V) concentration in the permeate exceeded the desire 10 µg/L WHO guideline value. Therefore, the amount of adsorbent initially dosed into the slurry reactor was increased to 5 g/L from 1 g/L to guarantee the As(V) permeate concentration below the WHO guideline value of 10 µg/L.

It is pertinent to mention, increasing the adsorbent dosage, caused a slight increase to the pH value of the permeate (ranging between 8.0 - 8.3), which can be attributed to the release of hydroxyl ion during adsorption of As(V) onto hydrous iron oxyhydroxide-based adsorbent (Eq. 2-21).

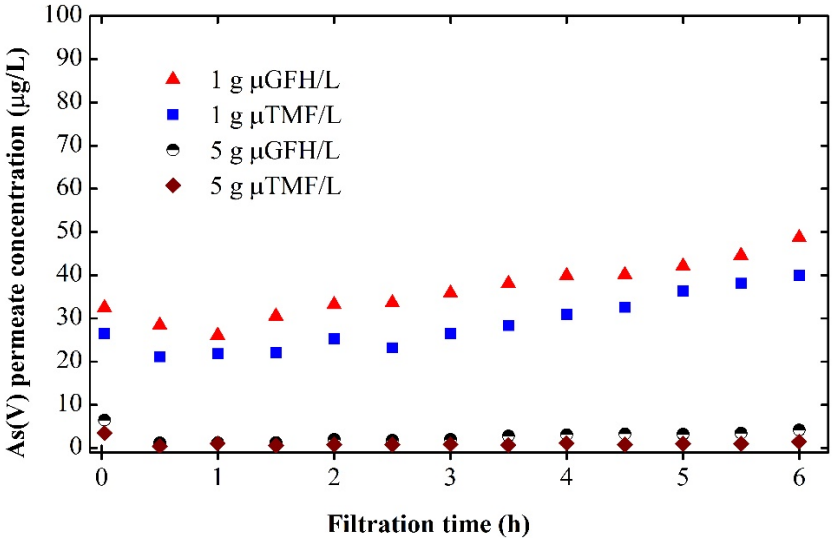

Figure 5.3. As(V) concentration in permeate over time in SMAHS with µGFH and µTMF for adsorbent dosages of 1 and 5 g/L with initial As(V) concentration of 190 µg/L, air bubbling rate = 2 $L_{air}/(min \cdot L_{slurry})$ and permeate pH= 8.0 - 8.3.

While at the dosage of 1 g/L of adsorbent initially dosed to the reactor a slight difference in the As(V) adsorption efficiency between the two adsorbents was observed, at the dosage of 5 g/L both adsorbent removed almost completely arsenic and final concentrations were very low even up to the end of the experiment, i.e., after 6 h. Furthermore, at the dosage of 1 g/L, there was a continuous increase in the As(V) permeate concentration with time which starts to be evident even from the first hour of the experiment, most likely because of the gradual exhaustion of the adsorbent sites. In the case of 5 g/L, only after 4 h of the experiment, a slight increase in the permeate concentrations starts to be detected, but in all measurements the As(V) permeate concentration is below 10 µg/L.

However, it is found in this work that that at an adsorbent dosage of 1 g/L both adsorbents failed to meet the guideline value of 10 µg/L for arsenic in drinking water, as indicated at the EU Directive 98/83/EC. In the first case, the dosed adsorbent corresponds to 0.19 mg As(V)/g of

adsorbent while in the second case the ratio is 5 times lower, thus equals to 3.8 x 10^{-2} mg As(V)/g adsorbent, under optimized conditions of air bubbling. During removal of nitrate in a SMAHS using ion exchange resins at water flux of 15 L/(m^2·h), Kalaruban et al. (2018b) used a ratio of 8 mg NO_3/g to lower the adsorbate concentration from 20 mg/L to less than 11.3 mg/L in the reactor or permeate concentration, which is the guideline value for nitrate. Under these conditions both adsorbent failed to maintain the nitration permeate concentration below 11.3 mg/L after 3-4 h at a hydraulic residence time (HRT) of 2.7 h in the slurry reactor.

5.2.3 Influence of hydraulic residence time

The residence time of interaction between the adsorbents and arsenic in the slurry reactor might be a limiting factor in the slurry reactor as the adsorption kinetic plot (Figure 5.1) shows that As(V) removal rate increased with increasing contact time. Therefore, the influence of HRT on the performance of SMAHS has been studied at membrane water fluxes of 10 L/(m^2·h) and 20 L/(m^2·h). Because the HRTs of As(V) in the slurry reactor are 2.8 h and 5.6 h at 20 L/(m^2·h) and 10 L/(m^2·h), respectively; accordingly the initial 3 h and 6 h contact times of As(V) with media in adsorption kinetics are considered. Figure 5.4 shows the As(V) permeate concentration profiles derived by monitoring the continuous flow SMAHS experiments using micro-sized iron oxyhydroxides. The results show that the addition of adsorbent results in a sudden decrease in As(V) concentration from 190 µg/L to a minimum value in the slurry reactor and after a day the As(V) concentration starts to increase with time.

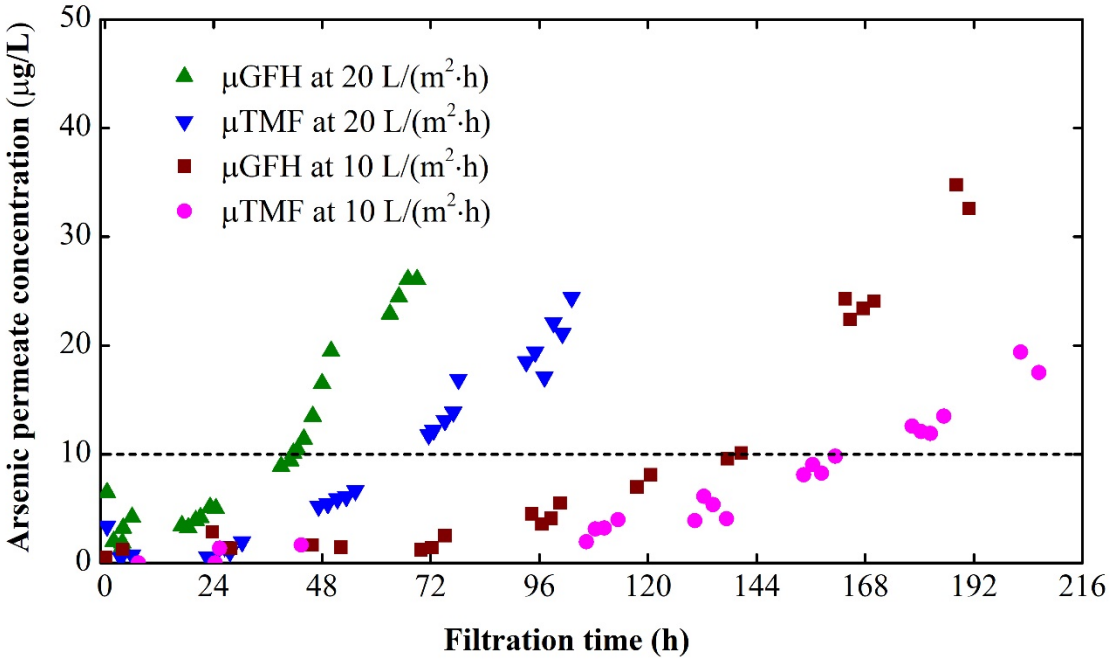

Figure 5.4. As(V) concentration in permeate vs. time for both media in the SMAHS at two different hydraulic residence times for adsorbent dosage=5 g/L with initial As(V) concentration= 190 µg/L, air bubbling rate = 2 L_{air}/(min·L_{slurry}) and permeate pH= 8.0 - 8.3. The dashed line indicates the WHO guideline value for arsenic in drinking water.

However, for the 10 L/(m^2·h), As(V) concentration in the reactor stayed at minimum value for 3 days and after which the As(V) concentration in the permeate starts to rise but at a slower rate than 20 L/(m^2·h). It can be seen from Figure 5.4 that As(V) permeate concentration profiles over time for both media in the hybrid system are effected by the membrane water fluxes. However, the increase in As(V) permeate concentration over time for µGFH is rapid at both water fluxes. This shows that the µTMF is more effective than µGFH in adsorbing As(V) in the presence of competing ions.

The performance of two applied iron oxyhydroxides was assessed in terms of the amount of As(V) adsorbed per unit mass of adsorbent and volume of treated water up to a guideline value of 10 µg/L. $Q_{10,\,SMAHS}$ was calculated by dividing the area above the As(V) concentration profile by the initially added dry mass of adsorbent.

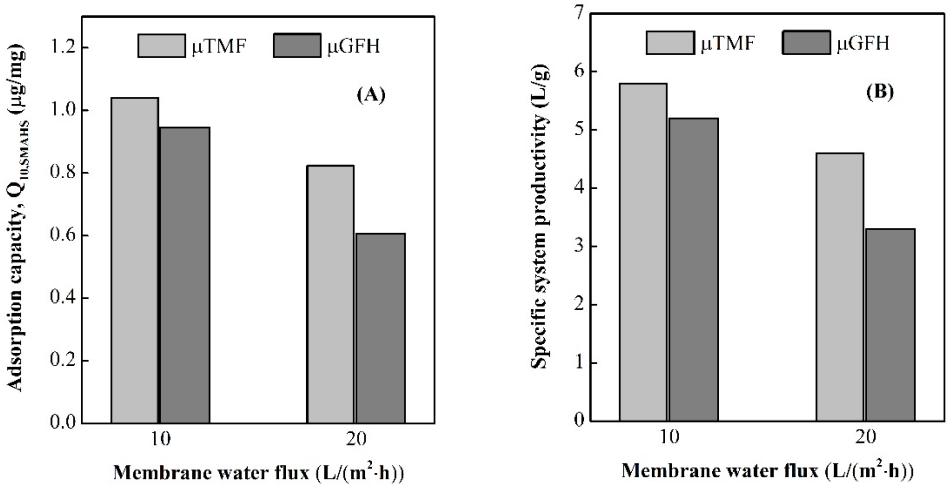

Figure 5.5. (A) Adsorption efficiency of both media in SMAHS; (B) specific system productivity at initial As(V)= 190 µg/L and permeate pH = 8.0 - 8.3.

It can be seen from Figure 5.5 that higher HRT (or lower flux of 10 L/(m^2 ·h)) increases the adsorption efficiency of media in removing As(V) from modeled groundwater and thus is favourable, although it produces less volumes of treatable water water per unit time. The amount of As(V) adsorbed per unit mass of media has been decreased at 20 L/(m^2·h). At 20 L/(m^2·h), the recorded adsorption capacity of µGFH is 36.2% less than that of µTMF. The difference decreases to 9.9% at 10 L/(m^2·h). This difference in $Q_{10,SMAHS}$ at shorter contact times can be explained by lower k_2 values of µGFH (Table 5.1). These results showed that although the kinetics of As(V) adsorption is much faster for µTMF (Figure 5.1), the amount of arsenic adsorbed is finally similar for both iron oxyhydroxides, and therefore, when the membrane flux was decreased, the difference in arsenic capacity of both adsorbents - before As(V) permeate concentration reaches 10 µg/L - has been reduced. It is concluded that particle size has a significant influence on practical adsorption capacity ($Q_{10,SMAHS}$) for drinking water production observed in a SMAHS, even though µGFH has large specific surface area and higher pH_{IEP} than µTMF.

The volume of water treated by unit mass of adsorbent to reach As(V) permeate concentration of 10 µg/L is calculated by defining as specific system productivity (SSP):

$$SSP = \frac{Q_v \, T_{10}}{V \, M_{ad}} \tag{5-1}$$

Where Q_v is the volumetric flow rate at corresponding membrane water flux, T_{10} is time taken to reach 10 µg As(V)/L concentration in permeate, V is the liquid volume in the reactor and M_{ad} is the mass of adsorbent initially dosed into the reactor. The results reveal (Figure 5.5(B)) that the system productivity is higher at lower membrane water flux and vice versa. Furthermore, the recorded system productivity using µTMF is higher, compared with µGFH at both water fluxes. Figure 5.6 shows TMF profile for constant flux filtration of 10 and 20 L/(m^2·h). Overall, it can be seen that the no fouling occurred during operation for both applied fluxes. It is recommended that membrane fouling behaviour must be considered for long term operation.

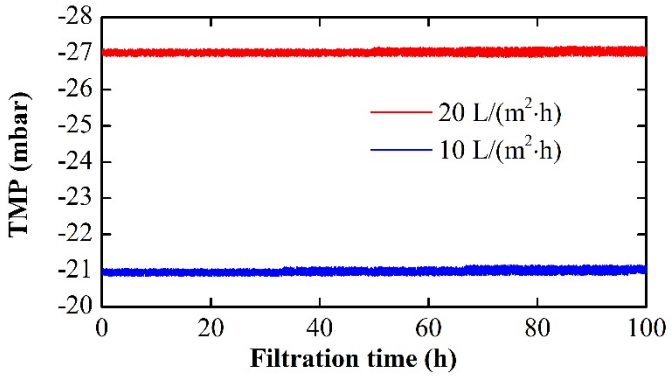

Figure 5.6. Trans-membrane pressure (TMP) profile during constant water flux in submerged membrane adsorption hybrid system.

5.2.4 Influence of initial As(V) concentration

The volume of water treated and amount of As(V) adsorbed per unit mass of adsorbent in the SMAHS using both adsorbents at varying As(V) feed concentrations and at identical flux is listed in Table 5.2. As anticipated, SSP using the micro-sized ion oxyhydroxides has been declined, when the As(V) feed concentration was increased from 190 µg/L to 380 µg/L. A reduction of 6 % and 10 % was recorded for µGFH and µTMF, respectively. However, $Q_{10,SMAHS}$ value was increased at the same membrane water flux for both iron oxyhydroxides since the amount of arsenic entering the slurry reactor per unit time was increased and subsequently, the concentration gradient between the adsorbate in solution and the media solid surface was increased and lead to the higher Q_{10} value of both adsorbents. The time taken to reach the As(V) permeate concentration of 10 µg/L was decreased in case of higher initial As(V) concentration of 380 µg/L.

Table 5.2. Volume of water treated and $Q_{10,SMAHS}$ value for As(V) concentration < 10 µg/L for two adsorbents at varying As(V) feed concentrations with adsorbent dosage = 5 g/L, water flux = 20 L/(m^2·h), pH = 8 ± 0.1 and air bubbling rate = 2 L_{air}/(min·L_{slurry}).

Adsorbent	Influent As(V) conc. (µg/L)	Total operation time (h)	Total volume filtrated (L)	T_{10} (h)	Amount of As(V) adsorbed (mg)[a]	SSP (L/g)[a]	$Q_{10,SMAHS}$ (µg/ mg)
µGFH	190	69	24.9	45.8	3.0	3.3	0.61
	380	68	27.5	43.0	5.8	3.1	1.15
µTMF	190	103	37.1	64.1	4.1	4.6	0.82
	380	102	36.6	57.0	7.7	4.1	1.54

[a]when As(V) concentration in permeate reached the WHO guideline value of 10 µg/L.

Hilbrandt et al. (2019a) reported that during adsorption of phosphate onto µGFH in an adsorption-membrane hybrid system that a sharp slope of the breakthrough curve is favorable as it indicates less influence of external film diffusion on adsorption. Due to which a sharp increase in As(V) permeate concentration was observed and target contaminant concentration of 10 µg/L in the treated permeate with As(V) feed concentration of 380 µg/L has been accomplished earlier than with 190 µg As(V)/L.

5.3 Performance evaluation of SMAHS and fixed-bed filtration filter

The performance of the SMAHS using micro-sized iron oxyhydroxides can be compared with laboratory- and full-scale fixed-bed adsorbers used for As(V) removal via adsorption onto granular fractions of iron oxyhydroxide-based adsorbents as well as iron oxide-coated sand (Table 5.3). Tresintsi et al. (2013a) obtained higher As(V) adsorption capacity (i.e., Q_{10} value) of GFH, with particle size ranging between 250-500 µm, in rapid small-scale column test (RSSCT) than that of SMAHS using µGFH (1.7 *vs.* 0.95 µg/mg at 10 L/(m^2·h) or 0.61 µg/mg at 20 L/(m^2·h)). This difference in adsorption capacity might be explained because the two studies were conducted under different experimental set-ups and conditions, since the actual adsorption capacity of an adsorbent for a specific pollutant depends on experimental set-ups, water matrix and solution pH.

Better performance of RSSCT packed with granular iron-oxyhydroxides for As(V) is associated to a larger concentration gradient between the adsorbate in solution and the media solid surface. The adsorbent in RSSCT is always in contact with the influent arsenic concentration, which results in a higher driving force over the whole adsorption process. However, in a SMAHS the influent arsenic concentration is in contact with slurry, which has very low liquid phase arsenic concentration especially at the start of adsorption process when all adsorption sites are empty and arsenic removal occurred very rapidly, due to which the mass transfer driving force (concentration

gradient) is very low compared to RSSCT. This is becoming more obvious when the initial arsenic concentration increased to 380 µg/L. This provided more contact of arsenic with the slurry of iron oxyhydroxides and caused an increase in $Q_{10,SMAHS}$ from 0.82 to 1.54 µg/mg for µTMF and from 0.61 to 1.15 µg/mg for µGFH respectively.

Regarding the experimental conditions, As(V) removal from the water via adsorption onto iron oxyhydroxides is known to be impacted by solution pH and presence of competing ions in the drinking water matrix (Chapter 4.4). Westerhoff et al. (2005) investigated the arsenic adsorption in GFH packed RSSCT using a different drinking water matrix with an As(V) influent concentration of 14 µg/L - where the concentration driving force might be in the same range as in SHAHS - even though the obtained Q_{10} value in RSSCT packed with GFH is lower than that of SMAHS using µGFH.

Concerning the pH value, both applied iron oxyhydroxides remove arsenic via adsorption more effectively at pH values below pH_{IEP} and their adsorptive capacities increase with decreasing pH. During adsorption of As(V) onto iron oxyhydroxides, synthesized in laboratory at kilogram scale, in RSSCT the Q_{10} value was increased from 2.8 to 6.8 to 10.7 µg/mg at 8, 7 and 6, respectively. This study demonstrated that by decreasing the solution pH by one unit from 8 to 7 the adsorption efficiency of adsorbent increased by 2.4 times. Similar results were obtained by Katsoyiannis and Zouboulis (2002), where As(V) adsorption was studied in fixed bed columns using amorphous iron oxides as adsorbent, the bed volumes treated before arsenic concentration reached the 10 µg/L were increased as the pH decreased from 9 to 7. This is because as the pH decreases the surface charge of the adsorbent becomes more positive and favors the adsorption of oxyanion species on their surface.

In summary this difference in adsorption capacity between two studies could be attributed to water matrix as well as solution pH in addition to As(V) influent concentration and therefore, it is relevant to mention that these factors play pivotal role while comparing the removal efficiencies of two water treatments systems for As(V) at roughly the same concentration driving force. From the above discussion it is concluded that the removal efficiencies of both treatment systems are comparable for As(V) especially when the concentration driving force is higher in the slurry reactor and also taking into account the effect of the water matrix and solution pH. In one system adsorbent media is fixed, while in hybrid system adsorbent media in suspension. Taking into account the experimental set-up difference, it may be concluded that the use of this adsorption onto micro-sized iron oxyhydroxides followed by membrane separation might be an efficient solution for treatment of high arsenic content waters, as found in many countries including India, Bangladesh, Pakistan, Nepal and China. This is because, at higher concentration driving force, the achieved Q_{10} values of both applied adsorbents have been increased significantly.

Table 5.3. As(V) adsorption capacity of different iron oxyhydroxide-based adsorbents in a fixed-bed adsorption filter and SMAHS.

Type of System	Test solution	pH	Phosphate conc. (mg/L)	Silica conc. (mg/L)	Influent As(V) conc. (µg/L)	Q_{10} (µg/mg)	Data source
GFH packed fixed-bed adsorber	Mitrousi (Greece) tap water	7.3	0.6	14	19	1.6	(Tresintsi et al. 2013a)
GFH packed RSSCT (lab-scale)	Thessaloniki (Greece) tap water	7.9	0.3	20	100	1.7	
GFH packed RSSCT (lab-scale)	Arizona (USA) groundwater	7.6	-	34	14	0.75	(Westerhoff et al. 2005)
GFH packed fixed-bed adsorber	Arizona (USA) groundwater	7.8	-	39	34	1.6	
SMAHS using µGFH at 20 LMH	Artificial groundwater	8	0.12	20	190	0.61	This work
		8	0.12	20	380	1.15	
SMAHS using µTMF at 20 LMH	Artificial groundwater	8	0.12	20	190	0.82	
		8	0.12	20	380	1.54	
Iron oxide-coated sand packed fixed-bed adsorber	Groundwater	7.6	-	-	1000	0.002	Callegari et al. (2018)
Amyloid fibril – carbon hybrid membranes	Ultrapure water	7	-	-	239	0.27	(Bolisetty et al. 2017)

Other types of fixed-bed filter uses low-cost sand coated with iron-oxide to remove arsenic from groundwater. Callegari et al., (2018) reported As(V) removal efficiency up to 99%. The iron oxide-coated sand fixed-bed filter could safely treat about 2 - 2.25 L water/L filter volume until 10 µg/L in the effluent was reached. With this volume of product water treated, the corresponding Q_{10} value of the iron oxide-coated sand is 0.002 µg/mg, which is at least three orders of magnitudes lower than the SMAHS using micro-sized iron oxyhydroxides even in the absence of competing ions. Additionally, the fixed bed filter packed with iron oxide-coated sand needs around 2.5 h to reach stable arsenic effluent concentration (below 10 µg/L), from a 1000 µg As(V)/L initial concentration. However, in a SMAHS using low-cost micro-sized iron oxyhydroxides the arsenic permeate concentration immediately reached arsenic concentrations below the drinking water guideline value starting from a 380 µg As(V)/L initial concentration. Moreover, the fined-sized adsorbent can be used in SMAHS in addition to simultaneous removal of colloids, microorganisms, and suspended solids. Furthermore, the examined hybrid system is a relatively simple, effective option to treat arsenic contaminated water and can find its application in decentralized water treatment system. Structural costs of the hybrid system are quite low, and the energy demand of pumps are relatively low that could be provided by solar photovoltaic panels.

The SMAHS performance can also be compared with similar studies using very advanced nanomaterials to achieve As(V) removal. The study of Bolisetty et al. (2017) shows that amyloid–carbon hybrid membranes containing 10 wt% amyloid fibrils indeed diminished the As(V) concentration in ultrapure water within the drinking water guideline value, but the adsorption capacity is only 0.27 µg/mg for As(V) and thus is almost 3 times lower than that those of µGFH and µTMF in the SMAHS, even without the presence of competing ions, showing that in the hybrid treatment system proposed in this study, the critical factor for optimized performance is the iron based materials.

5.4 Regenerability of spent fined-grained iron oxyhydroxide-based adsorbents

A MgO filter was able to achieve > 98 % As(V) removal efficiency when the influent concentration were in the range of 1-3 mg/L employing a EBCT 3 min (Figure A.6). According, EBCT of 3 min was applied for MgO filter for *in-situ* regeneration of µGFH in a SMAHS.

Figure 5.7 shows the As(V) concentration before MgO filter (in the slurry reactor) and after MgO packed adsorption filter for three sequential operation cycles using arsenic free NaOH solution.

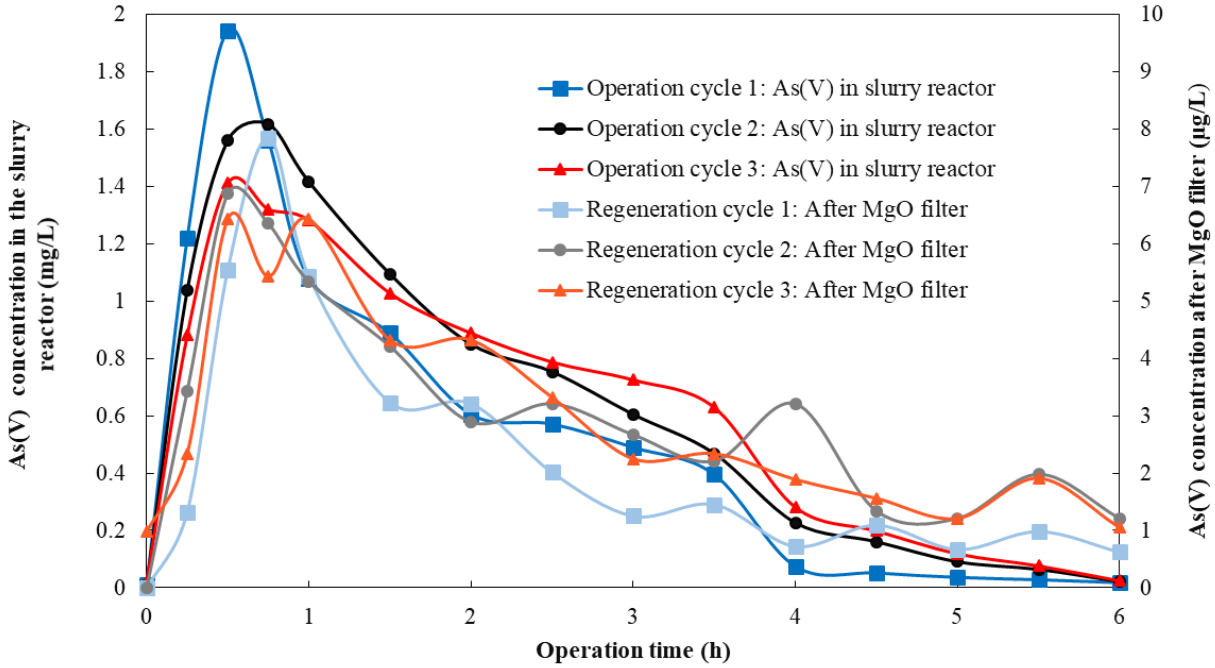

Figure 5.7. As(V) concentrations before and after MgO adsorption filter (applied regenerant concentration for regeneration cycles = 0.05 M NaOH).

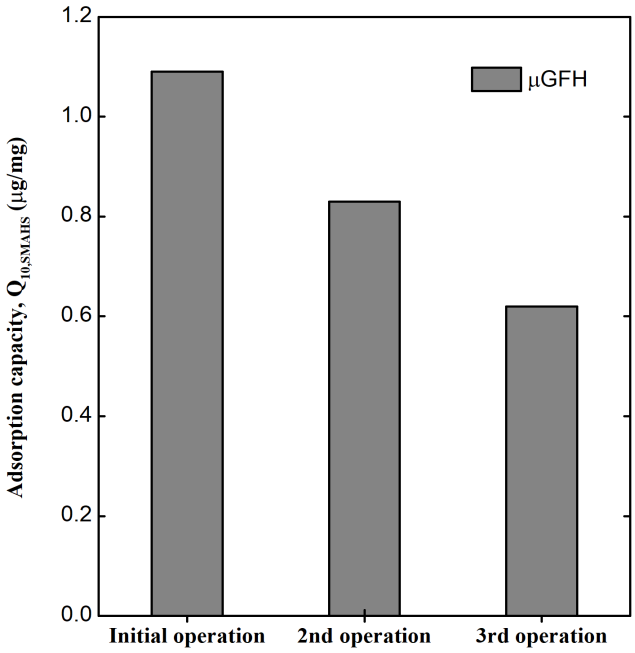

Figure 5.8. Achieved adsorption capacity ($Q_{10,SMAHS}$) by regenerated µGFH in SMAHS tests. Experimental conditions: As(V)= 380 µg/L in NSF water and initial pH = 8.0.

It can be seen from Figure 5.7 that the major part of the adsorbed arsenic from µGFH in the slurry reactor was desorbed within the first 2 h. In 6 h operation time with continuous pumping of 0.05 M NaOH solution, the arsenic concentration in the slurry reactor was 18, 24 and 28 µg/L for the

first, second and third filtration cycles. Moreover, 2 L of 0.05 M NaOH solution (pH 12.5) was initially used for the three regeneration cycles. At the end of the three regeneration cycles, a slight decrease in the strength of NaOH was observed (pH 12.4).

In the first regeneration cycle, arsenic leaching rates are fastest followed by second and third regeneration cycles. Moreover, in all 3 operation cycles, only a partial desorption was achieved, i.e. with each regeneration cycle adsorption sites were lost, and this has direct impact on achieved adsorption capacity of the regenerated µGFH (Figure 5.8). The adsorption capacity after regeneration was 0.83 µg As(V)/mg and 0.62 µg As(V)/mg, respectively, corresponding to 76.1 % and 56.9 % of the initial adsorption capacity (1.1 µg As(V)/mg). Similar results were obtained in the past during adsorption of phosphate from ultrapure water onto GFH fixed-bed filter. The adsorption capacity after regeneration was 84.9 % and 70.2 % of the initial adsorption capacity (Sperlich 2010). In this work, this loss in efficiency is mainly attributed to the loss of adsorption sites with each regeneration cycle as well as due to the interfering parameters such as phosphates originating from the modeled (NSF) water as indicated by batch tests during arsenic adsorption onto µGFH in NSF water (Chapter 4.4).

In addition, recorded arsenic concentration in the NaOH solution was < 10 µg/L (practically zero) for the three regeneration cycles, which indicates that desorbed arsenic from µGFH was successfully captured by MgO. This also indicates that that MgO filter packed with 65g MgO can be applied for at least 3 regeneration cycles.

6 Modeling arsenic adsorption onto fine-grained adsorbents in SMAHS

An optimized design of the SMAHS requires the proper selection of the variables such as type and particle size distribution of adsorbent, membrane water flux corresponding to the residence time of adsorbent in the reactor and mass of initially dosed adsorbent (M_{ad}) into the reactor. The required information are generally obtained by carrying out lab-scale studies as is the case in Chapter 5, which are not only time-consuming but also expensive. In this chapter, in the beginning a mathematical model based on the HSDM and the corresponding solute mass balance equation is formulated and developed (Chapter 6.1). Adsorption kinetics of As(V) on two different particle size fraction of each adsorbent are determined experimentally to estimate mass transfer coefficients for As(V) adsorption. The mass transfer coefficients are calculated simultaneously by fitting the experimental data with the model solution (Chapter 6.2). The developed model is then verified using experimentally determined As(V) breakthrough curves monitored in a SMAHS (Chapter 6.3). After validation at varying adsorbent doses and membrane fluxes, the developed mathematical model is used to predict the influence of different operating conditions on As(V) breakthrough curves (Chapter 6.4).

Selected contents of this chapter have been published in collaboration with Ioannis A. Katsoyiannis, M. Zarebanadkouki and M. Ernst: Journal of Hazardous Materials 2020. (Usman et al. 2020b): https://doi.org/10.1016/j.jhazmat.2020.123221

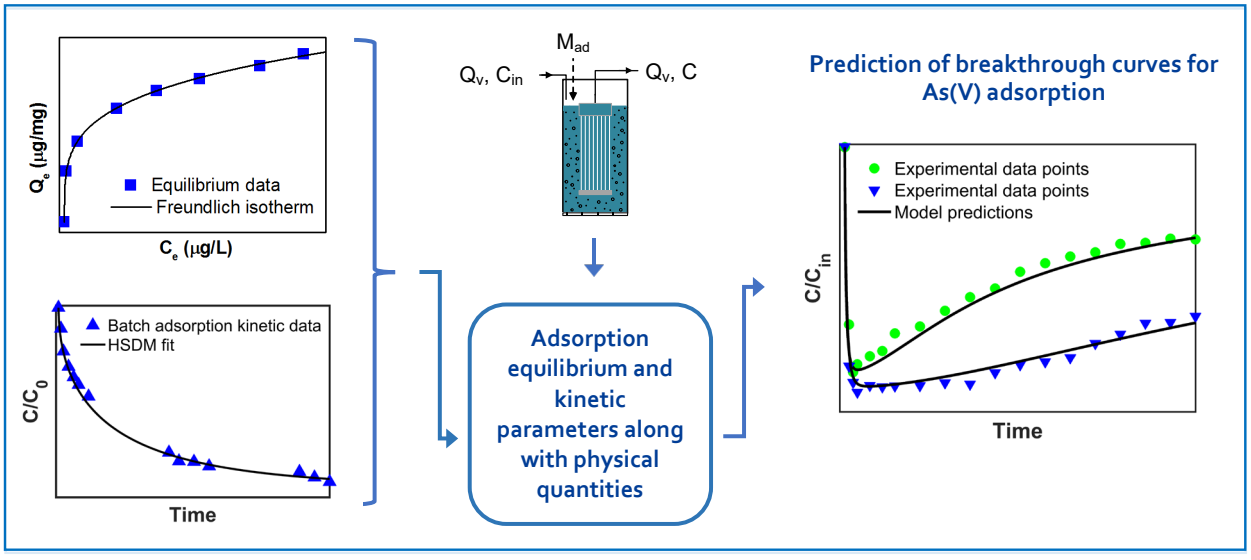

6.1 Formulation of mathematical model

For a continuous flow SMAHS with adsorbent in an initially dosed mode simulating a completely mixed stirred tank reactor, the solute mass balance in the slurry reactor can be expressed as:

$$Q_v\,(C_{in} - C) = \frac{d(V\,C + M_{ad}\,q_{avg})}{dt} \tag{6-1}$$

The left-hand side of above equation reflects the sink (the amount of adsorbate adsorbed onto adsorbent particle), whereas the right-hand side reflects the sum of mass change of the adsorbate that remains in the reactor in the liquid phase and that adsorbed onto the adsorbent particle over time.

q_{avg} represents the average adsorbed phase arsenic concentration and it is expressed as:

$$q_{avg}(t) = \frac{24}{d_p^3}\int_0^{d_p/2} q(r,t)\,r^2 dr \tag{6-2}$$

The change of adsorbate concentration in permeate of the SMAHS can be calculated by combing Eqs. 6-1 and 6-2 as follows:

$$\frac{dC}{dt} = \frac{Q_v}{V}\,(\,C_{in} - C\,) - \frac{M_{ad}}{V}\frac{dq_{avg}}{dt} \tag{6-3}$$

where Q_v is the volumetric flow rate, V is liquid volume in the reactor, C_{in} is the influent adsorbate concentration flowing into the slurry reactor, M_{ad} is the mass of adsorbent initially dosed into the reactor and d_p is the mean diameter of adsorbent particle.

6.1.1 Model implementation and parameterization

The set of derived equations based on the HSDM were solved numerically using a fully implicit finite difference method. First, both differential Eqs. 2-15 and 6-3 were substituted by their finite difference expressions based on the backward finite difference method (fully implicit) for temporal derivatives and backward finite difference method for spatial derivatives. The details of finite difference discretization are given in appendix B.1. Then the resulting sets of ordinary differential equations are solved simultaneously in MATLAB (R2015b) using an iterative method with regards to their initial and boundary conditions. This procedure allowed to calculate the profile of $q(r,t)$, $q_{avg}(t)$, and adsorbate concentration in the bulk solution ($C(t)$).

To predict the concentration profiles of adsorbate in the permeate of the SMAHS, the model input parameters were classified into three categories: (1) readily available (geometrical and mass related) model parameters which include the mass of adsorbent added initially added into the reactor, liquid volume in the reactor, the influent concentration of adsorbate, volumetric flow rate which governs the membrane water flux, particle size, and particle density; (2) equilibrium adsorption constants (K_F, n) which are determined by fitting the equilibrium isotherm's data

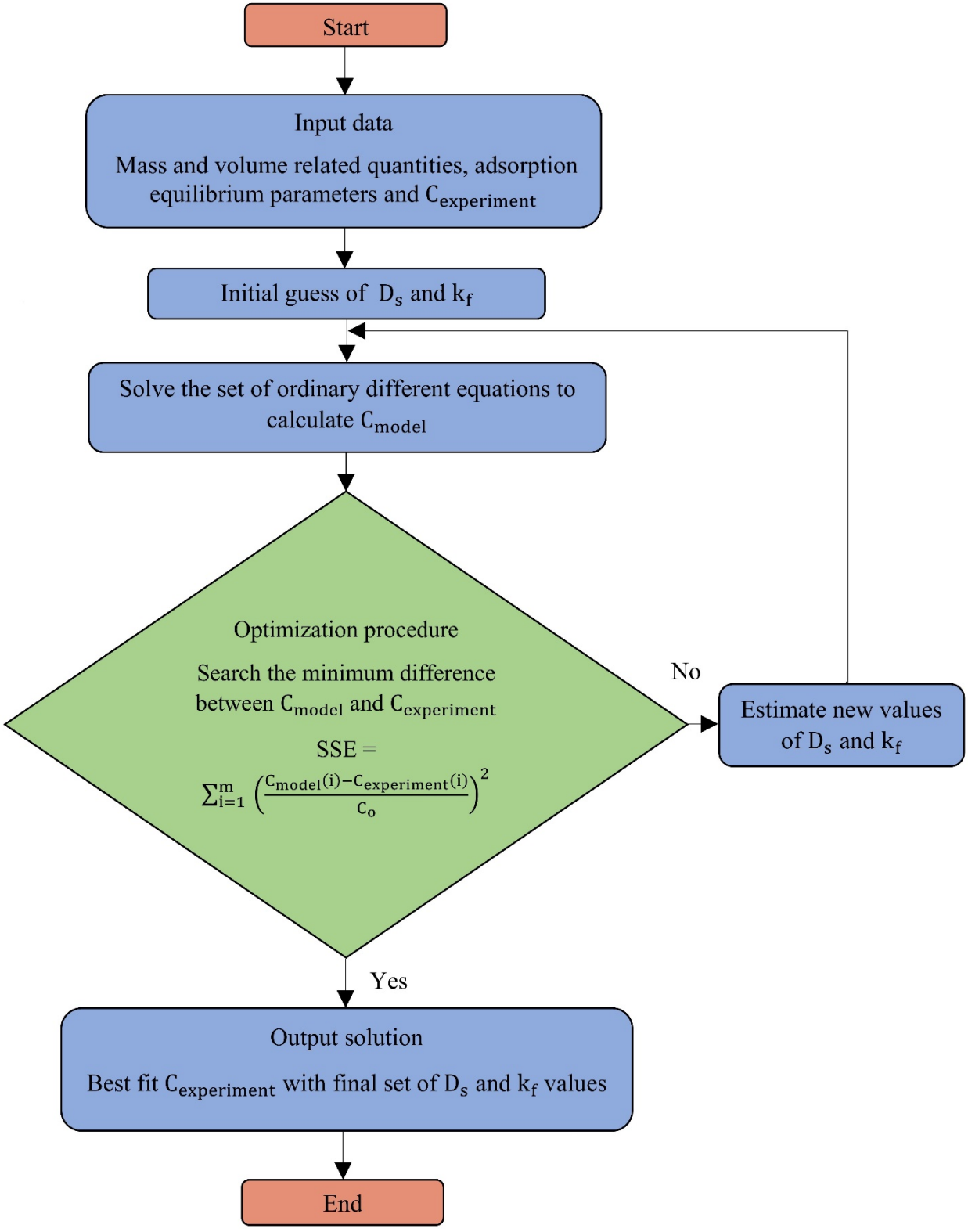

Figure 6.1. Flow chart of the adsorption kinetic coefficients using an optimization procedure.

(Figure A.10); (3) mass transfer (adsorption kinetic) coefficients (D_s, k_f) which cannot be measured directly. To determine the mass transfer coefficients simultaneously, the HSDM was first solved using initial estimates of D_s and k_f, and then these values were inversely adjusted to best reproduce the data collected from batch adsorption kinetic experiments. Figure 6.1 depicts the procedure adopted to estimate the adsorption kinetic coefficients of the HSDM.

The pattern search minimizer in MATLAB are used to minimize sum of squares of error (SSE) as:

$$\text{Sum of squares of error (SSE)} = \sum_{i=1}^{m} \left(\frac{C_{\text{model (i)}} - C_{\text{experiment (i)}}}{C_o} \right)^2 \quad (6\text{-}4)$$

where $C_{experiment}$ is the experimental data points, C_{model} is the modeling output data and m denotes the number of data points in time.

6.2 Determination of mass transfer coefficients for As(V) adsorption

The developed model is also adopted to determine the mass transfer coefficients from batch adsorption kinetics experiments. For batch tests, $Q_v = 0$. In this case, Eq. 6-3 reduces to:

$$V \frac{dC}{dt} = - M_{ad} \frac{dq_{avg}}{dt} \quad (6\text{-}5)$$

Eq. 6-5 describes the overall mass balance in a batch adsorption test. The right-hand and left-hand side of this represents the sum of mass change of As(V) that adsorbed onto adsorbent and that remains in the reactor (in the liquid phase) over time.

As(V) adsorption kinetics for µGFH (1 - 63 µm) and µTMF (1 - 63 µm) are shown in Figure 6.2(A). The results indicate a fast initial As(V) adsorption onto both iron oxyhydroxides followed by a slower removal which gradually approaches an equilibrium plateau. The faster kinetics of µTMF may be due to smaller mean particle size compared to µGFH as well as due to its large pore volume and mean pore diameter. The best fit values of D_s for the two-particle size fractions of each adsorbent along with values of sum of the square of the error (SSE) and determination coefficients (R^2) are reported in Table 6.1. Best fit D_s value for µGFH (1 - 250 µm) at pH 8 is 1.53 x 10^{-16} m^2/s with $R^2 > 0.99$ and SSE < 2.8 x 10^{-2}. The fitted D_s value is similar in magnitude to that reported for the adsorption of As(V) on GFH (18 – 250 µm) in differential column batch reactor (DCBR) at pH 7 in DI water spiked with 100 µg As(V)/L (Badruzzaman et al. 2004).

Representative best-fit model simulations together with kinetic data for two-particle size fractions of µTMF are shown in Figure 6.2(B). As anticipated based on Fick's second law of diffusion, the adsorption rate is faster with the smaller particles of the same adsorbent. The HSDM is based on Fick's law, which states that the adsorption rate is inversely proportional to the square of the radius of the particle. After 7 days of contact time, the residual concentration of As(V) in the solution for smaller and larger particle size fractions of µTMF is almost the same.

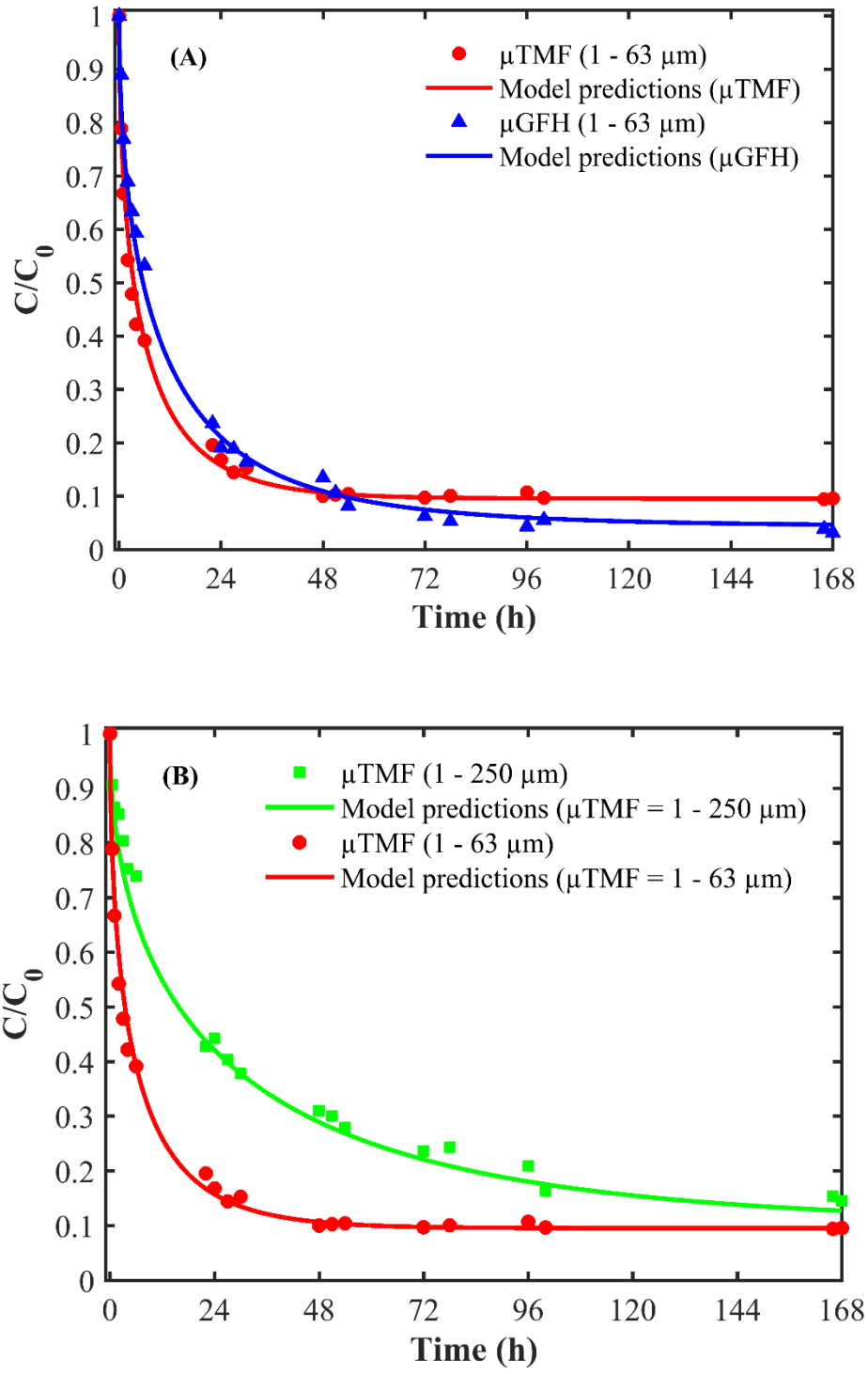

Figure 6.2. Model fit to the batch kinetic tests data at M_{ad} = 40 mg/L; **(A)** for powdered particle size fractions (1 – 63 μm) of iron oxyhydroxides, μGFH and μTMF; **(B)** for effect of particle size on As(V) adsorption rate for μTMF.

Table 6.1. Values of intraparticle diffusion coefficient (D_s), sum of square of error (SSE) and determination coefficients (R^2) estimated by fitting kinetic data by the HSDM.

Adsorbent media	Particle size fraction (µm)	Mean particle diameter (µm)	D_s (m^2/s)	SSE (x 10^{-2})	R^2	Bi	Data source
µGFH	1 - 63	3.5	1.09 x 10^{-18}	1.2	0.99	89	This work
µGFH	1 - 250	78.4	1.53 x 10^{-16}	2.8	0.98	192	This work
GFH	18 - 250	214	5.42 x 10^{-16}	-	-	190	(Badruzzaman et al. 2004)
GFH	250 - 600	426	1.12 x 10^{-15}	-	-	37	
GFH	800 - 1000	-	3.00 x 10^{-15}	-	-	183	(Sperlich et al. 2008)
µTMF	1 - 63	2.8	2.26 x 10^{-18}	1.0	0.99	56	This work
µTMF	1 - 250	40.0	1.01 x 10^{-16}	2.1	0.99	150	This work

6.3 Model verification

In this section, verification of the developed model has been carried out by comparing the results predicted by model with experimental data points for As(V) normalized permeate concentrations. Figure 6.3 shows experimentally determined As(V) breakthrough curves along with the model predictions for the two particle size fractions of µGFH, expressed as C/C_{in} over the filtration/operation time. The amount of adsorbent dosed into the reactor was kept at 1, 2 and 3 g/L, while the membrane flux was maintained at 200 L/(m^2·h). An excellent agreement between the experimentally and simulated breakthrough curves of As(V) was calculated with SSE < 1 x 10^{-2} and the corresponding R^2 values > 0.956 (R^2 and SSE are reported in Table A.1). However, for larger size fraction of µGFH (1 – 250 µm) of 1 g/L deviation of experimental data points from the model predicted values were noticed. D_s values depend strongly on the particle size as indicated by the adsorption kinetic data and the particle size distribution of larger sized µGFH (1 – 250 µm) varies over a wider range (shown in Figure 4.1). It is highly possible that the mean particle size of larger sized µGFH might be smaller than that was used in simulations. Due to which surface diffusion which is adsorbate diffusion along the inner surface of the adsorbent would have been changed and accordingly model tends to slightly under predict the normalized As(V) concentrations in the permeate of SMAHS from beginning of the experiment to operation time of 7 h.

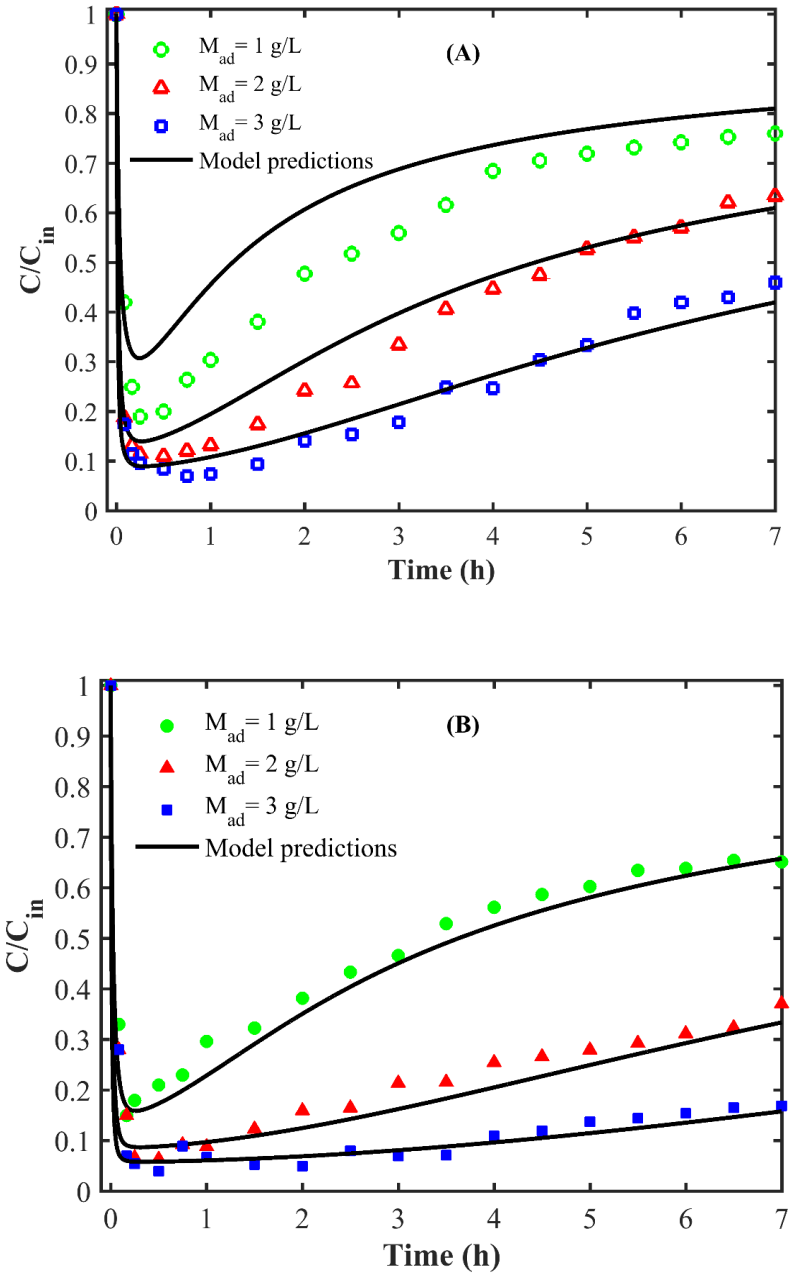

Figure 6.3. Model verification for continuous-flow SMAHS at C_{in} = 380 µg/L, pH = 8 and membrane water flux = 200 L/(m^2·h) using **(A)** µGFH (1 – 250 µm); **(B)** µGFH (1 – 63 µm).

To check the correctness of the model solution at varying membrane fluxes which determines the hydraulic residence time of As(V) in the slurry reactor, the SMAHS tests are also carried out at two membrane fluxes of 100 and 200 L/(m^2·h) for the larger and small fraction of each adsorbent media. The adsorbent dose is kept at 1 g/L to monitor a sharp increase in normalized As(V) permeate concentrations. Figure 6.4 shows the experimentally observed concentration profiles along with model solution at corresponding membrane flux for larger and smaller particle size

fractions of µGFH. The As(V) breakthrough curves for adsorption onto µTMF are shown in Figures A.11-A.14. The model predictions exhibit that the experimentally determined As(V) breakthrough curves for µTMF fit well as well.

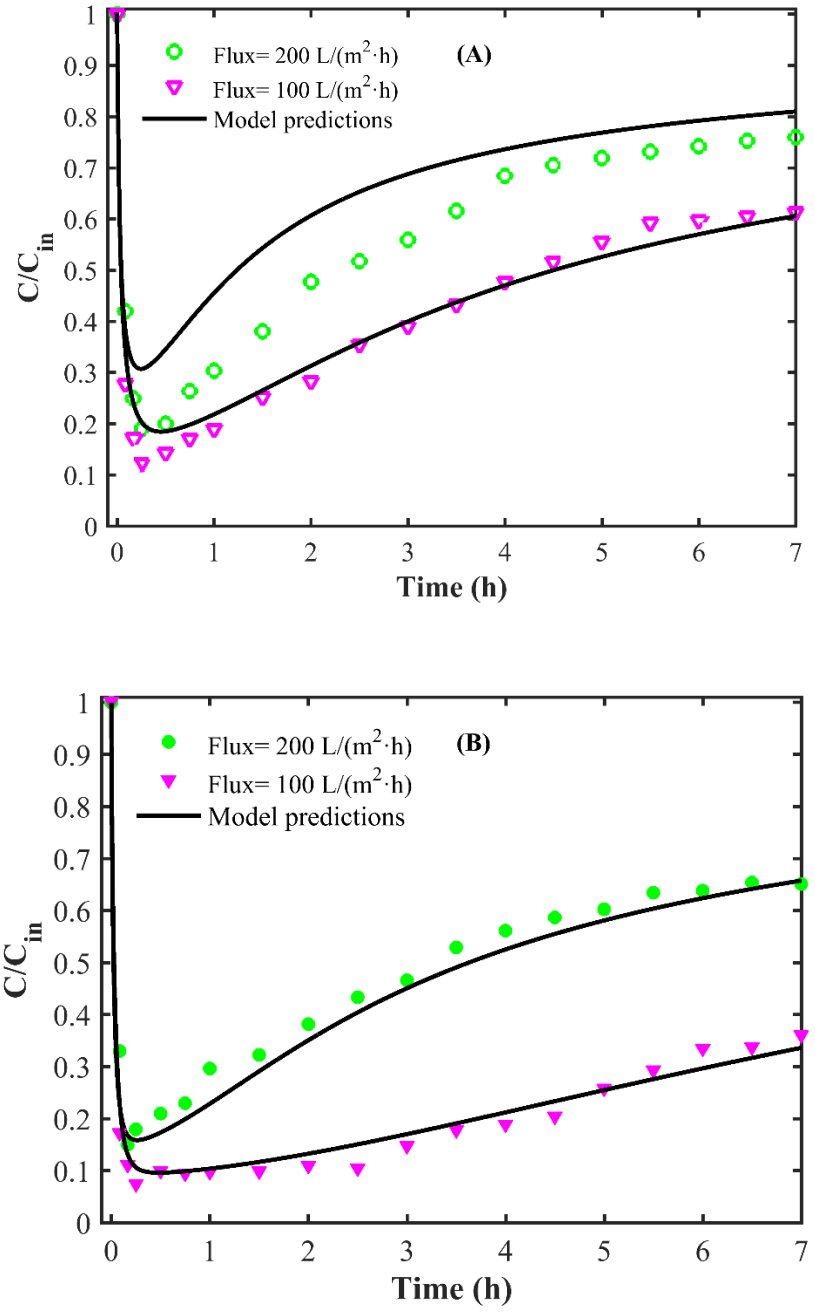

Figure 6.4. Model verification for SMAHS at C_{in}= 380 µg/L, pH= 8 using: **(A)** µGFH (1 – 250 µm); **(B)** µGFH (1 – 63 µm).

6.4 Model predictions

After the model has been developed and validated, it will be applied in the following section to derive information on possible technical variations of type of adsorbent, adsorbent mean particle size, along with the process parameters and conditions such as adsorbent dosage and membrane water flux (hydraulic residence time) on As(V) adsorption in a SMAHS. By this approach, the results of the mathematical model are transfer into a conceptual planning tool for the evaluation of process design boundary conditions.

6.4.1 Influence of adsorbent type

Figure 6.5 shows the predicted breakthrough curves of As(V) adsorption for µGFH (1 – 250 µm) and respective particle size fraction for µTMF at an adsorbent dosage of 3 g/L and at 100 L/(m^2·h). To better understand the influence of adsorbent type on As(V) breakthrough curves, five zones of the breakthrough curve as defined by Sontheimer (1988) are taken into consideration (Figure 6.6)

- Zone A (immediate breakthrough): Adsorbate concentration drops to the minimum effluent concentration after the starting up the filtration.
- Zone B (higher adsorption efficiency): After the sudden adsorbate breakthrough, a time span occurs in which the adsorbate effluent concentration stays at a nearly constant level. In this paper, this zone is until the breakthrough point of 0.1 and is termed as a working zone.
- Zone C (decreasing adsorption efficiency): This zone indicates the asymptotic shape of the breakthrough curve. In this zone, the adsorbate concentration changes rapidly and consequently, represents the main zone of the curve.
- Zone D (low adsorption efficiency): During this phase of the breakthrough curve, only a small part of the adsorbate is removed over time.
- Zone E (constant removal efficiency): In this zone, adsorption does not occur, and effluent concentration is almost the same as the influent level of the adsorbate.

An immediate decrease in adsorbate concentration in permeate is caused by the addition of micro-particles of iron oxyhydroxides. This immediate reduction in As(V) concentration is not only due to presence of large excess of adsorption sites but also due to the presence of high As(V) concentration gradient between the bulk solution and external surface adsorption sites of the adsorbent. The lowest As(V) concentration is achieved in the SMAHS using µTMF (1 – 250 µm) despite the adsorption capacity of µTMF for As(V) calculated through isotherm experiments is lower compared to µGFH. This might be explained by almost the same magnitude of D_s value for µTMF even though its mean particle size is almost half of µGFH mean particle size.

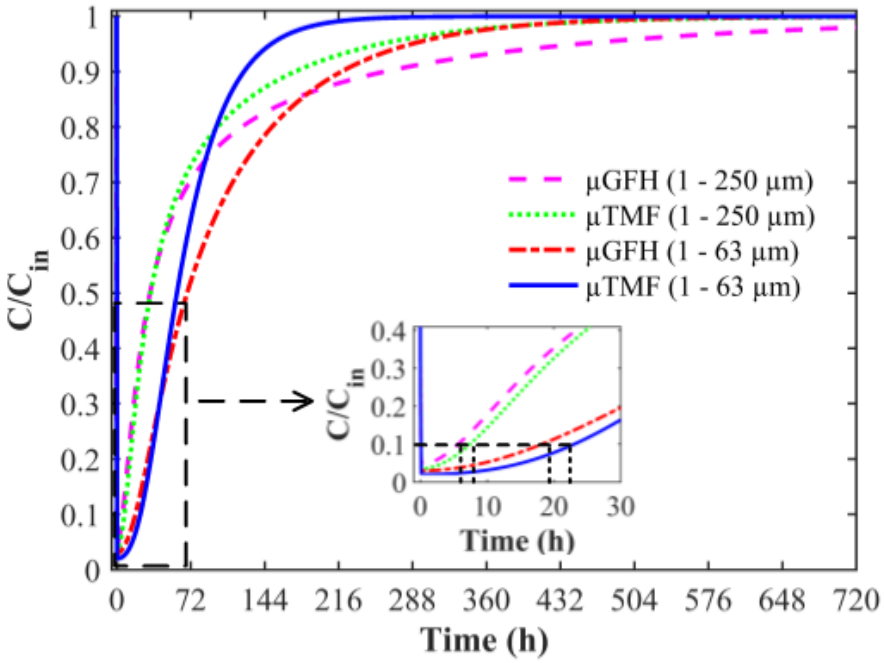

Figure 6.5. Simulated breakthrough curves for As(V) removal using iron oxyhydroxides in the SMAHS at at C_{in}= 380 µg/L, membrane flux= 100 L/(m^2·h) and adsorbent dose= 3 g/L. Dashed line in inset of figure reflects the working zone (B).

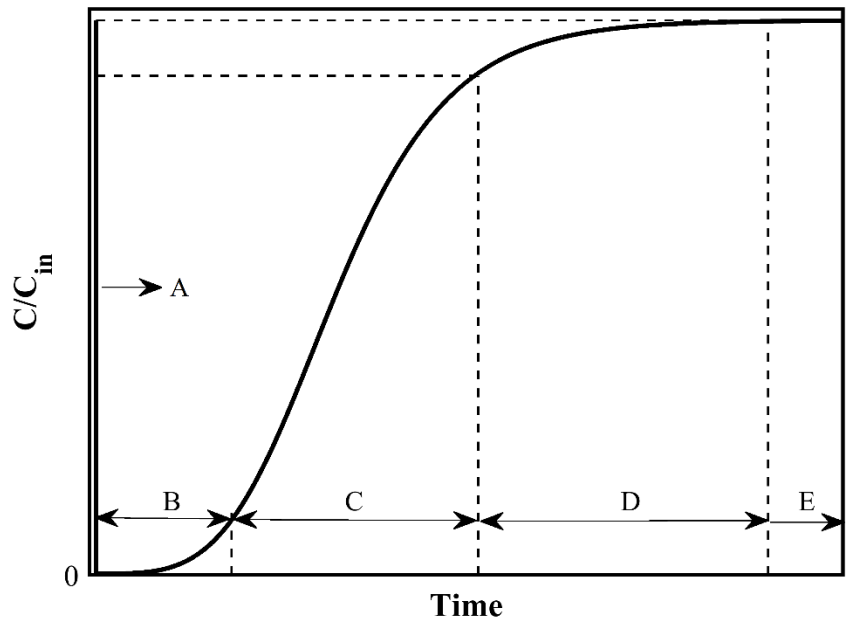

Figure 6.6. Criteria defined by Sontheimer (1988) for different zones of a typical breakthrough curve.

In the working zone (B), µTMF gives rise to longer times of higher adsorbate removal (inset Figure 6.5). In the zone (C) the steep increase in C/C_{in} can be seen for both adsorbents. This phase of the breakthrough curve suggests a decreasing intraparticle surface diffusion with time and represents an extremely slower rate of adsorption capacity for both adsorbents (Sperlich et al. 2005). However, the decrease in adsorption capacity of µTMF is faster in zone (C) and therefore, favourable for As(V) adsorption in the SMAHS. In general, the adsorption efficiency of the adsorbent decreases as the breakthrough curve becomes flatter.

Taken into account the complete breakthrough curve for As(V) in adsorption-submerged membrane hybrid system, Sperlich et al., (2008) categorized this type of breakthrough curve with surface diffusion-controlled mass transfer limitations (Bi > 30) and this type of breakthrough curve propounds an extremely slow intraparticle diffusion. Similar shape of breakthrough curves has been observed during adsorption of As(V) onto GFH in fixed-bed adsorbers (Saldaña-Robles et al. 2018; Sperlich et al. 2005; Sperlich et al. 2008; Westerhoff et al. 2005). Hilbrandt et al. (2018) also reported the similar trend of breakthrough curve for phosphate removal in fixed-bed filters packed with GFH and fine fraction of GFH, termed as µGFH in this work.

6.4.2 Influence of adsorbent size

Figure 6.5 also displays the model predictions for the As(V) removal using the two different particle size fractions of each adsorbent media. The smaller particle size fractions of both absorbents have prolonged the working zone of the breakthrough curve. It can be seen that the SMAHS results in longer times of higher As(V) removal using smaller particle size fractions (3.1 and 3.2 times for µTMF and µGFH, respectively). If operators are interested in 90% As(V) removal (i.e., $C/C_{in} = 0.1$), more volumes of water can be treated by smaller particle size fraction of iron oxyhydroxides. Moreover, 1.3 times more volume of water can be filtered by smaller fraction of µTMF in this hybrid membrane process than that of µGFH with same particle size fraction. In case of small particle size fractions of iron oxyhydroxides, steepness of the zone C (decreasing adsorption efficiency zone) of the breakthrough curve has been increased and also the complete As(V) breakthrough has been achieved earlier than larger diameter iron oxyhydroxides. At the end of 720 h operation, the adsorption sites of µGFH (1 – 63 µm) and µTMF (1 – 63 µm) are fully covered (full surface coverage), while the adsorption sites of µGFH (1 – 250 µm) are around 98 % covered.

A decrease in length of zone C and D of breakthrough curve following an elongated operating zone (B) indicates a lower dependency on the surface diffusion of As(V) into the adsorbent media. In case of µTMF (1 – 63 µm), the length of zone C and D has been shortened significantly and therefore favourable. This type of breakthrough curve does not vary too much from ideal s-shaped breakthrough curve and thus favourable. Therefore, it is concluded that long operation times of very low arsenic concentration (i.e., $C/C_{in} = 0.1$) in the permeate of the SMAHS can be achieved by applying powdered-sized fractions (1 – 63 µm) of the iron oxyhydroxide-based adsorbents.

6.4.3 Influence of membrane water flux

The influence of membrane flux was studied by varying the flux in the range of 20 - 200 L/(m^2·h) at a fixed adsorbent dosage of 5 g/L for each flux (Figure 6.7).

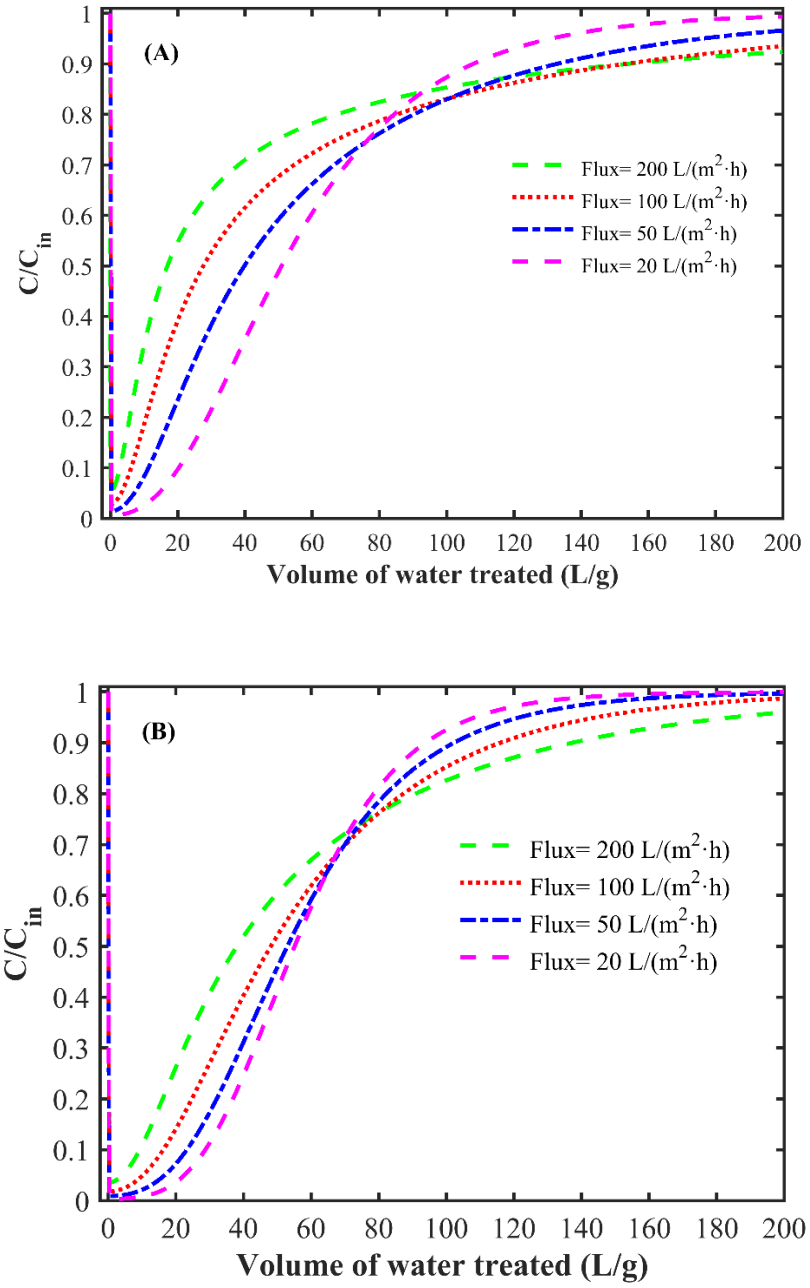

Figure 6.7. Model prediction for As(V) removal at different membrane fluxes at C_{in}= 380 µg/L, adsorbent dose= 5 g/L using; **(A)** µGFH (1 – 250 µm); **(B)** µGFH (1 – 63 µm).

The model simulations show that the membrane flux affects the immediate breakthrough of As(V) after the addition of the adsorbent. For instance, the normalized As(V) permeate concentration after the addition of adsorbent is 0.04 at the highest membrane flux (200 L/m^2·h). This normalized As(V) concentration in the permeate has been reduced to almost zero immediately after adsorbent's addition at a membrane flux of 20 L/(m^2·h). This is because the amount of As(V) entering the slurry reactor per unit time has been reduced by 10 times. This allows diffusion of As(V) along the inner surface within the adsorbent media, adsorption at binding sites, decreasing the As(V) concentration in the stagnant layer around the adsorbent particle and consequently, results in a larger concentration gradient between the bulk solution and the external adsorbent's surface. For a better comparison, volume of water treated per unit mass of adsorbent is considered to study the effect of membrane flux on the breakthrough curve. The model simulations exhibit that membrane flux can substantially alter the behavior of breakthrough curves for As(V) onto iron oxyhydroxides. For instance, more volumes of treated water can be generated with decreasing membrane flux. This is explained by larger HRT (= V/Q_v) of As(V) in the slurry reactor at lower membrane fluxes. At the lowest membrane water flux of 20 L/(m^2·h), the corresponding As(V) residence time has been increased from 17 min at 200 L/(m^2·h) to 170 min.

With the smaller particle size fraction of µGFH (1 - 63 µm), 1.8 times more water could be treated at 100 L/(m^2·h) with C/C_{in} = 0.1 in comparison to 200 L/(m^2·h). This increase rises to 3.1 times when the hybrid system operation was set at 20 L/(m^2·h). With the larger diameter of µGFH particles, lower membrane flux of 20 L/(m^2·h), with HRT of 170 min, provided an increment of almost 7 times to lower normalized As(V) permeate concentration. When both fractions of µGFH are compared in terms of volume of water treated until C/C_{in} = 0.1, the increase in volume of treated water was shrunk to 29% at 20 L/(m^2·h) from 70% at 200 L/(m^2·h). It was found the lowest membrane flux of 20 L/(m^2·h) is favourable in terms of more volume of treated water per unit mass of iron oxyhydroxide but the amount of product water generated per unit time until C/C_{in} reaches to 0.1 was decreased by 10 times.

Table 6.2. As(V) adsorption capacities (Q) of iron oxyhydroxides under investigation with corresponding As(V) = 380 µg/L.

Adsorbent media	Particle size fraction range (µm)	Q (µg/mg) at C/C_{in} = 1	Data source
µGFH	1 – 250	22.3	Integrating breakthrough curve
µGFH	1 – 63	22.4	Isotherm experiments from the present study
µGFH	1 – 63	22.4	Integrating breakthrough curve
µTMF	1 – 250	15.4	Integrating breakthrough curve
µTMF	1 – 63	15.4	Integrating breakthrough curve
µTMF	1 – 63	15.4	Isotherm experiments from the present study

The adsorption capacity of the adsorbent in the hybrid system is calculated by integrating the breakthrough curve until $C/C_{in} = 1$ with varying membrane fluxes. The calculated adsorption capacities recorded through continuous flow hybrid system along with adsorption capacities observed through batch isotherm experiments are summarized in Table 6.2. It can be seen that adsorption capacities recorded through two different experiment set ups at As(V) concentration of 380 µg/L are the same.

6.4.4 Influence of absorbent dosage

The influence of iron oxyhydroxides was examined by varying the adsorbent dosage in the range of 3 – 8 g/L and membrane flux was set at 100 L/(m^2·h) (Figure 6.8(A)). As(V) contaminated water flows continuously to the reactor containing a comparatively large amount of iron oxyhydroxides. The abundant amount of adsorbent initially dosed into the reactor affects not only the immediate breakthrough and working zone but also the later zones of the breakthrough curve. With increasing adsorbent dosage, the immediate decrease not only occurs faster but also achieves the lowest As(V) concentration in the reactor (~99.9%). It can be seen from Figure 6.8(A) that the increasing adsorbent dosage has elongated the length of the working zone. For instance, when M_{ad} is doubled (from 4 to 8 g/L) the time taken to reach C/C_{in}= 0.1 has been delayed by more than twice. This implies that adding more adsorbent at the start of the experiment is beneficial for longer time operations so that the time interval to supplement fresh or to start regeneration process can be prolonged. Using higher adsorbent dose in hybrid membrane system is also favorable in term of regeneration of adsorbent. It is generally expected that time taken to regenerate the different amounts of adsorbent under strong alkaline conditions are the same.

To investigate the combined effect of adsorbent dosage and hydraulic retention time of adsorbate, a parameter so-called “adsorbent load” has been defined (Eq. 6-6). This parameter represents the ratio of the total amount of adsorbent in the slurry reactor to the influent flow rate.

$$\text{Adsorbent load} = \frac{V\ M_{ad}}{Q} \tag{6-6}$$

Figure 6.8(B) shows the simulated effect of the adsorbent load on the breakthrough time to reach As(V) removal efficiency of 90% ($C/C_{in} = 0.1$). The results are shown as a function of membrane flux, for values 200 and 100 L/(m^2·h), corresponding HRT of 17 and 34 min. The influence of the operating parameters such as residence time and adsorbent dosage is similar for both adsorbents in the SMAHS.

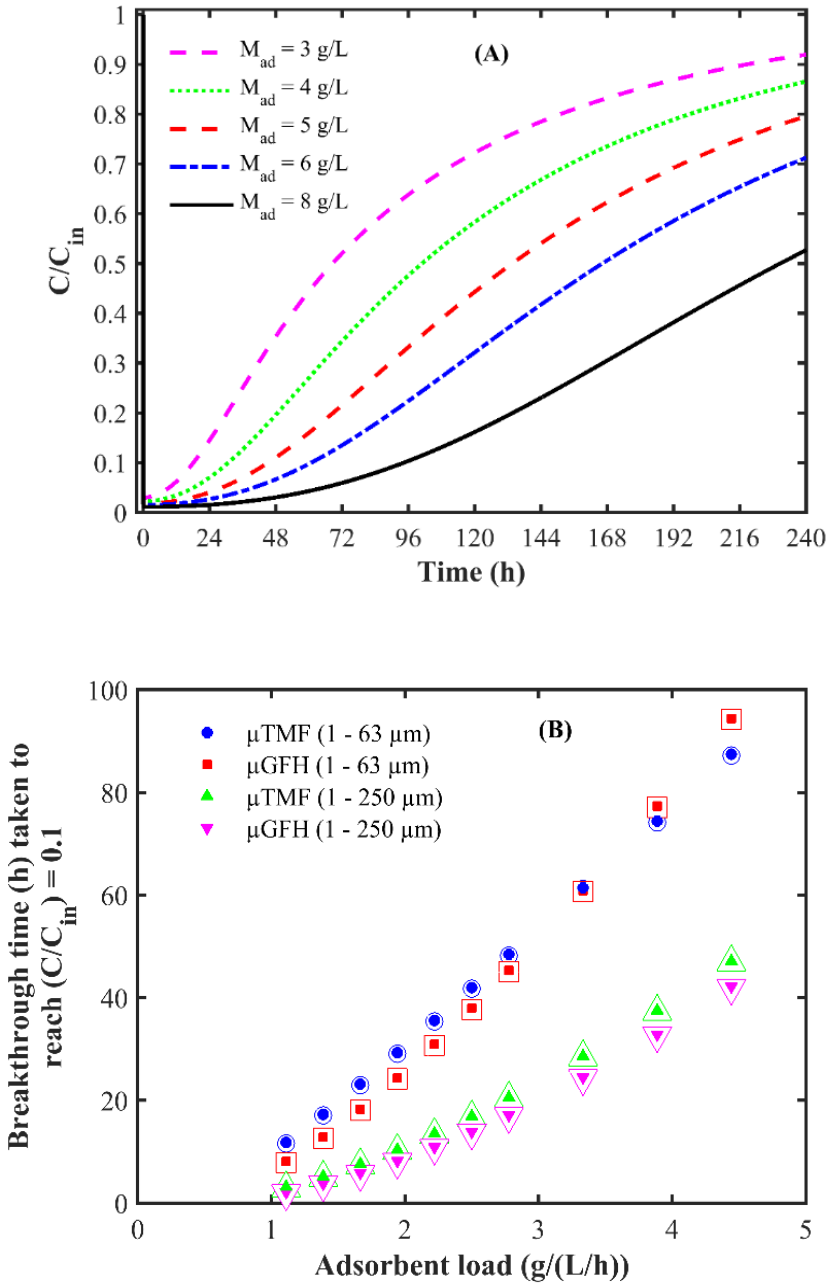

Figure 6.8. (A) Model prediction for As(V) removal using µGFH (1 – 63 µm) at C_{in}= 380 µg/L, adsorbent dosage and membrane flux= 100 L/(m^2·h); **(B)** Simulated effect of adsorbent load on breakthrough time of 0.1 for two particle size fractions of µGFH and µTMF. Small filled solid symbols represents the results at 200 L/(m^2·h), whereas large unfilled solid symbols at 100 L/(m^2·h).

The model simulations show a linear relationship between the breakthrough time and adsorbent load. This relationship is almost indistinguishable for the hybrid membrane system at varying residence times and iron oxyhydroxides dose. This implies that with a same particle size fraction,

longer times of higher As(V) removal (90%) can be achieved either at a higher adsorbent dose with smaller residence times or at lower adsorbent dosages with larger residence times. A minimum of one adsorbent load is necessary to achieve 90% removal using iron oxyhydroxides in the SMAHS.

7 Fine-grained arsenic adsorbents as dynamic membrane forming materials

The powdered-sized fraction (1-63 µm) of fine-grained iron oxyhydroxides have profound effect on As(V) adsorption rate (Figure 6.2(B)). This particle size fraction of iron oxyhydroxide-based adsorbents might be applied to form pre-deposited DMs to provide new insights into the use of powdered-sized iron oxyhydroxides as DM forming materials for remediation of arsenic polluted water. Hence, pre-deposited DM was formed *in-situ* by filtering slurry of powdered-sized adsorbents (1 - 63 µm) in ultrapure water at 0.5 bar applied pressure prior to the introduction of the arsenic contained feed solution. In chapter 7.2, the application of powdered-sized µGFH and µTMF pre-deposited DM was investigated in the MF process. The special attention was given to membrane water flux, amount of pre-deposited material per unit area of primary MF membrane, and arsenic feed concentration to find the best-operating conditions for optimum arsenic removal (Chapter 7.3). Moreover, the experimentally determined As(V) removal rates were then modeled using a mathematical model based on the HSDM and adsorbate mass balance over the DM filter (discussed in Chapter 7.1).

Selected contents of this chapter have been published in collaboration with Ioannis A. Katsoyiannis, and M. Ernst: Journal of Chemical Technology and Biotechnology 2021. (Usman et al. 2021): https://doi.org/10.1002/jctb.6728

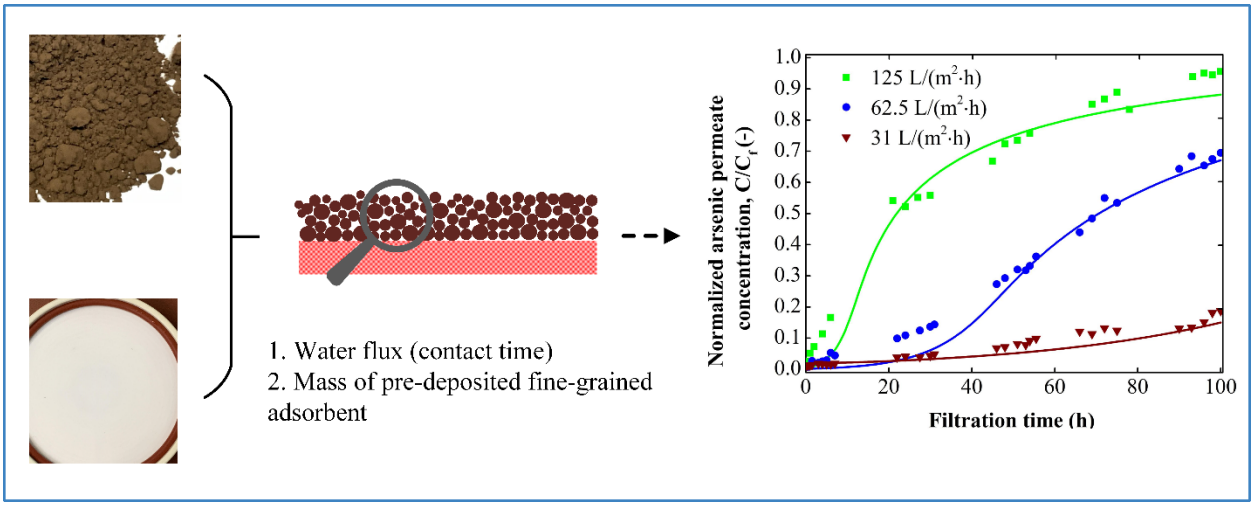

7.1 Formulation of mathematical model

The mass balance over an infinitesimal element of the pre-deposited DM filter in linear coordinates (z) is:

$$\varepsilon_B \frac{\partial C}{\partial t} + v_f \frac{\partial C}{\partial z} - \frac{3\,(1-\varepsilon_B)}{R} k_f\,(C - C_s) = 0 \qquad (7\text{-}1)$$

In Eq. 7-1, time is represented by t, filter velocity is represented by v_f, cake layer porosity is represented by ε_B, particle radius is represented by R, mass transfer coefficient due to the external film diffusion is represented by k_f, adsorbate liquid-phase concentrations in the pre-deposited iron oxyhydroxides layer and at the particle external surface are represented by C and C_s, respectively. In Eq. 7-1, the first term represents the mass in the void fraction (pores), the second term reflects solute entering and exiting the element by advective transport, and the last term represents the sink, i.e., the mass of solute adsorbed by the adsorbent grains. The more details can be found elsewhere (Sontheimer 1988; Sperlich et al. 2008).

This model differs from the former one (discussed in Chapter 6). The adsorbent pre-deposited DM filter act as a fixed-bed adsorption filter, where each adsorbent particle in the adsorbent cake layer accumulates adsorbate such as As(V) from the percolating feed solution as long as the state of equilibrium is not reached. This equilibration process proceeds successively, layer by layer, from the filter inlet to the filter outlet. Moreover, the adsorption process in a pre-deposited DM filter is a time- and distance-dependent process, whereas adsorption in a slurry reactor od the SMAHS is only a time-dependent process.

For model solution, a desktop software FAST 2.0 (Fixed-bed Adsorption Simulation Tool, http://www.fast-software.de/) developed by Sperlich et al. (2008) was applied. This software provides a numerical solution of Eqs. 7-1 and 2-15 to simulate the concentration profiles of anion over time of a fixed-bed adsorption filter packed with an adsorbent used in water treatment.

7.2 Dynamic membrane for As(V) removal

Figure 7.1 shows the normalized As(V) concentration in the permeate of DM filtration and a function of the volume of water treated for two iron oxyhydroxide materials as DM forming materials at pH 8 ± 0.1.

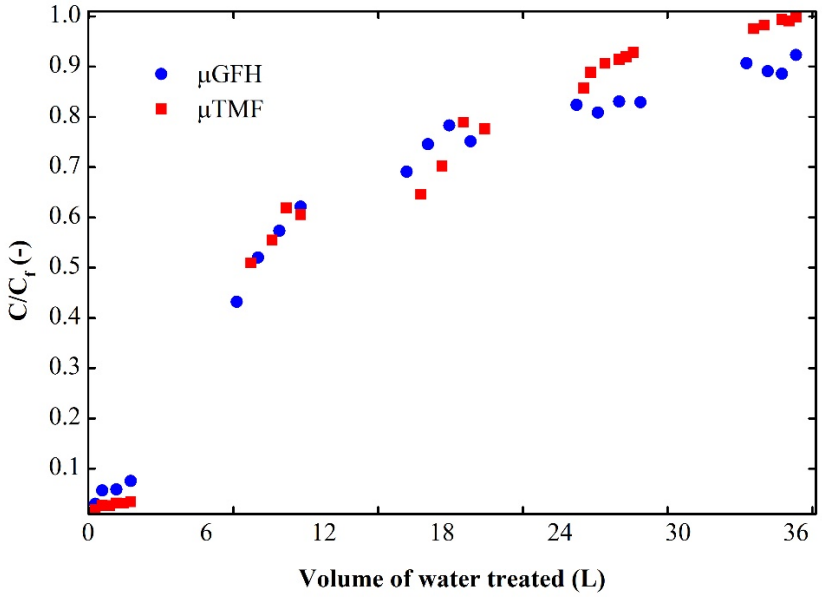

Figure 7.1. Normalized permeate concentrations of As(V) as a function of volume of water treated by dynamic membrane formed with μGFH and μTMF microparticles at 125 L/(m^2·h), amount of iron oxyhydroxides at 10.4 mg/cm^2, feed As(V) concentration= 380 μg/L and pH= 8.

At constant water flux 125 L/(m^2·h) and amount of iron oxyhydroxide pre-deposited per unit area of primary material 10.4 mg/cm^2, the results show that DM results in an immediate decrease in normalized As(V) permeate concentration with the As(V) concentration reaching a minimum value. DM achieved very high As(V) removal efficiency (90% which corresponds to C/C$_f$ = 0.1) for the first 3 L volume of water treated. After which the normalized As(V) permeate concentration starts to raise with an increasing volume of water treated (Figure 7.1). As the volume of water treated increases, the deposited iron oxyhydroxide layer will be saturated because of the continuous inflow of arsenic-contaminated feed solution, which causes the arsenic permeate concentration to rise. In case of μTMF formed DM, increase in normalized As(V) permeate concentration is slower than μGFH deposited layer, even though the achieved As(V) adsorption capacity of μTMF (15.4 μg/mg) is lower than μGFH (22.4 μg/mg) at 380 μg/L and pH 8. This is most likely due to the smaller particle size of μTMF even though the specific surface area and IEP of μTMF is lower than μGFH. The second explanation might be a large pore volume and mean pore diameter of μTMF, due to which the As(V) removal rate by μTMF pre-deposited layer was more rapid. A similar trend of As(V) removal rates by μTMF and μGFH was observed during As(V) batch adsorption tests carried out in slurry reactor setup (Figure 6.2(B)). As the volume of water treated water increases, the normalized As(V) permeate concentration has started to increase. Interestingly, an increase in normalized As(V) concentration was rapid in case of μTMF pre-deposited layer after 20 L of water treated. This is due to fact that the adsorption process is restricted to a limited number of available adsorption sites, the more active sites would have been consumed at the beginning of the process in case of μTMF. At the final stage of the process, remaining active sites of μTMF was consumed by As(V) at a faster rate than μGFH. Moreover,

the adsorption capacity of µTMF is smaller than µGFH, due to which recorded normalized concentration of As(V) to ≈ 1 has occurred at the end of the experiment (≈ 0.9 in case of µGFH) when 35 L of the volume of water was treated.

From the above discussion, it can be concluded that the iron oxyhydroxide pre-deposited DM lifetime depends on the type of DM forming material, micro-pores and particle size of the deposited material as well as on specific surface area which determines the number of active energy sites and the accessibility of the pollutant to the adsorbent material (Crittenden et al. 2012).

7.3 Modeling arsenic removal rates in permeate of a dynamic membrane microfilter

The model input parameters include Freundlich constants, intraparticle surface diffusion coefficient (D_s) and readily available mass related quantities. Feed volumetric flow rates are in the range of 1.5 – 6 mL/min at corresponding membrane water fluxes of 31, 62 and 125 L(m^2·h) and it was expected that the mass transfer due to external film diffusion would also control the arsenic adsorption process along with surface diffusion mass transfer during filtration of arsenic contaminated water passing through the thin cake layers (DM) of adsorbents deposited on the surface of the primary membrane. Accordingly, D_s value determined in Chapter 6.2 were used and optimum k_f value as evaluated through a constant optimization procedure until SSE (Eq. 6-4) was minimized. The SSE reflects the bias between the experimental and the simulated results. SSE value close to zero describes the low bias, whereas larger values indicate relatively higher bias between the experiment data and model output.

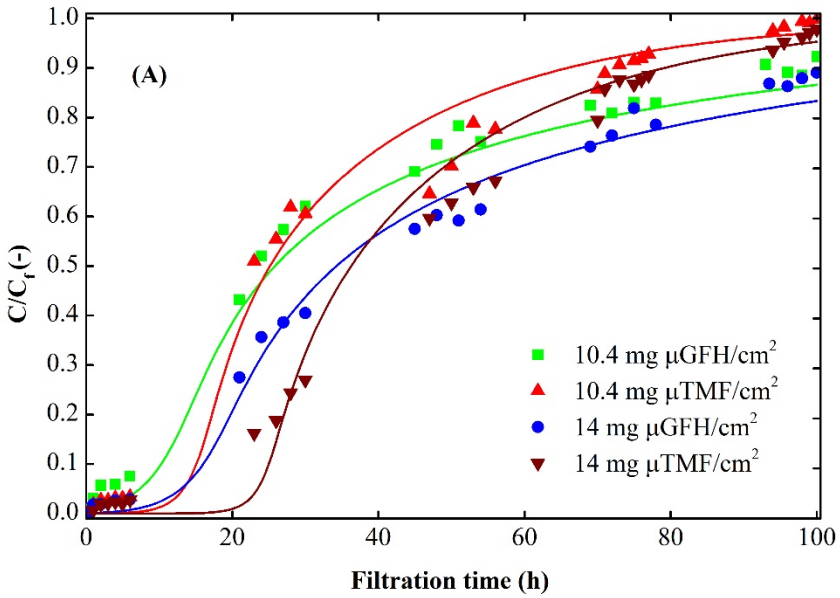

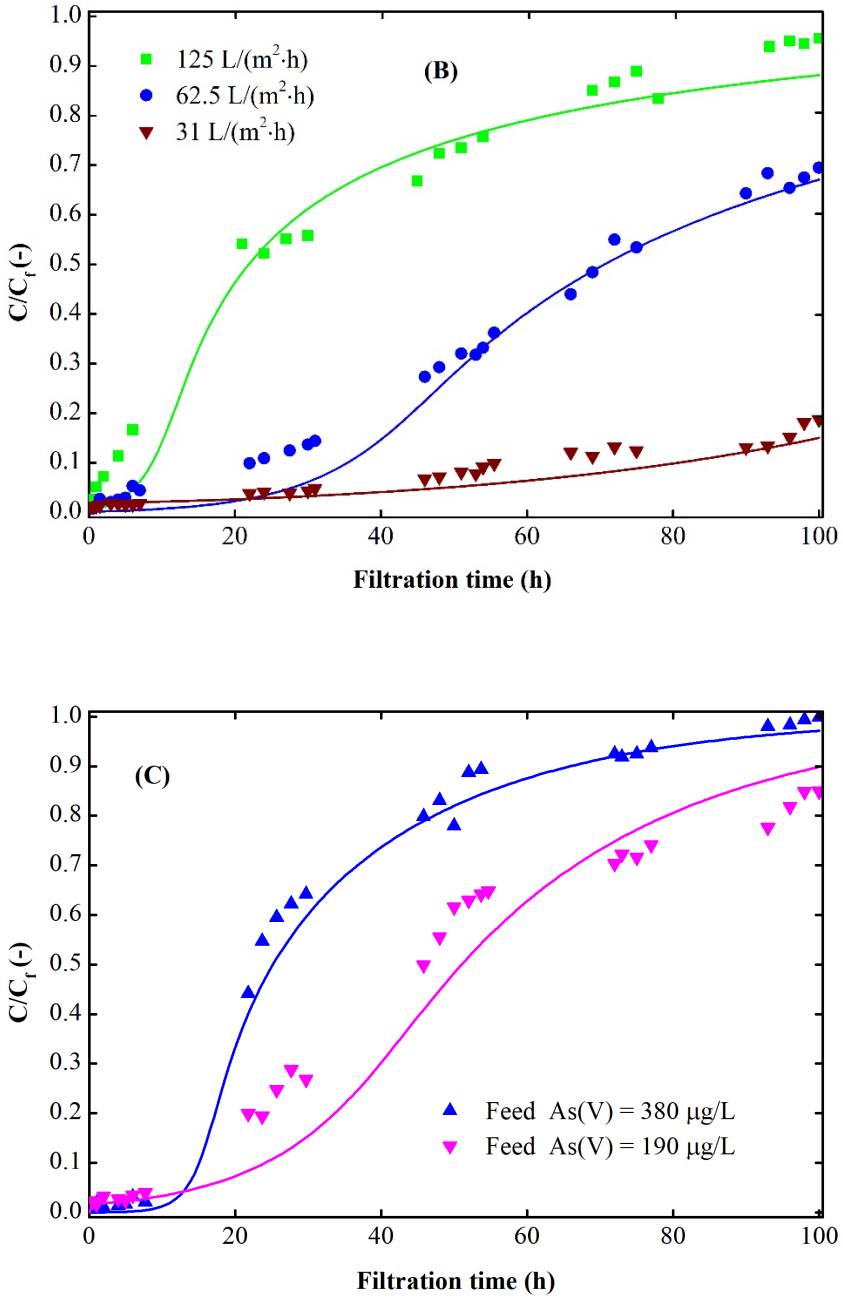

Figure 7.2. Model prediction of As(V) removal rates at pH 8 representing influence of **(A)** amount of µTMF and µGFH deposited per unit area of primary membrane; **(B)** membrane water flux for µGFH pre-deposited DM; **(C)** feed As(V) concentration onto µTMF dynamic membrane. Solid symbols reflect experimental data points, whereas model predictions are represented by solid lines at corresponding operating conditions.

The model fit to the experimental data is good (Figure 7.2) as evident from the high correlation (R^2) values and SSE values < 1 (Table 7.1). Figure 7.2 shows permeate As(V) concentration profiles along with the model predictions for the two iron oxyhydroxide formed DMs expressed

as C/C_f over the filtration time. The evaluated model parameters under different operating conditions are summarized in Table 7.1. Using the D_s values determined at As(V) concentration of 380 µg/L and same pH in ultrapure water, it is evident that the model can accurately predict the As(V) removal rates at varying amounts of iron oxyhydroxide pre-deposited per unit area of the primary membrane and membrane fluxes, which determine the contact time between the iron oxyhydroxides pre-deposited layer and feed solution. This is most likely due to the same concentration of arsenic applied in batch and continuous mode experiments. However, at lower feed As(V) concentration of 190 µg/L, the model tends to slightly over predict the As(V) removal rates as evident by low correlation (R^2) and high SSE values.

Table 7.1. The estimated parameters at different operating conditions.

Material	J ($L/m^2 \cdot h$)	M_a (mg/cm^2)	C_f (µg/L)	Volume of water treated (L)	Final As(V) concentration C/C_f(-)	D_s (x 10^{-18} m^2/s)	k_f (x 10^{-6} m/s)	R^2	SSE
µGFH	31	10.4	380	9	0.15	1.09	0.3	0.963	0.016
	62.5	10.4	380	18	0.67	1.09	1.0	0.995	0.042
	125	10.4	380	36	0.87	1.09	1.7	0.998	0.031
	125	14.0	380	36	0.83	1.09	1.8	0.993	0.027
	125	10.4	190	36	0.77	1.09	1.0	0.977	0.142
µTMF	31	10.4	380	9	0.21	2.26	0.07	0.980	0.019
	62.5	10.4	380	18	0.85	2.26	0.2	0.995	0.046
	125	10.4	380	36	0.98	2.26	1.0	0.998	0.029
	125	14.0	380	36	0.95	2.26	1.0	0.994	0.054
	125	10.4	190	36	0.90	2.26	0.3	0.974	0.169

Note. M_a is the amount of pre-deposited adsorbent per unit area of the primary MF membrane.

The fitted k_f values decreased significantly with decreasing membrane flux for both iron oxyhydroxide materials. This is possible due to lower amount of arsenic entering into membrane filtration cell per unit time and subsequently, leads to reduce As(V) mass transfer from liquid to solid (adsorbed) phase. Moreover, the k_f values were found to be higher for µGFH at same operating conditions. Large fitted k_f values for µGFH might be due to its higher adsorption capacity towards As(V) than µTMF. These results are in agreement to the results of

Kalaruban et al. (2018a), who has achieved larger k_f values for adsorbents with higher adsorbent capacity during adsorption of nitrate onto commercially available and laboratory prepared anion exchange resins in an adsorption-membrane hybrid process. A higher mass transfer at the external surface of material provides a larger sink for the target pollutant.

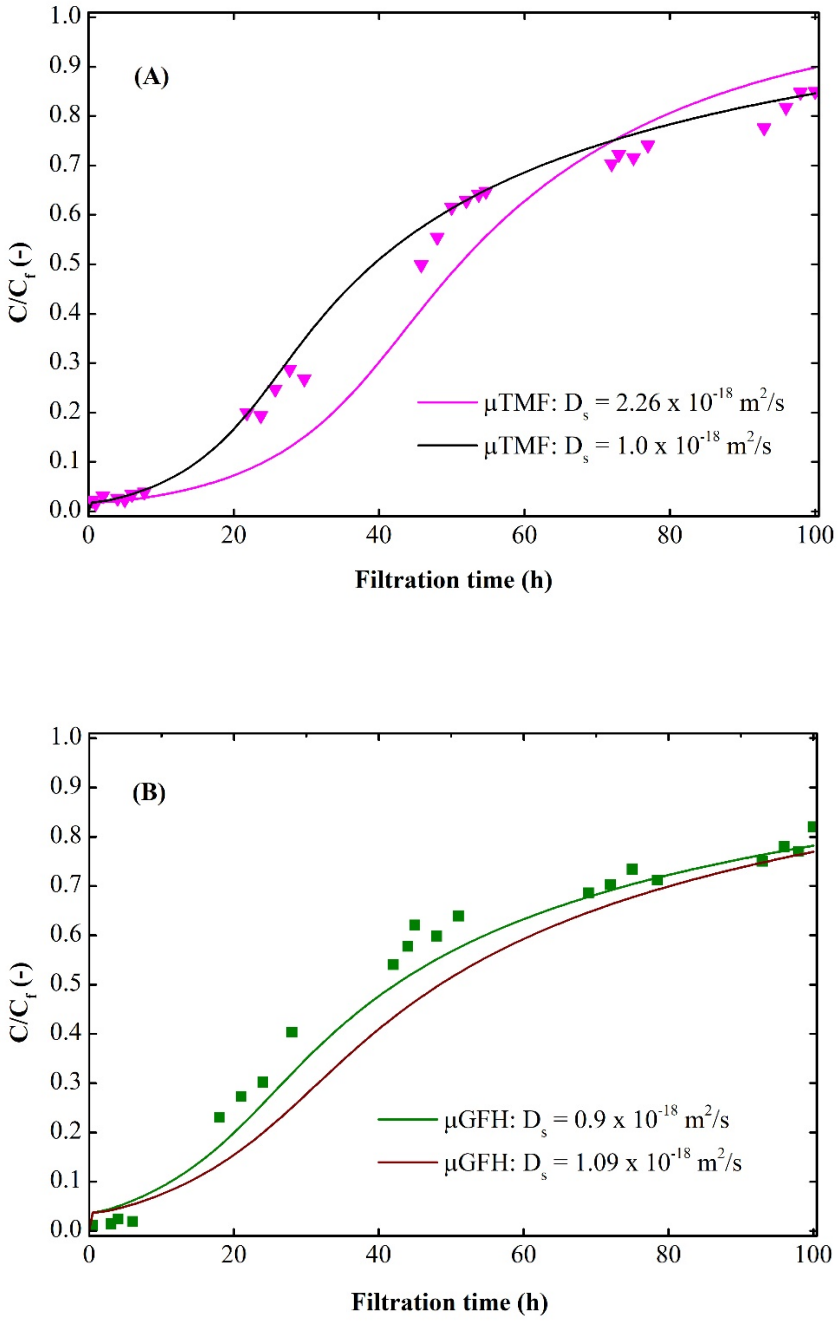

Figure 7.3. Model simulations of normalized As(V) concentrations employing different values of Ds for **(A)** μTMF pre-deposited DM; **(B)** μGFH pre-deposited DM. Experimental conditions: C_f = 190 μg/L, pH = 8 and membrane water flux = 125 L/(m^2·h).

At lower As(V) feed concentration of 190 µg/L, it can be seen from Table 7.1 that the SSE value is 0.142 for µGFH and 0.169 for µTMF, demonstrating that the mathematical model is fairly consistent with the experimental data but unable to describe accurately the experimentally determined arsenic removal rates. The possible reason for higher SSE values between experimental and model results at different feed As(V) concentrations is that D_s value applied in modeling approach was determined at higher As(V) concentration of 380 µg/L in batch mode experiments. When optimum values of D_s are applied in modeling approach, a strong agreement was observed as indicated by improved goodness of fit parameters (R^2=0. 99 and SSE = 0.043 for µGFH pre-deposited DM and R^2= 0.996 and SEE = 0.028 for µTMF pre-deposited DM).

Several model simulations are shown in Figure 7.3 employing values of D_s up to an order of magnitude lower. As it can be clearly seen that model simulations captures the experimental data points much better when the fitted values of D_s were decreased from 2.26 x 10^{-18} m^2/s to 1 x 10^{-18} m^2/s and 1.09 x 10^{-18} m^2/s to 0.9 x 10^{-18} m^2/s for µTMF and µGFH, respectively. The variation in D_s values might be because of the surface-loading dependence. The dependence of D_S on the surface loading may occur in the case of energetically heterogeneous adsorbents like µGFH and µTMF, and can be explained by the decrease of the adsorption energy with increasing surface loading that leads to an increase of adsorbate mobility (Worch 2012).

8 Conclusion

This final chapter summarizes the major conclusions drawn in the individual chapters of this thesis and highlights future research directions (Chapter 8.1). In closing, final remarks and implications for practice in the real world are provided in Chapter 8.2.

8.1 Conclusions and outcomes

Characterization and arsenic adsorption efficiency of applied fine-grained iron oxyhydroxides (Chapter 4)

Chapter 4.1 investigates the physicochemical properties of two applied akaganéite and feroxyhyte-based fined grained iron oxyhydroxides namely µGFH and µTMF, respectively.

- µGFH is produced from a ferric chloride solution by neutralization and precipitation with sodium hydroxide. It consists of akagenéite with an iron content 60% w/w on a dry basis, a mean particle size of 78.4 µm, a specific surface area of 283 ± 3 m^2/g, pore volume 0.28 mL/g, mean pore diameter 2.6 nm, pH at isoelectric point of 8 (Naeem et al. 2007), and around 50% w/w of moisture.
- The preparation of TMF involves the co-precipitation of $FeSO_4$ and $KMnO_4$. TMF is identified as feroxyhyte (Tresintsi et al. 2013b), with an iron content 44% w/w on a dry basis, a mean particle size of 40 µm, a specific surface area 178 ± 8 m^2/g, pore volume 0.35 mL/g, mean pore diameter 3.2 nm, pH at isoelectric point of 7.2 ± 0.1 (Tresintsi et al. 2013b), and less than 5% moisture.
- Compared to µGFH, µTMF has a smaller BET surface area, lower pH_{IEP} and iron content but larger mean pore diameter and smaller mean particle size of it than µGFH might play an important role on arsenic adsorption kinetics. Regarding the BET surface area of the adsorbents, the higher specific surface of µGFH might contribute to the higher adsorption capacity of arsenic under true equilibrium conditions, acting synergistically to the very high Fe content.

Chapter 4.2 focuses on investigating the effect of solution pH on the extent of arsenic adsorption through batch tests utilizing µGFH and µTMF as adsorbents. As the solution pH controls the net surface charge of the adsorbents.

- The value of solution/equilibrium pH was found to be the factor that has the most impact on the As(V) adsorption by both applied iron oxyhydroxides. This is associated with the surface charge characteristics of an adsorbent and As(V) species. As pH_{IEP} of µGFH and µTMF lies at 8 and 7.2, respectively; As(V) adsorption diminishes with increasing pH due to the decrease in net positive surface charge on the adsorbent. As(V) species are influenced by changes in pH value. As the equilibrium pH rises, divalent $HAsO_4^{2-}$ gradually predominates in the equilibrium solution in proportion to monovalent $H_2AsO_4^-$ and consequently, divalent As(V) consumes two

active sites in the adsorption process on adsorbent's surface compared to monovalent As(V), which takes up one active adsorption site.

- As(III) adsorption onto µGFH is unaffected by changes in pH value. This is due to the fact that As(III) species predominantly present in an aqueous medium in the pH range of 3-9 is uncharged H_3AsO_3, which cannot undergo electrostatic interaction with the adsorbent. In the case of µTMF, it is more sensitive to changes in pH value due to the mediating role of Mn(IV) that oxidizes As(III) and facilitates the adsorption of arsenic in the form of As(III) by iron atoms onto µTMF.
- Adjusting solution pH 8 to 6.5-7 may further improve the adsorption efficiency of applied iron oxyhydroxides, particularly µGFH towards As(V). Although pH control adds cost and complexity to an adsorption system, that cost may be offset by improved adsorption capacity.

Chapter 4.3 focuses on the arsenic adsorption onto applied iron oxyhydroxides in a single solute system. The chosen arsenic initial concentration of 190 µg/L reflects the concentration often found in polluted environments and the applied pH of 8 is identical to pH of HH tap water. The adsorbents were not evaluated according to their maximum adsorption capacity but to the adsorption capacity which corresponds to a residual arsenic concentration of 10 µg/L.

- Among applied isotherm models, the Freundlich isotherm model has described the arsenic equilibrium data better than the Langmuir isotherm which was identified by high R^2 (>0.98) and low chi-squared (< 1) values. The adsorption capacity (Q_{10}) of µGFH – derived by setting the Freundlich isotherm constants and residual arsenic concentration of 10 µg/L in the Freundlich isotherm equation – is 6.9 and 3.5 µg/mg for As(V) and As(III), respectively. The difference in Q_{10} value may be attributed to the stronger interaction of As(V) with the µGFH through electrostatic forces of attraction. The Q_{10} value of µTMF is 5.7 and 4.8 µg/mg for As(V) and As(III), respectively. The higher adsorption efficiency of µTMF towards As(III) is associated with the homogenous distribution of Mn(IV) into crystal unit of TMF. The improved efficiency of µTMF for As(III) demonstrates the high practical impact of µTMF over µGFH in water treatment when raw water contains a large proportion of arsenic in the form of As(III).
- Information from Gibbs free energy (ΔG°) at 20 °C indicates that the adsorption process of As(III) and As(V) onto both applied iron oxyhydroxides was spontaneous in nature.
- Information about the energy of adsorption, E (free energy change when 1 mol of the arsenic ion is transferred from infinity in the solution to the surface of the adsorbent) values calculated through the D-R isotherm suggests that the arsenic adsorption is predominantly chemical in nature.

Chapter 4.4 studies the effect of water matrix using HH tap water and NSF water to get reliable and realistic information concerning the particular adsorbents' applicability in real water treatment. It is a well-known fact that arsenic adsorption is heavily dependent on the type and concentration of different ions present in the source water. Batch adsorption results have demonstrated that the water matrix has substantial impact on the adsorption capacity of both

applied adsorbents. The impact is more substantial in NSF water matrix followed by HH tap water at equilibrium pH 8 ± 0.1. The water matric effect in the case of As(III) is higher than As(V) for both adsorbents (Figure 8.1). These obtained values of Q_{10} through batch tests can be used to estimate the adsorption efficiency or lifetime of iron oxyhydroxide-based adsorbents if applied in an integrated water treatment concept combing adsorption onto these fine-grained adsorbents and subsequent separation of arsenic loaded adsorbent particles with MF unit submerged in a slurry-bed reactor (Chapter 5.2). It can be seen that the Q_{10} values are different not only for different adsorbent–adsorbate systems but also for different water matrices.

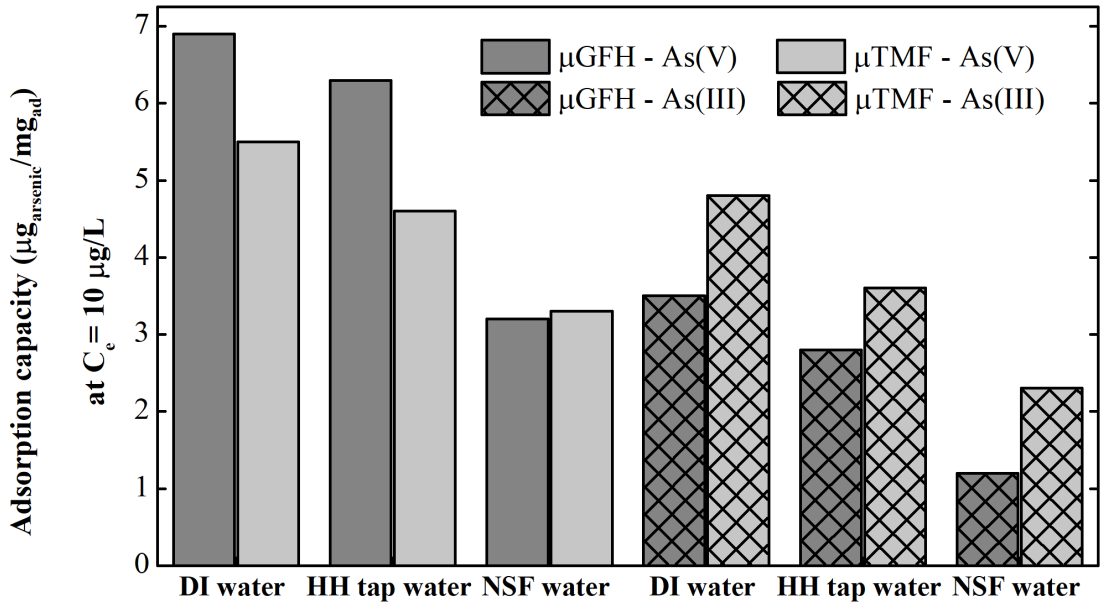

Figure 8.1. Adsorption capacity (Q_{10}) value in three different water matrices with initial arsenic concentration of 190 µg/L at pH 8 ± 0.1.

Chapter 4.5 investigates the regeneration of spent µGFH and µGFH through batch tests at varying NaOH concentrations. The regenerability is necessary to enhance the (environmental) sustainability of the overall adsorption process as well as for efficient use of resources.

- The results show that approximately 86 % of the initially bound As(V) can be desorbed with either with 0.05 or 0.1 M NaOH, which suggests arsenic adsorption is primarily reversible with very limited percentage of irreversible bonding. As(V) desorption decreases significantly at lower NaOH concentration (0.01 M), implying both longer regeneration time and lower desorption efficiency (≈ 75 %). These results suggest that the regeneration of applied iron oxyhydroxides can be an economically favorable option compared to a single use. It is expected that the adsorbents could be applied in the SMAHS for multiple operation cylces.

Application of fine-grained iron oxyhydroxides in submerged membrane adsorption hybrid system (Chapter 5)

Chapter 5.1 has assessed the importance of contact time of interaction between As(V) and adsorbents in modeled groundwater (NSF water) at pH 8 through batch tests.

- The results show that the As(V) adsorption rate increases as the contact time increases. The increase in adsorption rate was sharper for µTMF than for µGFH most probably due to its smaller particle size. The benefit of short contact time for As(V) adsorption onto µTMF was diminished with increasing contact time. Faster arsenic adsorption kinetics would favor (in terms of more volume of treatable product water produced per unit time) its application in the SMAHS at short residence times in the slurry reactor
- Adsorption reaction kinetic models were applied to gain an understanding of the adsorption process kinetics. Adsorption rate data are more accurately described by a pseudo-second-order kinetic model than a pseudo-first-order kinetic model.

Chapter 5.2 focuses on application of fine-grained iron oxyhydroxides in hybrid water treatment system consisting of adsorption in a slurry-bed reactor and liquid-solid separation by submerged MF unit for removal of As(V) from artificial groundwater.

- Both applied low-cost fine-grained adsorbents were proven to be efficient in removing As(V) from artificial groundwater for drinking water production. Within the given SMAHS set up air bubbling rate of ≥ 2 $L_{air}/(min \cdot L_{slurry})$ was necessary not only to promote the interaction between arsenic and fine-grained adsorbent but also to reach optimal conditions for the required mass transfer of As(V) in the slurry reactor. The SMAHS benefits from a higher adsorbent dose to achieve the WHO guideline value for arsenic in drinking water. The high residence time of ~ 6 h in the slurry reactor was favorable to achieve longer times of product water with arsenic permeate concentration of < 10 µg/L and subsequently, more volumes of treated product water. The results focusing on the effect of influent arsenic concentration indicates that treatable volumes of product water are inversely linked with the influent concentration of arsenic, decreasing with increasing influent concentration. However, the decreases in treatable volumes of product water per unit mass of adsorbent is maximum of 15 % at tested experimental conditions. The material costs are estimated to be as low as 0.30 € µGFH/m^3 when the SMAHS is operated at long residence time of ~ 6 h with arsenic contaminated water at pH 8.
- The Q_{10} values of µGFH and µTMF obtained through laboratory scale SMAHS in slurry-bed reactor were compared with literature Q_{10} values of GFH and TMF fixed-bed filters. The comparison suggests that adsorption efficiency of fine-grained and conventional adsorbents are in similar ranges when taken into consideration the complete difference in the two compared units including the arsenic concentration gradient in the slurry reactor.

Chapter 4.5 investigated the possibility of MgO application as a regeneration medium for arsenic adsorbents (µGFH as an example was used) using 0.05 M NaOH as regenerant. For an economic use of the regenerant, the reuse of NaOH solution is desired.

- MgO filter employing an empty bed contact time of 3 min was able to capture the arsenic-rich water coming from the slurry reactor of the SMAHS. The arsenic concentration in the effluent of MgO filter was practically zero (< 10 µg/L) even when the arsenic in the influent of the MgO filter - in the slurry reactor - was approximately 2 mg/L. Three regeneration cycles were carried out to investigate the regenerability of the µGFH as a representative of iron oxyhydroxide-based adsorbents for multiple cycles.
- The determined adsorption capacities (Q_{10} value) of the regenerated adsorbents for three sequential operation cycles were found to be 1.08, 0.83, and 0.62 µg As(V)/mg, respectively. A decrease in each operation was realized due to the continuous loss of adsorption sites in each regeneration cycle and presence of the competing ions in raw water. The outcomes suggest that spent adsorbents could be *in-situ* regenerated in the slurry reactor of a SMAHS and subsequently, the lifetime of an adsorbent in the slurry reactor can be extended. For regeneration of spent adsorbents, an adsorption filter packed with low-cost MgO – which is 100 % cheaper than the iron oxyhydroxide-based arsenic adsorbents (Tresintsi et al. 2014a), regenerant (NaOH solution), and additional investments (tanks, etc) are needed. The additional costs for regeneration should trade-off saved material costs. The cost of media replacement could be saved by *in-situ* regeneration and reuse of the adsorbent media.

Mathematical approach predicting the product water quality of a submerged membrane adsorption hybrid system (Chapter 6)

From an engineering point of view, a reliable prediction of operation time to achieve certain adsorbate removal and thus breakthrough of applied adsorbent based on easily accessible data is generally needed to design a SMAHS using slurry reactor. Chapter 6.1 focuses on the development of a mathematical model using mass transfer model such as the homogeneous surface diffusion model (HSDM) to predict the arsenic adsorption onto fine-grained adsorbent in the SMAHS. The model input parameters include the mass of adsorbent added initially added into the reactor, liquid volume in the reactor, the influent concentration of adsorbate, volumetric flow rate which governs the membrane water flux, particle size, and particle density, equilibrium adsorption constants which are obtained through equilibrium isotherm experiments and the mass transfer coefficients obtained from kinetic data of batch slurry reactor setup.

Chapter 6.2 assesses not only As(V) adsorption onto two particle size fractions of each applied fine-grained adsorbent but also focuses on identification and quantification of the mass transport processes that control the As(V) adsorption rate in slurry reactor setup.

- Two particle size fractions of µGFH and µTMF were applied in batch kinetic tests. Smaller particle size fraction (1 – 63 µm) of both iron oxyhydroxides have shown a profound effect on

As(V) adsorption kinetics. Film (k_f) and intraparticle surface diffusion (D_s) coefficients of the HSDM were derived by fitting with kinetic data of respective adsorbent and its particle size fraction. The fitted diffusion coefficients of larger (1 - 250 µm) diameter particles of µGFH and µTMF were estimated to be 1.53×10^{-16} m^2/s and 1.01×10^{-16} m^2/s, respectively. A decrease in D_s value (by two orders of magnitudes) was computed for the smaller (1 - 63 µm) particle size fraction of both adsorbents. The estimated values of surface diffusion coefficients were 1.09×10^{-18} m^2/s, and 2.26×10^{-18} m^2/s for smaller (1 - 63 µm) diameter particles of µGFH and µTMF, respectively. The results further suggest that surface diffusion is a mass transfer process that controls the overall adsorption of As(V) onto porous applied adsorbents.

Chapter 6.3 assesses the predictability of the HSDM using the input readily available parameters including the Freundlich isotherm constants and mass transfer coefficients determined in Chapter 6.2.

- The results suggested As(V) concentration in permeate of a SMAHS using suspended µGFH and µTMF (both particle size fractions) in a slurry-bed reactor can be predicted with a good agreement (Figures 6.3 and 6.4). The results further show that the developed model is capable of mathematically model As(V) adsorption by the suspended fine-grained adsorbents at varying membrane water flux and amount of adsorbent added into a reactor. It was found that the design and development of a water treatment system involving slurry-bed reactor for arsenic remediation shall take into account surface diffusion limitations.

Chapter 6.4 investigates the complete As(V) breakthrough in a SMAHS using model simulations.

- The use of smaller particle size fraction (1 – 63 µm) leads to accelerated As(V) adsorption rate than larger particle size fraction (1 – 250 µm) of both applied adsorbent. When comparing the performance of both iron oxyhydroxides in the SMAHS, µTMF elongated the time taken to a breakthrough point of 0.1 (90 % As(V) removal) by 1.3 times than that of µGFH because of fast arsenic adsorption rate. Also, the complete As(V) breakthrough of µTMF was reached earlier than µTMF for both particle size fractions which is beneficial in water treatment involving a slurry reactor. However, the breakthrough curves for As(V) onto fine-grained iron oxyhydroxide-based adsorbent were significantly different from ideal s-shaped breakthrough curve due to surface diffusion-controlled mass transfer limitations. To overcome the matter in discussion the operation of the SMAHS in cyclical on-off modes could be adopted in the future for arsenic remediation at higher membrane flux (influent flow rates). Upon restarting the operation of the hybrid system, a higher concentration gradient would exist between the bulk solution in the reactor and adsorbent surface because of adsorption at the internal adsorption sites which would reduce the adsorbent concentration in the stagnant layer around the adsorbent particle. This would lead to a short-term improvement in the arsenic adsorption rate.
- Lower operation flux shows more benefit in terms of longer times of 90 % arsenic removal because of the longer residence time between arsenic and adsorbent. This thesis shows that the effect of surface diffusion-controlled mass transfer limitations can be lowered by operating

SMAHS at low membrane flux of 20 L/(m^2·h) with a corresponding arsenic residence time of ~ 3 h.

- Like low membrane flux, large amounts of adsorbent initially added into the reactor could delay the target arsenic removal, i.e., 90 %. In initially dosed mode operation, a certain adsorbate removal efficiency can be achieved by ensuring that C/C_{in} does not exceed a specific value if the equilibrium and mass transfer coefficients are known. An adsorbent dose of 8 g/L was found optimum that could be applied for real applications in advanced water treatment.
- The model simulations have shown that a parameter so-called adsorbent load is an important process parameter that could be used to help in the selection of process design parameters for full-scale arsenic treatment systems. This thesis shows that the developed mathematical model is a useful planning tool to reduce the time and associated costs of full-scale SMAHS involving slurry-bed reactors. Further, the developed model should be used to determine process design parameters such as membrane water flux and/or influent volumetric flow rate, and volume of reactor.
- The developed model could also be used to optimize the process at different water quality parameters, e.g., pH, influent arsenic concentration, and water matric when the equilibrium and mass transfer coefficients are available.

Iron oxyhydroxide pre-deposited dynamic membrane for arsenic removal (Chapter 7)

In chapter 7, a pre-coated DM filter was built up *in-situ* at low pressure of 0.5 bar by depositing powdered-sized fractions of fine-grained iron oxyhydroxide on the primary MF membrane, wherein powdered-sized (1-63 µm) µGFH and µTMF deposited layers have acted as a filtration barrier to remove arsenic from water applied in the MF process at varying operating conditions. Experimentally determined arsenic removal rates were described by a mathematical model based on surface diffusion and external film diffusion.

Chapter 7.2 assesses the potential of powdered-sized fractions of iron oxyhydroxide with individual particle size of 3.5 µm for µGFH and 2.8 µm for µTMF as DM forming materials for arsenic remediation in water treatment. The DM shows remarkable arsenic removal efficiencies (as high as ~ 99 %).

- Microparticles (mean particle size of ~ 3 µm) of µGFH and µTMF have been proven to be emerging pre-coating materials of DMs and equally good to be applied in water treatment systems targeting arsenic remediation. Like fine-grained iron oxyhydroxide-based adsorbents application in a slurry-bed reactor of the SMAHS, adsorbing potential of µGFH and µTMF depends strongly on the particle size and mean pore diameter. Due to the larger mean pore diameter of µTMF, the full surface coverage of it was achieved earlier than a large diameter µGFH (1-63 µm). In a 4-day bench-scale filtration experiment, the adsorption sites of µTMF (1 – 63 µm) are fully covered, whereas 95% coverage was recorder for µGFH (1 – 63 µm).

Chapter 7.3 investigates the effect of different operating parameters on arsenic removal rates of a DM microfilter

- Parametric study of pre-coated DM's indicates that arsenic removal rates of DM's can be controlled by changing the membrane water flux and amount of pre-coating agent per unit area of the primary membrane. Longer filtration times with very low arsenic concentrations in the permeate of DM filter can be achieved by increasing from 10.4 mg/cm^2 to 14 mg/cm^2 of pre-coating material over the primary membrane. Similarly, lowest membrane water flux of 31 L/(m^2·h), which governs the highest contact time of interaction between the arsenic-contaminated feed solution and deposited cake layer of adsorbent, found to be the most beneficial in terms of longer filtration times with very low arsenic concentrations. Treatable volumes of water were augmented when the As(V) feed concentration was reduced from 380 µg/L to 190 µg/L.
- As(V) removal rates can be accurately predicted using the applied mathematical model based on the HSDM. The surface diffusion parameter of the HSDM can be considered as independent of membrane water flux and the amount of iron oxyhydroxide used to form pre-coated DM. Under the same operating conditions, mass transfer due to film diffusion is affected by the adsorption capacity of adsorbent. The magnitude of k_f value increases with increasing adsorption capacity.
- The outcome of this chapter suggests that low-pressure DM filtration is a sustainable and effective approach that can be applied for remediation of arsenic-contaminated waters in water treatment.

In this work, iron oxyhydroxides particles forming DM are significantly larger (one order of magnitude) than the primary membrane pores. Therefore, the primary membrane pore size was not expected to have a significant effect on the formation of pre-deposited DM. However, further research is needed to study the effect of the depositing particles on the surface morphology and strength of the primary membrane. These investigations would provide more insights into the repeating use of the primary membrane for formation and deformation of DM.

Analog to earlier provided research directions, in future research should aim to extend the DM filtration technology with repeated use of the exhausted iron-based oxyhydroxide materials to reduce the quantity of produced waste (spent adsorbent) for environmental sustainability and to obtain more information on practical applications.

In future research, iron oxyhydroxide pre-deposited DM might be considered for removal of other oxyanions forming toxic metals (vanadium, chromium, selenium, antimony, and uranium) because of higher adsorption efficiency of iron oxyhydroxides towards these environmental pollutants (Hilbrandt et al. 2019a; Hilbrandt et al. 2019b; Kalaitzidou et al. 2019; Naeem et al. 2007; Simeonidis et al. 2017).

8.2 Final remarks and implications for practice

This work proposes the application of fine-grained iron oxyhydroxide as arsenic adsorbents in an integrated water treatment concept combining adsorption and an MF unit. The outcomes of this thesis confirm that micro-sized iron oxyhydroxides, by-products of conventional adsorbent

production processes, can successfully be employed in the proposed hybrid membrane process to achieve drinking water guideline value for arsenic without considerable fouling of the submerged MF membrane under tested experimental conditions. This thesis suggests that either groundwater or drinking water purification are the potential applications of the SMAHS involving the use of fine-grained adsorbents in a slurry reactor. The use of µGFH over µTMF should be considered when raw water contains larger percentages of pentavalent arsenic in the pH range of 3-8, whereas µTMF should be preferred for raw water with a large proportion of trivalent arsenic. The SMAHS permits the use of powdered-sized fractions (individual particle size of ~ 3 µm) of applied adsorbents. This is remarkable considering almost half of µGFH particles are smaller than 10 µm particles. The SMAHS not only allows employment of powdered-sized fractions of µGFH but also leads to much sharper breakthrough curves (close to ideal s-shaped breakthrough curves) with longer filtration times of very low arsenic concentration in the permeate of the SMAHS.

Fixed-bed adsorption filter packed with various adsorbents including GFH and its counterpart (Bayoxide, E33) is a well-established water treatment process demanding less labor and low operation costs. The SMAHS could potentially be a strong competitor as an arsenic remediation process as both hybrid system and fixed-bed adsorption filters are dynamic and continuous flow water treatment systems. The SMAHS using low-cost adsorbents (µGFH is currently five times cheaper than GFH) offers simultaneous removal of microorganisms and colloids as an advantage over the fixed-bed filter. However, the SMAHS requires an additional pump for sucking product water as well as air supply which adds to more energy demand and accordingly, higher costs for product water. This thesis further indicates that the SMAHS might be preferred over fixed-bed filters when raw water is polluted with elevated concentrations of arsenic. The adsorption capacity at guideline value of 10 µg/L of employing adsorbent is almost the same when influence parameters such as water quality parameters (water matrix and pH) are taken into account.

The fine grains of the spent adsorbent could be *in-situ* regenerated without compromising environmental sustainability and reused in the slurry reactor without removing them from the reactor. This thesis indicates that the life of the adsorbent material could be significantly extended by *in-situ* regeneration of the spent adsorbent. Accordingly, the need for the new adsorbent material could be decrease, which indicates that the *in-situ* regeneration process with the MgO adsorption filter is an economically viable option that should be considered in full-scale arsenic treatment system involving a slurry reactor.

Applying sufficient aeration to the adsorbent suspension keeps the adsorbent particles completely dispersed in the slurry reactor and helps to reduce the solid deposition on the membrane surface by the air scouring effect. Both applied fine-grained performed better at longer residence times in the slurry reactor of the SMAHS/ lower membrane water flux. However, longer residence times in real water treatment systems involving a slurry reactor would increase the footprint installations and overall operation costs would thus be high. This might overshadow the advantage of the application of low-cost adsorbents in the SMAHS. Short residence times offer large volumes of treatable product water, which decreases the operations costs but, in this case, the optimum

adsorption efficiency of adsorbent was not fully utilized. Therefore, a trade-off should be considered between footprint installations and adsorbate residence time in the reactor.

Moreover, hydrodynamic conditions in the reactor provided to help alleviate the membrane fouling and constrain particle deposition due to permeation drag should be controlled and under strong aeration, breakage (puncture) of individual membrane fibers might occur due to excessive membrane movement in the reactor. Moreover, as the membrane is submerged in the slurry reactor, therefore any unexpected water quality together with strong aeration might damage the membrane. Installment of pretreatment processes such as rapid sand filters might be considered. Extra care should be given for the operation of SMAHS especially when the water quality fluctuations are high.

In conclusion, the application of fine-grained adsorbents (µGFH and µTMF) in a slurry reactor of the SMAHS is a viable option for arsenic remediation in water treatment due to their fast kinetics, affordability, especially in the developing countries and high adsorption capacity. In addition to these benefits, spent adsorbent could be *in-situ* regenerated and reused in an integrated approach that leads to a more environmental sustainability and resource efficient process. This thesis has contributed to arsenic remediation technologies by introducing an innovative integrated water treatment process that is a potentially strong counterpart of conventional fixed-bed adsorption filter under optimized operating conditions.

References

Abejón A, Garea A, Irabien A (2015) Arsenic removal from drinking water by reverse osmosis: Minimization of costs and energy consumption. Separation and Purification Technology 144:46–53. https://doi.org/10.1016/j.seppur.2015.02.017

Aghili F, Ghoreyshi AA, Rahimpour A, Rahimnejad M (2017) Coating of mixed-matrix membranes with powdered activated carbon for fouling control and treatment of dairy effluent. Process Safety and Environmental Protection 107:528–539. https://doi.org/10.1016/j.psep.2017.03.013

Akhondi E, Zamani F, Tng K, Leslie G, Krantz W, Fane A, Chew J (2017) The performance and fouling control of submerged hollow fiber (HF) systems: A Review. Applied Sciences 7:765. https://doi.org/10.3390/app7080765

Al-Abed SR, Jegadeesan G, Purandare J, Allen D (2007) Arsenic release from iron rich mineral processing waste: Influence of pH and redox potential. Chemosphere 66:775–782. https://doi.org/10.1016/j.chemosphere.2006.07.045

Amy GL (2005) Adsorbent treatment technologies for arsenic removal. AWWA Research Foundation [and] American Water Works Association, Denver, CO

Anantharaman A, Chun Y, Hua T, Chew JW, Wang R (2020) Pre-deposited dynamic membrane filtration - A review. Water Res 173:115558. https://doi.org/10.1016/j.watres.2020.115558

Asere TG, Stevens CV, Du Laing G (2019) Use of (modified) natural adsorbents for arsenic remediation: A review. Science of the Total Environment 676:706–720. https://doi.org/10.1016/j.scitotenv.2019.04.237

AWWARF A (1993) Research Foundation. NOM Adsorption onto Iron Oxide-coated Sand, AWWA, Denver, Colorodo

Badruzzaman M, Westerhoff P, Knappe DRU (2004) Intraparticle diffusion and adsorption of arsenate onto granular ferric hydroxide (GFH). Water Research 38:4002–4012. https://doi.org/10.1016/j.watres.2004.07.007

Bahr C (2012) Entfernung von Uran aus Trinkwasser durch Adsorption an Granuliertem Eisenhydroxid (GEH). Doctoral Thesis, Technische Universität Berlin, Fakultät III - Prozesswissenschaften

Banerjee K, Nour S, Selbie M, Prevost M, Blumenschein CD, Chen HW, Amy GL (2003) Optimization of process parameters for arsenic treatment with granular ferric hydroxide. In: Proceedings of the AWWA Annual Conference, Anaheim, CA, USA, pp 15–19

Banerjee K, Amy GL, Prevost M, Nour S, Jekel M, Gallagher PM, Blumenschein CD (2008) Kinetic and thermodynamic aspects of adsorption of arsenic onto granular ferric hydroxide (GFH). Water Research 42:3371–3378. https://doi.org/10.1016/j.watres.2008.04.019

Barrett EP, Joyner LG, Halenda PP (1951) The Determination of Pore Volume and Area Distributions in Porous Substances. I. Computations from Nitrogen Isotherms. Journal of the American Chemical society 73:373–380. https://doi.org/10.1021/ja01145a126

Bhatnagar A, Sillanpää M (2011) A review of emerging adsorbents for nitrate removal from water. Chemical Engineering Journal 168:493–504. https://doi.org/10.1016/j.cej.2011.01.103

Bolisetty S, Reinhold N, Zeder C, Orozco MN, Mezzenga R (2017) Efficient purification of arsenic-contaminated water using amyloid-carbon hybrid membranes. Chemical Communications 53:5714–5717

Bretzler A, Nikiema J, Lalanne F, Hoffmann L, Biswakarma J, Siebenaller L, Demange D, Schirmer M, Hug SJ (2020) Arsenic removal with zero-valent iron filters in Burkina Faso: Field and laboratory insights. Science of the Total Environment 737:139466. https://doi.org/10.1016/j.scitotenv.2020.139466

Cai B, Ye H, Yu L (2000) Preparation and separation performance of a dynamically formed MnO2 membrane. Desalination 128:247–256. https://doi.org/10.1016/S0011-9164(00)00039-4

Cai Z, Benjamin MM (2011) NOM fractionation and fouling of low-pressure membranes in microgranular adsorptive filtration. Environmental and Science Technology 45:8935–8940. https://doi.org/10.1021/es202219e

Callegari A, Ferronato N, Rada EC, Capodaglio AG, Torretta V (2018) Assessment of arsenic removal efficiency by an iron oxide-coated sand filter process. Environmental Science and Pollution Research 25:26135–26143

Campos C, Marinas BJ, Snoeyink VL, Baudin I, Lainé JM (2000) PAC-membrane filtration process. II: Model application. Journal of Environmental Engineering 126:104–111

Chang S, Waite TD, Fane AG (2003) Optimization of combined PAC adsorption-submerged membrane system for organics removal. In: Proceedings of Fifth International Membrane Science and Technology Conference, Sydney, Australia

Chang H, Liang H, Qu F, Liu B, Yu H, Du X, Li G, Snyder SA (2017) Hydraulic backwashing for low-pressure membranes in drinking water treatment: A review. Journal of Membrane Science 540:362–380. https://doi.org/10.1016/j.memsci.2017.06.077

Chen W, Parette R, Zou J, Cannon FS, Dempsey BA (2007) Arsenic removal by iron-modified activated carbon. Water Reseearch 41:1851–1858. https://doi.org/10.1016/j.watres.2007.01.052

Chen ASC, Sorg TJ, Wang L (2015) Regeneration of iron-based adsorptive media used for removing arsenic from groundwater. Water Research 77:85–97. https://doi.org/10.1016/j.watres.2015.03.004

Choi B-B, Choi Y-J, Choi J-S, Lee S, Oh H-J (2009) Energy management in submerged microfiltration systems by optimum control of aeration. Desalination 247:233–238. https://doi.org/10.1016/j.desal.2008.12.027

Chu H-q, Cao D-w, Jin W, Dong B-z (2008) Characteristics of bio-diatomite dynamic membrane process for municipal wastewater treatment. Journal of Membrane Science 325:271–276. https://doi.org/10.1016/j.memsci.2008.07.040

Chwirka JD, Thomson BM, Stomp JM (2000) Removing arsenic from groundwater. Journal - American Water Works Association 92:79–88. https://doi.org/10.1002/j.1551-8833.2000.tb08911.x

Cornelis G, Johnson CA, van Gerven T, Vandecasteele C (2008) Leaching mechanisms of oxyanionic metalloid and metal species in alkaline solid wastes: A review. Applied Geochemistry 23:955–976. https://doi.org/10.1016/j.apgeochem.2008.02.001

Cornell RM, Schwertmann U (2003) The Iron Oxides. Wiley

Crittenden JC, Trussell RR, Hand DW, Howe KJ, Tchobanoglous G (2012) MWH's Water Treatment. John Wiley & Sons, Inc, Hoboken, NJ, USA

Ćurko J, Matošić M, Crnek V, Stulić V, Mijatović I (2016) Adsorption Characteristics of Different Adsorbents and Iron(III) Salt for Removing As(V) from Water. Food Technol Biotechnol 54:250–255. https://doi.org/10.17113/ftb.54.02.16.4064

Deliyanni EA, Bakoyannakis DN, Zouboulis AI, Matis KA (2003) Sorption of As(V) ions by akaganéite-type nanocrystals. Chemosphere 50:155–163. https://doi.org/10.1016/S0045-6535(02)00351-X

Dotto GL, Salau NPG, Piccin JS, Cadaval TRS'A, Pinto LAA de (2017) Adsorption kinetics in liquid phase: Modeling for discontinuous and continuous systems. In: Adsorption Processes for Water Treatment and Purification. Springer, pp 53–76

Douven S, Paez CA, Gommes CJ (2015) The range of validity of sorption kinetic models. J Colloid Interface Sci 448:437–450. https://doi.org/10.1016/j.jcis.2015.02.053

Driehaus W (2002) Arsenic removal - experience with the GEH® process in Germany. Water Science and Technology: Water Supply 2:275–280. https://doi.org/10.2166/ws.2002.0073

Drouiche M, Lounici H, Belhocine D, Grib H, Piron D, Mameri N (2001) Economic study of the treatment of surface water by small ultrafiltration units. Water SA 27:199–204

Dubinin MM (1960) The Potential Theory of Adsorption of Gases and Vapors for Adsorbents with Energetically Nonuniform Surfaces. Chem Rev 60:235–241. https://doi.org/10.1021/cr60204a006

El-Khaiary MI (2008) Least-squares regression of adsorption equilibrium data: Comparing the options. Journal of Hazardous Materials 158:73–87. https://doi.org/10.1016/j.jhazmat.2008.01.052

Ersahin ME, Ozgun H, Dereli RK, Ozturk I, Roest K, van Lier JB (2012) A review on dynamic membrane filtration: Materials, applications and future perspectives. Bioresource Technolology 122:196–206. https://doi.org/10.1016/j.biortech.2012.03.086

Essington ME (2015) Soil and water chemistry: An integrative approach. CRC Press

Fan B, Huang X (2002) Characteristics of a self-forming dynamic membrane coupled with a bioreactor for municipal wastewater treatment. Environmental Science and Technology 36:5245–5251. https://doi.org/10.1021/es025789n

Ferguson JF, Gavis J (1972) A review of the arsenic cycle in natural waters. Water Research 6:1259–1274. https://doi.org/10.1016/0043-1354(72)90052-8

Ferrer O, Lefèvre B, Prats G, Bernat X, Gibert O, Paraira M (2015) Reversibility of fouling on ultrafiltration membrane by backwashing and chemical cleaning: Differences in organic fractions behaviour. Desalination and Water Treatment 57:8593–8607. https://doi.org/10.1080/19443994.2015.1022807

Flora SJS (2015) Arsenic: Chemistry, occurrence, and exposure. In: Handbook of Arsenic toxicology. Elsevier, pp 1–49

Foo KY, Hameed BH (2010) Insights into the modeling of adsorption isotherm systems. Chemical Engineering Journal 156:2–10. https://doi.org/10.1016/j.cej.2009.09.013

Freundlich HMF (1906) Over the adsorption in solution. J. Phys. Chem 57:1100–1107

Garelick H, Jones H, Dybowska A, Valsami-Jones E (2008) Arsenic pollution sources. Reviews of Environmental Contamination Volume 197:17–60. https://doi.org/10.1007/978-0-387-79284-2_2

Garelick H, Jones H, Dybowska A, Valsami-Jones E (2009) Arsenic pollution sources. In: Reviews of Environmental Contamination Volume 197. Springer, pp 17–60

Genz A, Kornmüller A, Jekel M (2004) Advanced phosphorus removal from membrane filtrates by adsorption on activated aluminium oxide and granulated ferric hydroxide. Water Research 38:3523–3530. https://doi.org/10.1016/j.watres.2004.06.006

Ghurye GL, Clifford DA, Tripp AR (1999) Combined arsenic and nitrate removal by ion exchange. Journal - American Water Works Association 91:85–96. https://doi.org/10.1002/j.1551-8833.1999.tb08718.x

Goldberg S, Johnston CT (2001) Mechanisms of Arsenic Adsorption on Amorphous Oxides Evaluated Using Macroscopic Measurements, Vibrational Spectroscopy, and Surface Complexation Modeling. Journal of Colloidal Interface and Science 234:204–216. https://doi.org/10.1006/jcis.2000.7295

Guan X, Du J, Meng X, Sun Y, Sun B, Hu Q (2012) Application of titanium dioxide in arsenic removal from water: A review. Journal of Hazardous Materials 215-216:1–16. https://doi.org/10.1016/j.jhazmat.2012.02.069

Gude JCJ, Rietveld LC, van Halem D (2017) As(III) oxidation by MnO_2 during groundwater treatment. Water Research 111:41–51. https://doi.org/10.1016/j.watres.2016.12.041

Guha Mazumder D, Dasgupta UB (2011) Chronic arsenic toxicity: Studies in West Bengal, India. Kaohsiung Journal of Medical Science 27:360–370. https://doi.org/10.1016/j.kjms.2011.05.003

Hall KR, Eagleton LC, Acrivos A, Vermeulen T (1966) Pore- and solid-diffusion kinetics in fixed-bed adsorption under constant-pattern conditions. Industrial and Engineering Chemistry Fundamentals 5:212–223. https://doi.org/10.1021/i160018a011

Hashlamon A, Mohammad AW, Ahmad A (2017) The effect of wastewater pretreatment on nanofiltration membrane performance. Journal of Water Reuse and Desalination 7:45–52. https://doi.org/10.2166/wrd.2016.083

Henke KR (2009) Arsenic: Environmental chemistry, health threats and waste treatment / by Kevin Henke, David Atwood, Lisa Blue. Wiley-Blackwell, Oxford

Herawati N, Suzuki S, Hayashi K, Rivai IF, Koyama H (2000) Cadmium, copper, and zinc levels in rice and soil of Japan, Indonesia, and China by soil type. Bulletin of Environmental Contamination and Toxicology 64:33–39. https://doi.org/10.1007/s001289910006

Hering JG, Katsoyiannis IA, Theoduloz GA, Berg M, Hug SJ (2017) Arsenic Removal from Drinking Water: Experiences with Technologies and Constraints in Practice. J. Environ. Eng. 143:3117002. https://doi.org/10.1061/(ASCE)EE.1943-7870.0001225

Hilbrandt I, Ruhl A, Jekel M (2018) Conditioning fixed-bed filters with fine fractions of granulated iron hydroxide (μGFH). Water 10:1324. https://doi.org/10.3390/w10101324

Hilbrandt I, Shemer H, Ruhl AS, Semiat R, Jekel M (2019a) Comparing fine particulate iron hydroxide adsorbents for the removal of phosphate in a hybrid adsorption/ultrafiltration system. Separation and Purification Technology 221:23–28. https://doi.org/10.1016/j.seppur.2019.03.044

Hilbrandt I, Ruhl AS, Zietzschmann F, Molkenthin M, Jekel M (2019b) Competition in chromate adsorption onto micro-sized granular ferric hydroxide. Chemosphere 218:749–757. https://doi.org/10.1016/j.chemosphere.2018.11.152

Hindmarsh JT, McCurdy RF (1986) Clinical and environmental aspects of arsenic toxicity. CRC Critical Reviews in Clinical Laboratory Sciences 23:315–347. https://doi.org/10.3109/10408368609167122

Hobson JP (1969) Physical adsorption isotherms extending from ultrahigh vacuum to vapor pressure. The Journal of Physical Chemistry 73:2720–2727. https://doi.org/10.1021/j100842a045

Hu Y, Wang XC, Tian W, Ngo HH, Chen R (2016) Towards stable operation of a dynamic membrane bioreactor (DMBR): Operational process, behavior and retention effect of dynamic membrane. Journal of Membrane Science 498:20–29. https://doi.org/10.1016/j.memsci.2015.10.009

Huang H, Schwab K, Jacangelo JG (2009) Pretreatment for low pressure membranes in water treatment: A review. Environmental Science and Technology 43:3011–3019. https://doi.org/10.1021/es802473r

Huang Y-H, Shih Y-J, Cheng F-J (2011) Novel $KMnO_4$-modified iron oxide for effective arsenite removal. Journal of Hazardous Materials 198:1–6. https://doi.org/10.1016/j.jhazmat.2011.10.010

Jekel M, Czekalla C (eds) (2017) Wasseraufbereitung - Grundlagen und Verfahren: DVGW Lehr- und Handbuch Wasserversorgung Band 6, 2nd edn. DVGW Lehr- und Handbuch Wasserversorgung, vol 6. Deutscher Industrieverlag, München

Jia Y, Wang R, Fane AG (2009a) Hybrid PAC-submerged membrane system for trace organics removal. Chemical Engineering Journal 155:155–160. https://doi.org/10.1016/j.cej.2009.07.032

Jia Y, Wang R, Fane AG (2009b) Hybrid PAC-submerged membrane system for trace organics removal II: System simulation and application study. Chemical Engineering Journal 149:42–49. https://doi.org/10.1016/j.cej.2008.09.044

Jia Y, Wang R, Fane A (2005) Atrazine adsorption from aqueous solution using powdered activated carbon—Improved mass transfer by air bubbling agitation. Chemical Engineering Journal. https://doi.org/10.1016/j.cej.2005.10.014

Kalaitzidou K, Nikoletopoulos A-A, Tsiftsakis N, Pinakidou F, Mitrakas M (2019) Adsorption of Se(IV) and Se(VI) species by iron oxy-hydroxides: Effect of positive surface charge density. Science of the Total Environment 687:1197–1206. https://doi.org/10.1016/j.scitotenv.2019.06.174

Kalaruban M, Loganathan P, Shim W, Kandasamy J, Vigneswaran S (2018a) Mathematical modelling of nitrate removal from water using a submerged membrane adsorption hybrid system with four adsorbents. Applied Sciences 8:194. https://doi.org/10.3390/app8020194

Kalaruban M, Loganathan P, Kandasamy J, Vigneswaran S (2018b) Submerged membrane adsorption hybrid system using four adsorbents to remove nitrate from water. Environmental Science Pollution Research 25:20328–20335. https://doi.org/10.1007/s11356-017-8905-9

Kang M, Kawasaki M, Tamada S, Kamei T, Magara Y (2000) Effect of pH on the removal of arsenic and antimony using reverse osmosis membranes. Desalination 131:293–298. https://doi.org/10.1016/S0011-9164(00)90027-4

Katsoyiannis IA, Zouboulis AI, Mitrakas M, Althoff HW, Bartel H, others (2013) A hybrid system incorporating a pipe reactor and microfiltration for biological iron, manganese and arsenic removal from anaerobic groundwater. Fresenius Environmental Bulletin 22:3848–3853

Katsoyiannis IA, Mitrakas M, Zouboulis AI (2015a) Arsenic occurrence in Europe: Emphasis in Greece and description of the applied full-scale treatment plants. Desalination and Water Treatment 54:2100–2107. https://doi.org/10.1080/19443994.2014.933630

Katsoyiannis IA, Voegelin A, Zouboulis AI, Hug SJ (2015b) Enhanced As(III) oxidation and removal by combined use of zero valent iron and hydrogen peroxide in aerated waters at neutral pH values. Journal of Hazardous Materials 297:1–7. https://doi.org/10.1016/j.jhazmat.2015.04.038

Katsoyiannis I, Zouboulis A (2002) Removal of arsenic from contaminated water sources by sorption onto iron-oxide-coated polymeric materials. Water Research 36:5141–5155. https://doi.org/10.1016/s0043-1354(02)00236-1

Khan SU, Farooqi IH, Usman M, Basheer F (2020) Energy efficient rapid removal of arsenic in an electrocoagulation reactor with hybrid Fe/Al electrodes: Process optimization using CCD and kinetic modeling. Water 12:2876. https://doi.org/10.3390/w12102876

Kim Y, Kim C, Choi I, Rengaraj S, Yi J (2004) Arsenic removal using mesoporous alumina prepared via a templating method. Environmental Science and Technology 38:924–931. https://doi.org/10.1021/es0346431

Knox RC, Canter LW (1996) Prioritization of ground water contaminants and sources. Water Air Soil Pollution 88:205–226. https://doi.org/10.1007/BF00294102

Koltuniewicz AB, Witek A, Bezak K (2004) Efficiency of membrane-sorption integrated processes. Journal of Membrane Science 239:129–141. https://doi.org/10.1016/j.memsci.2004.02.037

Laîné J-M, Vial D, Moulart P (2000) Status after 10 years of operation — overview of UF technology today. Desalination 131:17–25. https://doi.org/10.1016/S0011-9164(00)90002-X

Lakshmipathiraj P, Narasimhan BRV, Prabhakar S, Bhaskar Raju G (2006) Adsorption of arsenate on synthetic goethite from aqueous solutions. Journal of Hazardous Materials 136:281–287. https://doi.org/10.1016/j.jhazmat.2005.12.015

Langmuir I (1916) The constitution and fundamentals properties of solids and liquids. Part I. Solids. J. Am. Chem. Soc. 38:2221–2295. https://doi.org/10.1021/ja02268a002

Lebeau T, Lelièvre C, Buisson H, Cléret D, van de Venter LW, Côté P (1998) Immersed membrane filtration for the production of drinking water: Combination with PAC for NOM and SOCs removal. Desalination 117:219–231. https://doi.org/10.1016/S0011-9164(98)00101-5

Li X, Xu W, Wang S, Tang M, Shen X (2014) Effect of SO_3 and MgO on portland cement clinker: Formation of clinker phases and alite polymorphism. Construction and Building Materials 58:182–192. https://doi.org/10.1016/j.conbuildmat.2014.02.029

Li L, Xu G, Yu H (2018) Dynamic membrane filtration: Formation, filtration, cleaning, and applications. Chemical Engineering Technology 41:7–18

Liu Y, Li Q, Gao S, Shang JK (2011) Exceptional As(III) sorption capacity by highly porous magnesium oxide nanoflakes made from hydrothermal synthesis. Journal of the American Ceramic Society 94:217–223. https://doi.org/10.1111/j.1551-2916.2010.04043.x

Liu X, Zhang G, Lin L, Khan ZH, Qiu W, Song Z (2018) Synthesis and characterization of novel Fe-Mn-Ce ternary oxide biochar composites as highly efficient adsorbents for As(III) removal from aqueous solutions. Materials (Basel) 11. https://doi.org/10.3390/ma11122445

Lu D, Cheng W, Zhang T, Lu X, Liu Q, Jiang J, Ma J (2016) Hydrophilic Fe_2O_3 dynamic membrane mitigating fouling of support ceramic membrane in ultrafiltration of oil/water emulsion. Separation and Purification Technology 165:1–9. https://doi.org/10.1016/j.seppur.2016.03.034

Mahramanlioglu M, Kizilcikli I, Bicer IO (2002) Adsorption of fluoride from aqueous solution by acid treated spent bleaching earth. Journal of Fluorine Chemistry 115:41–47. https://doi.org/10.1016/S0022-1139(02)00003-9

Maity JP, Nath B, Kar S, Chen C-Y, Banerjee S, Jean J-S, Liu M-Y, Centeno JA, Bhattacharya P, Chang CL, Santra SC (2012) Arsenic-induced health crisis in peri-urban Moyna and Ardebok villages, West Bengal, India: An exposure assessment study. Environmental Geochemistry Health 34:563–574. https://doi.org/10.1007/s10653-012-9458-y

Mandal B (2002) Arsenic round the world: A review. Talanta 58:201–235. https://doi.org/10.1016/S0039-9140(02)00268-0

Manna BR, Dey S, Debnath S, Ghosh UC (2003) Removal of arsenic from groundwater using crystalline hydrous ferric oxide (CHFO). Water Quality Research Journal 38:193–210. https://doi.org/10.2166/wqrj.2003.013

Manning BA, Fendorf SE, Goldberg S (1998) Surface structures and stability of arsenic(III) on Goethite: Spectroscopic evidence for inner-sphere complexes. Environmental Science and Technology 32:2383–2388. https://doi.org/10.1021/es9802201

Marcinkowsky AE, Kraus KA, Phillips HO, Johnson JS, Shor AJ (1966) Hyperfiltration studies. IV. Salt rejection by dynamically formed hydrous oxide membranes[1]. Journal of the American Chemical Society 88:5744–5746. https://doi.org/10.1021/ja00976a013

Masscheleyn PH, Delaune RD, Patrick WH (1991) Effect of redox potential and pH on arsenic speciation and solubility in a contaminated soil. Environmental Science and Technology 25:1414–1419. https://doi.org/10.1021/es00020a008

Matsuyama H, Shimomura T, Teramoto M (1994) Formation and characteristics of dynamic membrane for ultrafiltration of protein in binary protein system. Journal of Membrane Science 92:107–115. https://doi.org/10.1016/0376-7388(94)00038-7

Mitrakas MG, Panteliadis PC, Keramidas VZ, Tzimou-Tsitouridou RD, Sikalidis CA (2009) Predicting Fe^{3+} dose for As(V) removal at pHs and temperatures commonly encountered in natural waters. Chemical Engineering Journal 155:716–721. https://doi.org/10.1016/j.cej.2009.09.011

Mohan D, Pittman CU (2007) Arsenic removal from water/wastewater using adsorbents--A critical review. Journal of Hazardous Materials 142:1–53. https://doi.org/10.1016/j.jhazmat.2007.01.006

Mukherjee A, Sengupta MK, Hossain MA, Ahamed S, Das B, Nayak B, Lodh D, Rahman MM, Chakraborti D (2006) Arsenic contamination in groundwater: A global perspective with emphasis on the Asian scenario. Journal of Health, Population and Nutrition:142–163

Naeem A, Westerhoff P, Mustafa S (2007) Vanadium removal by metal (hydr)oxide adsorbents. Water Research 41:1596–1602. https://doi.org/10.1016/j.watres.2007.01.002

Nguyen VL, Chen W-H, Young T, Darby J (2011) Effect of interferences on the breakthrough of arsenic: Rapid small scale column tests. Water Research 45:4069–4080. https://doi.org/10.1016/j.watres.2011.04.037

Nidheesh PV, Singh TSA (2017) Arsenic removal by electrocoagulation process: Recent trends and removal mechanism. Chemosphere 181:418–432. https://doi.org/10.1016/j.chemosphere.2017.04.082

Noor MJMM, Ahmadun FR, Mohamed TA, Muyibi SA, Pescod MB (2002) Performance of flexible membrane using kaolin dynamic membrane in treating domestic wastewater. Desalination 147:263–268. https://doi.org/10.1016/S0011-9164(02)00548-9

Nyobe D, Ye J, Tang B, Bin L, Huang S, Fu F, Li P, Hu Q (2019) Build-up of a continuous flow pre-coated dynamic membrane filter to treat diluted textile wastewater and identify its dynamic membrane fouling. Journal of Environmental Management 252:109647. https://doi.org/10.1016/j.jenvman.2019.109647

O'Day PA, Vlassopoulos D, Meng X, Benning LG (eds) (2005) Advances in arsenic research. ACS symposium series. American Chemical Society, Washington, DC

Organization WH (2004) Guidelines for drinking-water quality, vol 1. World Health Organization

Pal P (2015) Introduction to the arsenic contamination problem. In: Groundwater arsenic remediation. Elsevier, pp 1–23

Pal BN (2001) Granular ferric hydroxide for elimination of arsenic from drinking water. Technologies for arsenic removal from drinking water:59–68

Pan Y, Wang T, Sun H, Wang W (2012) Preparation and application of titanium dioxide dynamic membranes in microfiltration of oil-in-water emulsions. Separation and Purification Technology 89:78–83. https://doi.org/10.1016/j.seppur.2012.01.010

Podgorski J, Berg M (2020) Global threat of arsenic in groundwater. Science 368:845–850. https://doi.org/10.1126/science.aba1510

Podgorski JE, Eqani SAMAS, Khanam T, Ullah R, Shen H, Berg M (2017) Extensive arsenic contamination in high-pH unconfined aquifers in the Indus Valley. Sci Adv 3:e1700935. https://doi.org/10.1126/sciadv.1700935

Radushkevich MDL (1947) The equation of the characteristic curve of the activated charcoal USSR Phys. Chem Sect 55:331

Saldaña-Robles A, Saldaña-Robles N, Saldaña-Robles AL, Damian-Ascencio C, Rangel-Hernández VH, Guerra-Sanchez R (2017) Arsenic removal from aqueous solutions and the impact of humic and fulvic acids. Journal of Cleaner Production 159:425–431. https://doi.org/10.1016/j.jclepro.2017.05.074

Saldaña-Robles A, Damian-Ascencio CE, Guerra-Sanchez RJ, Saldaña-Robles AL, Saldaña-Robles N, Gallegos-Muñoz A, Cano-Andrade S (2018) Effects of the presence of organic matter on the removal of arsenic from groundwater. Journal of Cleaner Production 183:720–728. https://doi.org/10.1016/j.jclepro.2018.02.161

Salomons W, Förstner U, Mader P (2012) Heavy metals: Problems and solutions. Springer Science & Business Media

Sato Y, Kang M, Kamei T, Magara Y (2002) Performance of nanofiltration for arsenic removal. Water Research 36:3371–3377. https://doi.org/10.1016/s0043-1354(02)00037-4

Selatile MK, Ray SS, Ojijo V, Sadiku R (2018) Recent developments in polymeric electrospun nanofibrous membranes for seawater desalination. RSC Advances 8:37915–37938. https://doi.org/10.1039/C8RA07489E

Shanmuganathan S, Nguyen TV, Jeong S, Kandasamy J, Vigneswaran S (2015) Submerged membrane – (GAC) adsorption hybrid system in reverse osmosis concentrate treatment. Separation and Purification Technology 146:8–14. https://doi.org/10.1016/j.seppur.2015.03.017

Shannon MA, Bohn PW, Elimelech M, Georgiadis JG, Mariñas BJ, Mayes AM (2008) Science and technology for water purification in the coming decades. Nature 452:301–310. https://doi.org/10.1038/nature06599

Siddiqui SI, Chaudhry SA (2018) A review on graphene oxide and its composites preparation and their use for the removal of As^{3+} and As^{5+} from water under the effect of various parameters: Application of isotherm, kinetic and thermodynamics. Process Safety and Environmental Protection 119:138–163. https://doi.org/10.1016/j.psep.2018.07.020

Simeonidis K, Papadopoulou V, Tresintsi S, Kokkinos E, Katsoyiannis I, Zouboulis A, Mitrakas M (2017) Efficiency of iron-based oxy-hydroxides in removing antimony from groundwater to levels below the drinking water regulation limits. Sustainability 9:238. https://doi.org/10.3390/su9020238

Simonin J-P (2016) On the comparison of pseudo-first order and pseudo-second order rate laws in the modeling of adsorption kinetics. Chemical Engineering Journal 300:254–263. https://doi.org/10.1016/j.cej.2016.04.079

Singh R (2015) Introduction to membrane technology. In: membrane technology and engineering for water purification. Elsevier, pp 1–80

Singh J, Yadav P, Pal AK, Mishra V (2020) Water pollutants: Origin and status. In: Sensors in water pollutants monitoring: Role of material. Springer, pp 5–20

Smith AH, Hopenhayn-Rich C, Bates MN, Goeden HM, Hertz-Picciotto I, Duggan HM, Wood R, Kosnett MJ, Smith MT (1992) Cancer risks from arsenic in drinking water. Environmental health perspectives 97:259

Sontheimer H (1988) Activated carbon for water treatment. DVGW-Forschungsstelle Engler-Bunte-Inst. Universität Karlsruhe (TH), Karlsruhe

Sorlini S, Gialdini F (2010) Conventional oxidation treatments for the removal of arsenic with chlorine dioxide, hypochlorite, potassium permanganate and monochloramine. Water Research 44:5653–5659. https://doi.org/10.1016/j.watres.2010.06.032

Sperlich A (2010) Phosphate adsorption onto granular ferric hydroxide (GFH) for wastewater reuse. ITU-Schriftenreihe, Bd. 14. Papierflieger, Clausthal-Zellerfeld

Sperlich A, Werner A, Genz A, Amy G, Worch E, Jekel M (2005) Breakthrough behavior of granular ferric hydroxide (GFH) fixed-bed adsorption filters: Modeling and experimental approaches. Water Research 39:1190–1198. https://doi.org/10.1016/j.watres.2004.12.032

Sperlich A, Schimmelpfennig S, Baumgarten B, Genz A, Amy G, Worch E, Jekel M (2008) Predicting anion breakthrough in granular ferric hydroxide (GFH) adsorption filters. Water Research 42:2073–2082. https://doi.org/10.1016/j.watres.2007.12.019

Stoquart C, Servais P, Bérubé PR, Barbeau B (2012) Hybrid Membrane Processes using activated carbon treatment for drinking water: A review. Journal of Membrane Science 411-412:1–12. https://doi.org/10.1016/j.memsci.2012.04.012

Stylianou S, Simeonidis K, Mitrakas M, Zouboulis A, Ernst M, Katsoyiannis IA (2018) Reductive precipitation and removal of Cr(VI) from groundwaters by pipe flocculation-microfiltration. Environmental Science and Pollution Research 25:12256–12262. https://doi.org/10.1007/s11356-017-9967-4

Tajernia H, Ebadi T, Nasernejad B, Ghafori M (2014) Arsenic removal from water by sugarcane bagasse: An application of response surface methodology (RSM). Water Air Soil Pollution 225:1829. https://doi.org/10.1007/s11270-014-2028-4

Tanny GB, Johnson JS (1978) The structure of hydrous Zr(IV) oxide–polyacrylate membranes: Poly(acrylic acid) deposition. Journal of Applied Polymer Science 22:289–297. https://doi.org/10.1002/app.1978.070220121

Tantry BA, Shrivastava D, Taher I, Nabi Tantry M (2015) Arsenic exposure: Mechanisms of action and related health effects. Journal of Environmental & Analytical Toxicology 5:1. https://doi.org/10.4172/2161-0525.1000327

Thanawatpoontawee S, Imyim A, Praphairaksit N (2016) Iron-loaded zein beads as a biocompatible adsorbent for arsenic(V) removal. Journal of Industrial and Engineering Chemistry 43:127–132. https://doi.org/10.1016/j.jiec.2016.07.058

Thirunavukkarasu OS, Viraraghavan T, Subramanian KS (2003) Arsenic removal from drinking water using granular ferric hydroxide. WSA 29. https://doi.org/10.4314/wsa.v29i2.4851

Traegner U, Suidan M (1989) Evaluation of surface and film diffusion coefficients for carbon adsorption. Water Research 23:267–273. https://doi.org/10.1016/0043-1354(89)90091-2

Tran HN, You S-J, Hosseini-Bandegharaei A, Chao H-P (2017) Mistakes and inconsistencies regarding adsorption of contaminants from aqueous solutions: A critical review. Water Research 120:88–116. https://doi.org/10.1016/j.watres.2017.04.014

Tresintsi S, Simeonidis K, Vourlias G, Stavropoulos G, Mitrakas M (2012) Kilogram-scale synthesis of iron oxy-hydroxides with improved arsenic removal capacity: Study of Fe(II) oxidation--precipitation parameters. Water Res 46:5255–5267. https://doi.org/10.1016/j.watres.2012.06.049

Tresintsi S, Simeonidis K, Zouboulis A, Mitrakas M (2013a) Comparative study of As(V) removal by ferric coagulation and oxy-hydroxides adsorption: Laboratory and full-scale case studies. Desalination and Water Treatment 51:2872–2880. https://doi.org/10.1080/19443994.2012.748011

Tresintsi S, Simeonidis K, Estradé S, Martinez-Boubeta C, Vourlias G, Pinakidou F, Katsikini M, Paloura EC, Stavropoulos G, Mitrakas M (2013b) Tetravalent manganese feroxyhyte: A

novel nanoadsorbent equally selective for As(III) and As(V) removal from drinking water. Environmental Science and Technology 47:9699–9705. https://doi.org/10.1021/es4009932

Tresintsi S, Simeonidis K, Katsikini M, Paloura EC, Bantsis G, Mitrakas M (2014a) A novel approach for arsenic adsorbents regeneration using MgO. Journal of Hazardous Materials 265:217–225. https://doi.org/10.1016/j.jhazmat.2013.12.003

Tresintsi S, Simeonidis K, Mitrakas M (2014b) Mn-feroxyhyte: The role of synthesis conditions on As(III) and As(V) removal capacity. Chemical Engineering Journal 251:192–198. https://doi.org/10.1016/j.cej.2014.04.033

Tresintsi S, Mitrakas M, Simeonidis K, Kostoglou M (2015) Kinetic modeling of As(III) and As(V) adsorption by a novel tetravalent manganese feroxyhyte. Journal of Colloidal Interface and Science 460:1–7. https://doi.org/10.1016/j.jcis.2015.07.075

Tripathy SS, Raichur AM (2008) Enhanced adsorption capacity of activated alumina by impregnation with alum for removal of As(V) from water. Chemical Engineering Journal 138:179–186. https://doi.org/10.1016/j.cej.2007.06.028

Tubić A, Agbaba J, Dalmacija B, Ivancev-Tumbas I, Dalmacija M (2010) Removal of arsenic and natural organic matter from groundwater using ferric and alum salts: A case study of central Banat region (Serbia). Journal of Environmentla Science and Health: Part A 45:363–369. https://doi.org/10.1080/10934520903467931

Usman M, Waseem M, Mani N, Andiego G (2018a) Optimization of soil aquifer treatment by chemical oxidation with hydrogen peroxide addition. Pollution 4:369–379. https://doi.org/10.22059/POLL.2018.247639.354

Usman M, Katsoyiannis I, Mitrakas M, Zouboulis A, Ernst M (2018b) Performance evaluation of small sized powdered ferric hydroxide as arsenic adsorbent. Water 10:957. https://doi.org/10.3390/w10070957

Usman M, Katsoyiannis I, Rodrigues JH, Ernst M (2020a) Arsenate removal from drinking water using by-products from conventional iron oxyhydroxides production as adsorbents coupled with submerged microfiltration unit. Environmental Science and Pollution Research. https://doi.org/10.1007/s11356-020-08327-w

Usman M, Zarebanadkouki M, Waseem M, Katsoyiannis IA, Ernst M (2020b) Mathematical modeling of arsenic(V) adsorption onto iron oxyhydroxides in an adsorption-submerged membrane hybrid system. Journal of Hazardous Materials 400:123221. https://doi.org/10.1016/j.jhazmat.2020.123221

Usman M, Belkasmi AI, Katsoyiannis IA, Ernst M (2021) Pre-deposited dynamic membrane adsorber formed of microscale conventional iron oxide-based adsorbents to remove arsenic from water: Application study and mathematical modeling. Journal of Chemical Technology and Biotechnology. https://doi.org/10.1002/jctb.6728

Víctor-Ortega MD, Ratnaweera HC (2017) Double filtration as an effective system for removal of arsenate and arsenite from drinking water through reverse osmosis. Process Safety and Environmental Protection 111:399–408. https://doi.org/10.1016/j.psep.2017.08.001

Vieira BRC, Pintor AMA, Boaventura RAR, Botelho CMS, Santos SCR (2017) Arsenic removal from water using iron-coated seaweeds. Journal of Environmental Management 192:224–233. https://doi.org/10.1016/j.jenvman.2017.01.054

Vigneswaran S, Chaudhary DS, Ngo HH, Shim WG, Moon H (2003) Application of a PAC-membrane hybrid system for removal of organics from secondary sewage effluent: experiments and modelling. Separation Science and Technology 38:2183–2199. https://doi.org/10.1081/SS-120021619

Vijayaraghavan K, Padmesh TVN, Palanivelu K, Velan M+ (2006) Biosorption of nickel(II) ions onto sargassum wightii: Application of two-parameter and three-parameter isotherm models. Journal of Hazardous Materials 133:304–308. https://doi.org/10.1016/j.jhazmat.2005.10.016

Violante A, Ricciardella M, Del Gaudio S, Pigna M (2006) Coprecipitation of arsenate with metal oxides: Nature, mineralogy, and reactivity of aluminum precipitates. Environmental Science and Technology 40:4961–4967. https://doi.org/10.1021/es052321m

Wang J-Y, Chou K-S, Lee C-J (1998) Dead-end flow filtration of solid suspension in polymer fluid through an active kaolin dynamic membrane. Separation Science and Technology 33:2513–2529. https://doi.org/10.1080/01496399808545316

Wang L, Chen ASC, Sorg TJ, Fields KA (2002) Field evaluation of as removal by IX and AA. Journal - American Water Works Association 94:161–173. https://doi.org/10.1002/j.1551-8833.2002.tb09460.x

Wang L, Chen ASC, Sorg TJ, Supply W (2011) Costs of arsenic removal technologies for small water systems: US EPA arsenic removal technology demonstration program. Cincinnati: United States Environmental Protection Agency:92

Wang LH (2009) Heavy metals in the environment. CRC Press, Boca Raton

Ware GW, Albert LA, Crosby DG, Voogt P de, Hutzinger O, Knaak JB, Mayer FL, Morgan DP, Park DL, Tjeerdema RS, Whitacre DM, Yang RSH, Gunther FA (eds) (2005) Reviews of environmental contamination and toxicology. Reviews of Environmental Contamination and Toxicology. Springer New York, New York, NY

Wedepohl KH, Correns CW, Shaw DM, Turekian KK, Zemann J (1969) Handbook of Geochemistry

Westerhoff P, Highfield D, Badruzzaman M, Yoon Y (2005) Rapid small-scale column tests for arsenate removal in iron oxide packed bed columns. Journal of Environmental Engineering 131:262–271. https://doi.org/10.1061/(ASCE)0733-9372(2005)131:2(262)

Wilcox J (2012) Carbon capture. Springer, New York

Wilde FGN-d, Buckley CA, Cawdron MPR (1988) Dynamically formed hydrous zirconium (IV) oxide/polyacrylic membranes; low pressure formation, high pressure evaluation. Desalination 70:121–136. https://doi.org/10.1016/0011-9164(88)85048-3

Worch E (2012) Adsorption technology in water treatment: Fundamentals, processes, and modeling. De Gruyter, Berlin

Xie B, Fan M, Banerjee K, van Leeuwen JH (2007) Modeling of arsenic(V) adsorption onto granular ferric hydroxide. Journal - American Water Works Association 99:92–102. https://doi.org/10.1002/j.1551-8833.2007.tb08083.x

Yang B-Y, Cao Y, Qi F-F, Li X-Q, Xu Q (2015) Atrazine adsorption removal with nylon6/polypyrrole core-shell nanofibers mat: Possible mechanism and characteristics. Nanoscale Research Letters 10:207. https://doi.org/10.1186/s11671-015-0903-6

Ye M, Zhang H, Wei Q, Lei H, Yang F, Zhang X (2006) Study on the suitable thickness of a PAC-precoated dynamic membrane coupled with a bioreactor for municipal wastewater treatment. Desalination 194:108–120. https://doi.org/10.1016/j.desal.2005.11.005

Yu X-Y, Luo T, Jia Y, Zhang Y-X, Liu J-H, Huang X-J (2011) Porous hierarchically micro-/nanostructured MgO: Morphology control and their excellent performance in As(III) and As(V) removal. Journal of Physical Chemistry C 115:22242–22250. https://doi.org/10.1021/jp207572y

Zhang G, Qu J, Liu H, Liu R, Wu R (2007) Preparation and evaluation of a novel Fe-Mn binary oxide adsorbent for effective arsenite removal. Water Research 41:1921–1928. https://doi.org/10.1016/j.watres.2007.02.009

Zhang G, Liu H, Liu R, Qu J (2009) Adsorption behavior and mechanism of arsenate at Fe-Mn binary oxide/water interface. Journal of Hazardous Materials 168:820–825. https://doi.org/10.1016/j.jhazmat.2009.02.137

Zhang X, Wang Z, Wu Z, Lu F, Tong J, Zang L (2010) Formation of dynamic membrane in an anaerobic membrane bioreactor for municipal wastewater treatment. Chemical Engineering Journal 165:175–183. https://doi.org/10.1016/j.cej.2010.09.013

Zhang J, Gong C, Lu L, Wang S, Hou P (2015) Effect of MgO on the composition and properties of belite-barium calcium sulphoaluminate cement in the presence of Na_2O and K_2O. Ceramics-Silikáty 59:135–144

Zhao Y, Tan Y, Wong F-S, Fane AG, Xu N (2006) Formation of $Mg(OH)_2$ dynamic membranes for oily water separation: Effects of operating conditions. Desalination 191:344–350. https://doi.org/10.1016/j.desal.2005.06.042

Zouboulis A, Katsoyiannis I (2002) Removal of arsenates from contaminated water by coagulation-direct filtration. Separation Science and Technology 37:2859–2873. https://doi.org/10.1081/SS-120005470

A. Appendix I – Supporting information

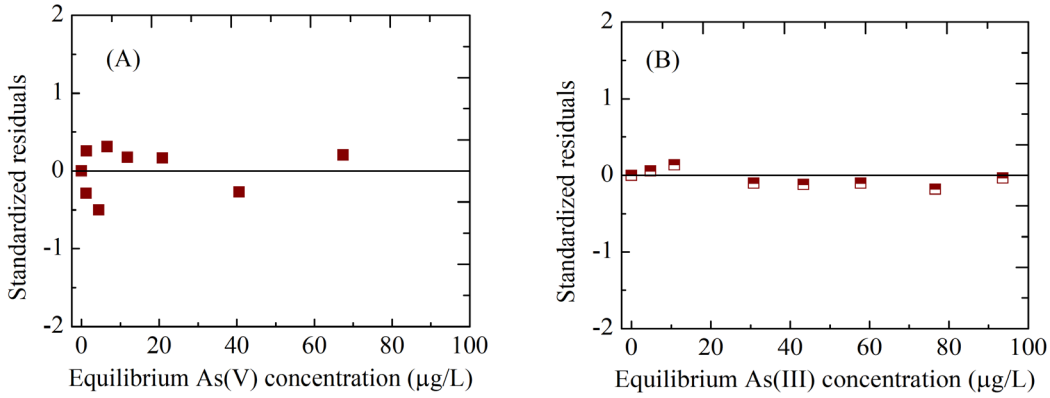

Figure A.1. Standardized residuals for the Freundlich isotherm (A) As(V) adsorption; (B) As(III) adsorption onto µGFH.

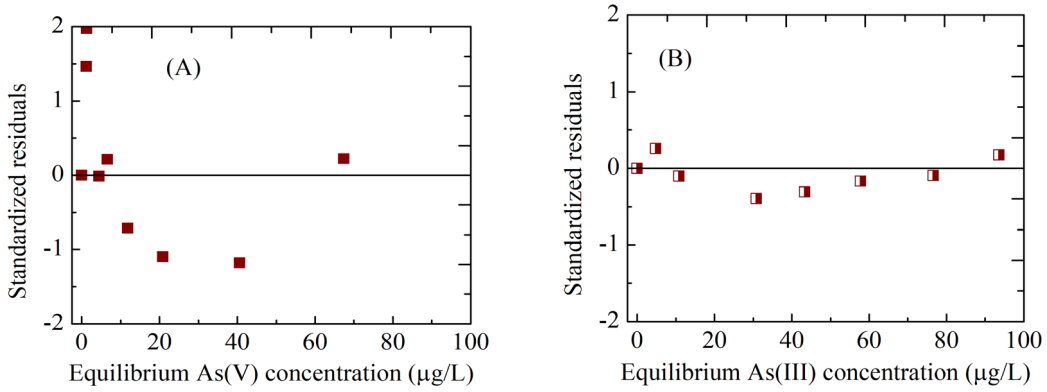

Figure A.2. Standardized residuals for the Langmuir isotherm **(A)** As(V) adsorption; **(B)** As(III) adsorption onto µGFH.

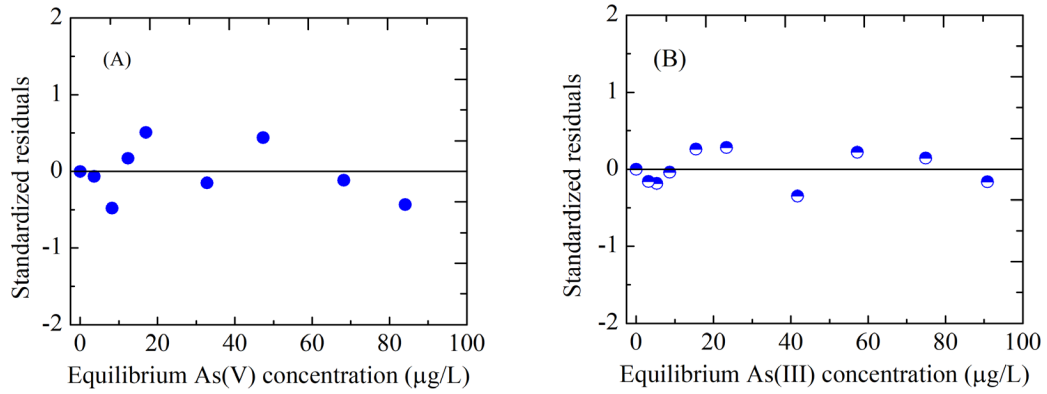

Figure A.3. Standardized residuals for the Freundlich isotherm **(A)** As(V) adsorption; **(B)** As(III) adsorption onto µTMF.

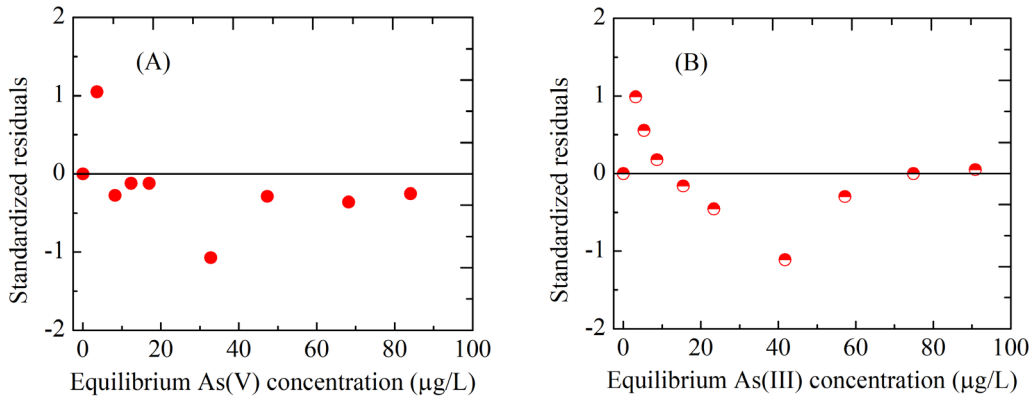

Figure A.4. Standardized residuals for the Langmuir isotherm (A) As(V) adsorption; (B) As(III) adsorption onto µTMF.

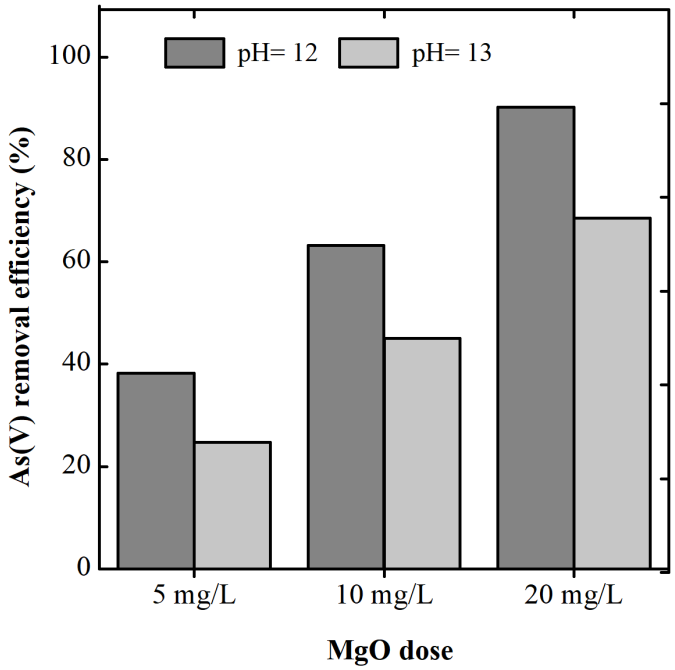

Figure A.5. Effect of MgO dose on As(V) removal (n= 2). Experimental conditions: Initial arsenic concentration = 190 µg/L in DI water, and T = 20 + 1 °C.

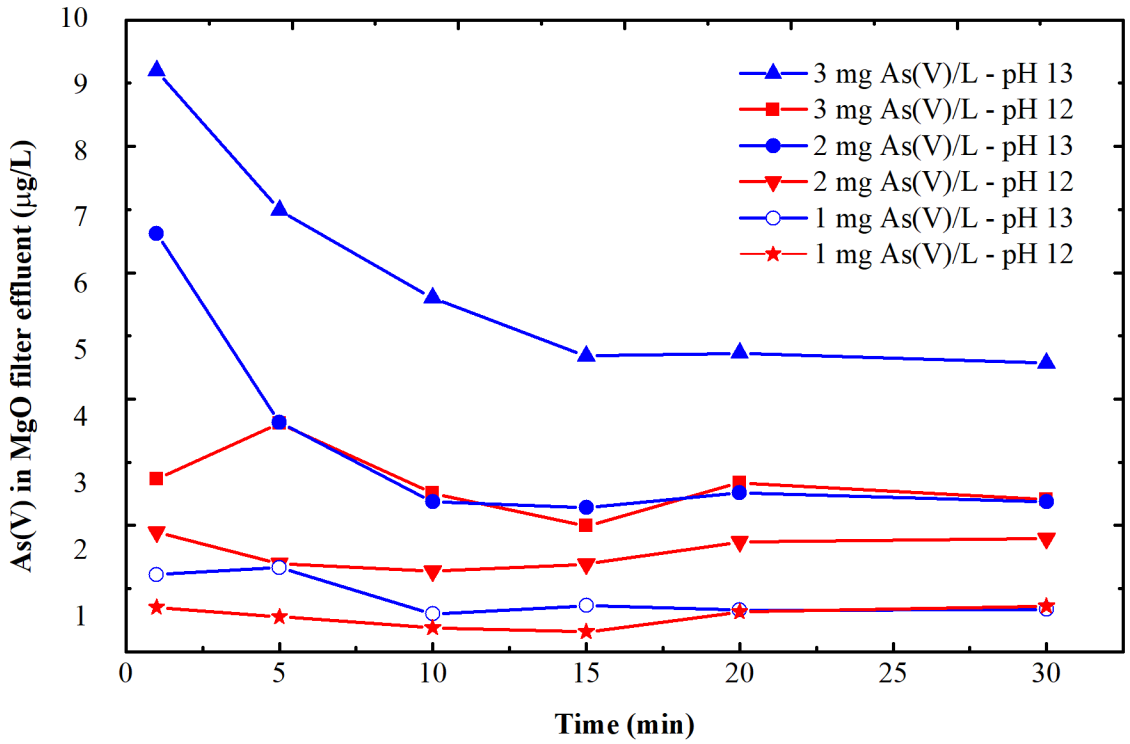

Figure A.6. As(V) concentration in the MgO filter effluent at varying pH and influent As(V) concentration with EBCT = 3 min.

Discretization of partial differential equations of the HSDM to ordinary differential equations

Eq. 2-15 was solved by method of lines (MOL), which discretizes the partial differential equations (PDEs) to ordinary differential equations (ODEs) by finite differences. The radial of the adsorbent particle (Figure 2.10) was divided into nr increments, $\Delta r = R/nr$, and the jth radial distance inside the particle is defined as, $r_j = (j - 1)\Delta r$.

The first group on the right hand side of the Eq. 2-15 was converted as follows:

At center of adsorbent j = 1:

$$\frac{\partial q^2(r,t)}{\partial t} = 2\frac{q(i,j+1)-q(i,j)}{\Delta r^2} \quad \text{(A-1)}$$

At the interior grid points j = 2, ……., nr -1:

$$\frac{\partial q^2(r,t)}{\partial t} = \frac{q(i,j+1) - 2q(i,j) + q(i,j-1)}{\Delta r^2} \quad \text{(A-2)}$$

At the surface of the adsorbents j =nr:

$$\frac{\partial q^2(r,t)}{\partial t} = \frac{q_f(i,j) - 2q(i,j) + q(i,j-1)}{\Delta r^2} \tag{A-3}$$

where

$$q_f(i,j) = q(i,j-1) + \frac{2R\,k_f}{\rho_p D_s}\left\{c(i) - \left[\frac{q(i,nr)}{K_F}\right]^{1/n}\right\} \tag{A-4}$$

The second group on the right side of the Eq. 2-15 was converted as follows:

At center of adsorbent j = 1:

$$\frac{2\,\partial q(r,t)}{r\,\partial r} = 4\,\frac{q(i,j+1)-q(i,j)}{\Delta r^2} \tag{A-5}$$

At the interior grid points j = 2,….., nr -1:

$$\frac{2\,\partial q(r,t)}{r\,\partial r} = \frac{2}{r_j}\,\frac{q(i,j+1)-q(i,j-1)}{2\,\Delta r} \tag{A-6}$$

At the surface of the adsorbent j =nr:

$$\frac{2\,\partial q(r,t)}{r\,\partial r} = \frac{2R\,k_f}{\rho_p D_s}\left\{c(i) - \left[\frac{q(i,nr)}{K_F}\right]^{1/n}\right\} \tag{A-7}$$

Altogether Eq. 2-15 becomes

At center of adsorbent j = 1:

$$\frac{\partial q(r,t)}{\partial t} = D_s\left[2\,\frac{q(i,j+1)-q(i,j)}{\Delta r^2} + 4\,\frac{q(i,j+1)-q(i,j)}{\Delta r^2}\right] \tag{A-8}$$

At the interior grid points j = 2,….., nr -1:

$$\frac{\partial q(r,t)}{\partial t} = D_s\left[\frac{q(i,j+1) - 2q(i,j) + q(i,j-1)}{\Delta r^2} + \frac{2}{r_j}\,\frac{q(i,j+1)-q(i,j-1)}{2\,\Delta r}\right] \tag{A-9}$$

At the surface of the adsorbent j =nr:

$$\frac{\partial q(r,t)}{\partial t} = D_s\left[\frac{q(i,j-1)+\frac{2R\,k_f}{\rho_p D_s}\left\{c(i)-\left[\frac{q(i,nr)}{K_F}\right]^{1/n}\right\} - 2q(i,j) + q(i,j-1)}{\Delta r^2} + \frac{2R\,k_f}{\rho_p D_s}\left\{c(i) - \left[\frac{q(i,nr)}{K_F}\right]^{1/n}\right\}\right] \tag{A-10}$$

Effect of electrical stir on particle size distribution

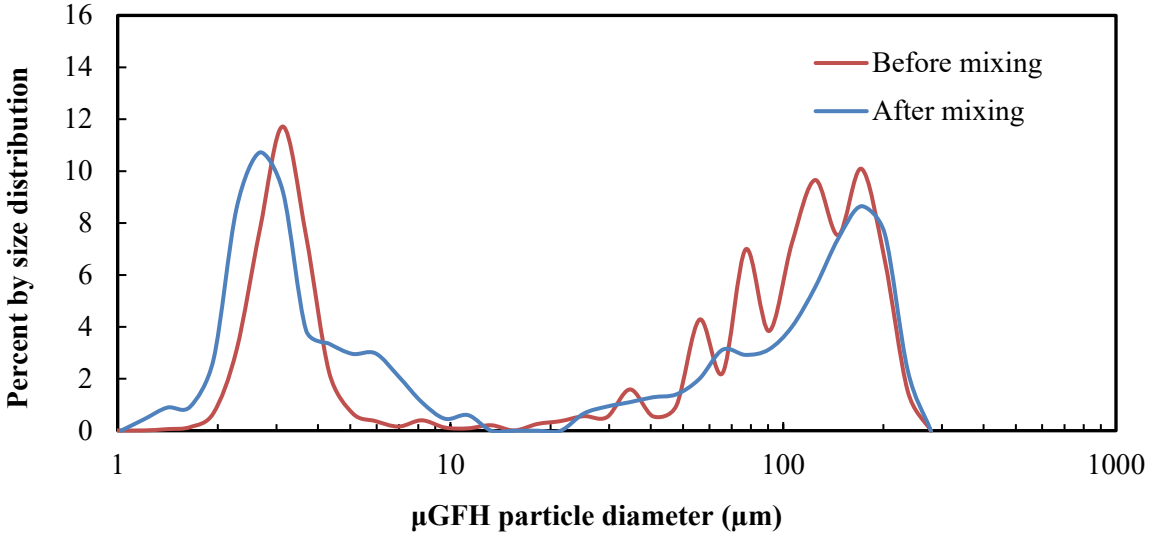

Figure A.7. Particle size distribution of µGFH (1–250 µm) determined using particle size analyzer (EyeTech) device.

Particle size distribution of powdered-sized iron oxyhydroxides

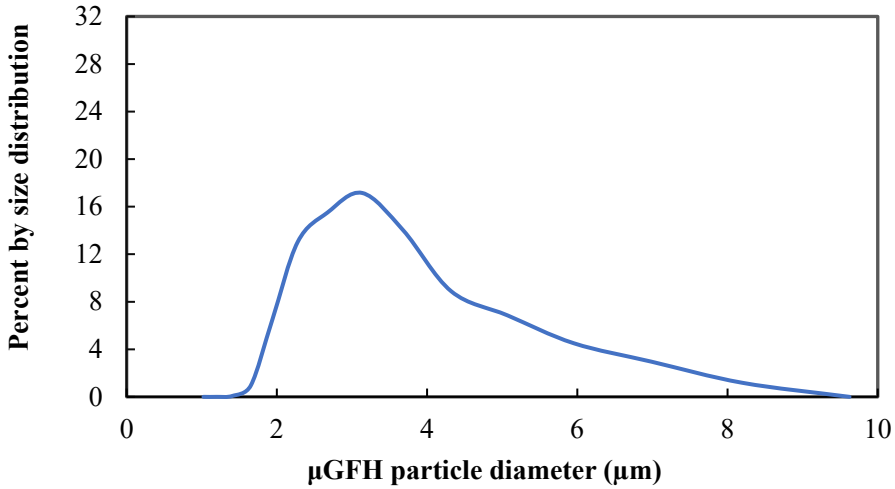

Figure A.8. Particle size distribution of µGFH (1 – 63 µm).

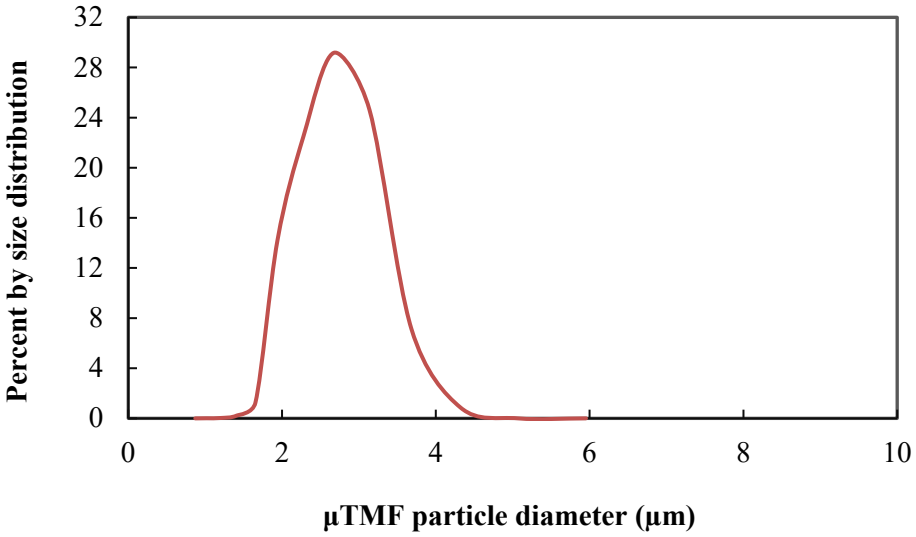

Figure A.9. Particle size distribution of µTMF (1–63 µm).

Equilibrium parameters for As(V) adsorption

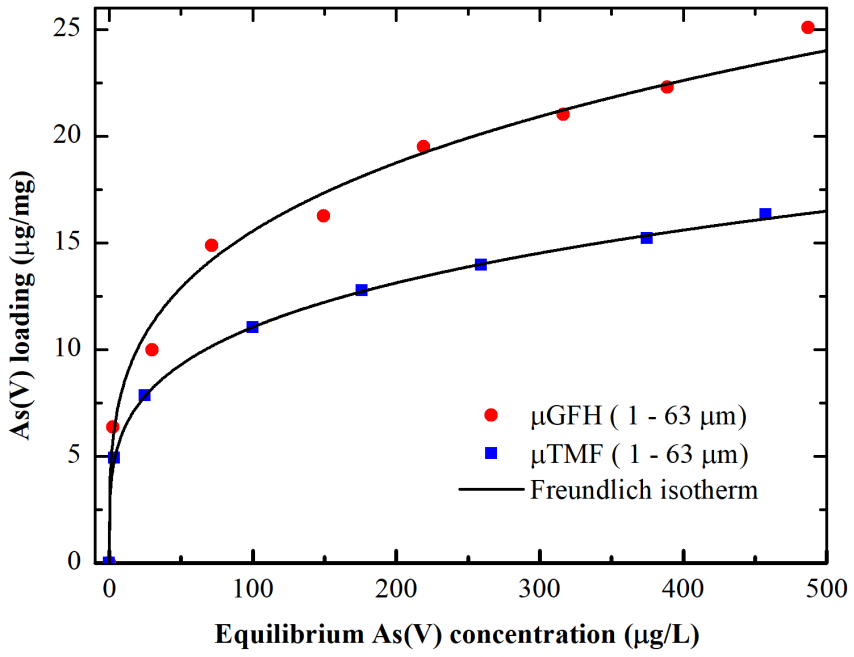

Figure A.10. Freundlich isotherms for µGFH and µTMF developed using powdered-sized fractions (1–63 µm). K_F and n determined by fitting are: 4.5 (µg/mg)/(L/µg)^n and 0.27 for µGFH and 3.5 (µg/mg)/(L/µg)^n and 0.25 for µTMF, respectively.

Modeling of experimentally determined breakthrough curves for As(V) adsorption onto µTMF in the SMAHS

Influence of adsorbent dose on the breakthrough curves for As(V) adsorption onto µTMF

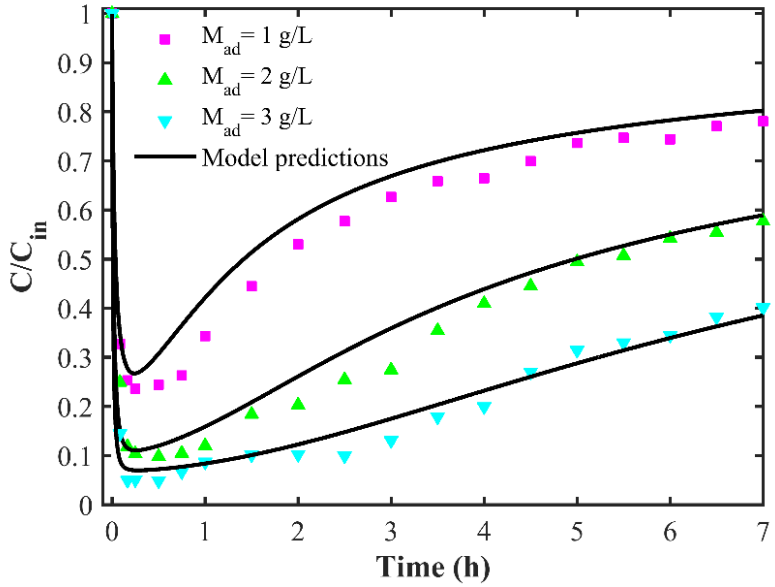

Figure A.11. Model verification for continuous-flow SMAHS at C_{in} = 380 µg/L, pH = 8 and membrane water flux = 200 L/(m^2·h) using µTMF (1 – 250 µm).

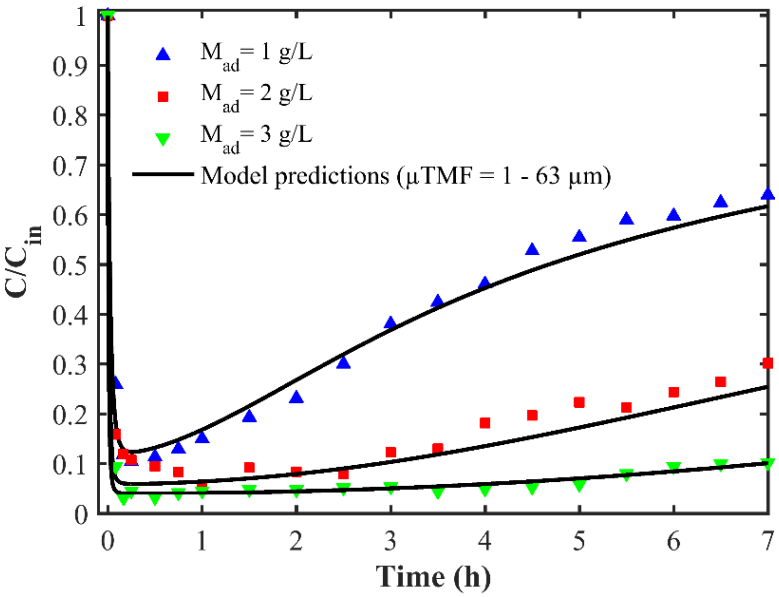

Figure A.12. Model verification for continuous-flow SMAHS at C_{in} = 380 µg/L, pH = 8 and membrane water flux = 200 L/(m^2·h) using µTMF (1 – 63 µm).

Influence of membrane flux on the breakthrough curves for As(V) adsorption onto µTMF

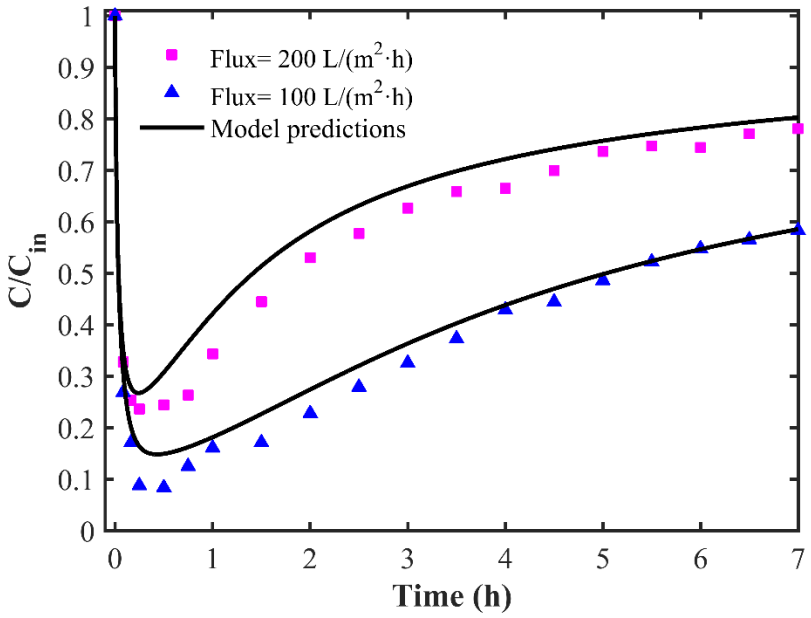

Figure A.13. Model verification for continuous-flow SMAHS at C_{in} = 380 µg/L, pH = 8 using µTMF (1 – 250 µm).

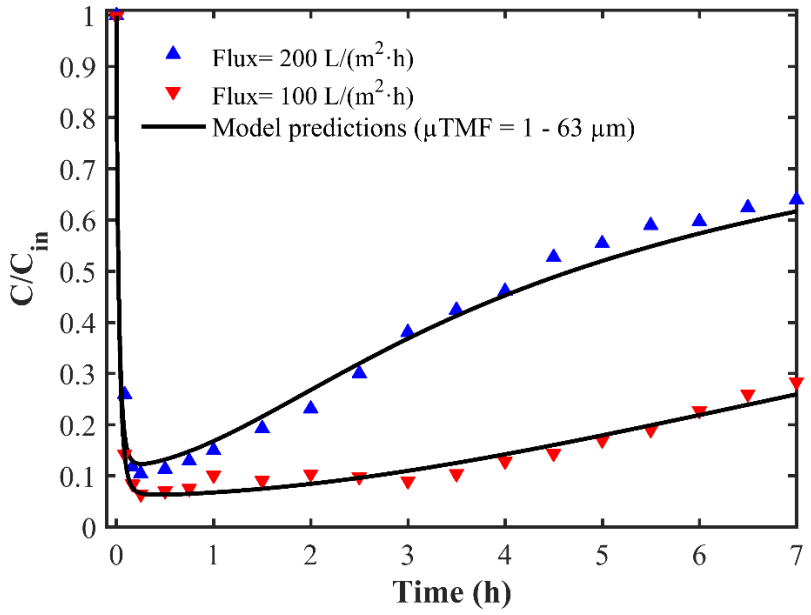

Figure A.14. Model verification for continuous-flow SMAHS at C_{in} = 380 µg/L, pH = 8 using µTMF (1 – 63 µm).

Table A.1. Values of sum of square of error (SSE) and coefficient of determination between the experimentally and simulated breakthrough curves of As(V).

Adsorbent media	Mean particle size (µm)	Water flux (L/(m^2·h))	M_{ad} (g/L)	SSE (x 10^{-2})	R^2
µGFH	78.4	200	3	1.7	0.983
µGFH	78.4	200	2	5.2	0.971
µGFH	78.4	200	1	1.7	0.956
µGFH	78.4	100	1	2.5	0.986
µGFH	3.5	200	3	4.3	0.974
µGFH	3.5	200	2	5.3	0.961
µGFH	3.5	200	1	2.1	0.991
µGFH	3.5	100	1	1.3	0.987
µTMF	40.0	200	3	1.3	0.986
µTMF	40.0	200	2	3.2	0.977
µTMF	40.0	200	1	4.4	0.983
µTMF	40.0	100	1	2.4	0.996
µTMF	2.8	200	3	0.3	0.996
µTMF	2.8	200	2	2.7	0.986
µTMF	2.8	200	1	3.9	0.995
µTMF	2.8	100	1	0.5	0.994

Reproducibility of dynamic membrane formed from powdered-sized iron oxyhydroxides

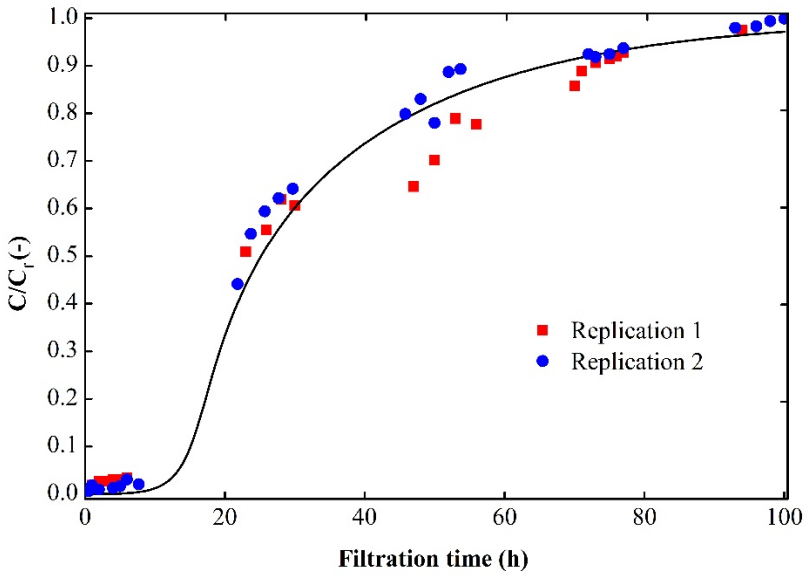

Figure A.15. Reproducibility of pre-deposited dynamic membrane formed from µTMF (1 - 63 µm) at membrane water flux= 125 L/(m^2·h), M_a = 10.4 mg/cm^2, As(V)= 380 µg/L, pH= 8 ± 0.1. Solid symbols reflect experimental data points, whereas model predictions are represented by solid lines at corresponding operating conditions.

B. Appendix II – List of publications

Selected contents of this thesis have been published as follows:

- Usman, M., Belkasmi, AI., Katsoyiannis, IA., & Ernst, M. (2021). Pre-deposited dynamic membrane adsorber formed of microscale conventional iron oxide-based adsorbents to remove arsenic from water: Application study and mathematical modeling. *Journal of Chemical Technology and Biotechnology (in press)*. https://doi.org/10.1002/jctb.6728.
- Usman, M., Katsoyiannis, IA., Rodrigues, JH., & Ernst, M. (2020a). Arsenate removal from drinking water using by-products from conventional iron oxyhydroxides production as adsorbents coupled with submerged microfiltration unit. *Environmental Science and Pollution Research (in press)*. https://doi.org/10.1007/s11356-020-08327-w.
- Usman, M., Zarebanadkouki, M., Waseem, M., Katsoyiannis, IA., & Ernst, M. (2020b). Mathematical modeling of arsenic (V) adsorption onto iron oxyhydroxides in an adsorption-submerged membrane hybrid system. *Journal of Hazardous Materials*, 400, 123221. https://doi.org/10.1016/j.jhazmat.2020.123221.
- Usman, M., Katsoyiannis, IA., Mitrakas, M., Zouboulis, A., & Ernst, M. (2018). Performance evaluation of small sized powdered ferric hydroxide as arsenic adsorbent. *Water*, 10(7), 957. https://doi.org/10.3390/w10070957.

C. Appendix III – List of supervised student theses

The following student works were conducted within the scope of this thesis:

M.Sc. Theses

- Belkasmi, A.I. Dynamic membrane pre-coated with powdered-sized iron oxyhydroxides for arsenic removal. M.Sc. thesis, January 2019
- Waseem, M. Assessment of arsenic removal by micro-sized iron oxyhydroxides in an adsorption-submerged membrane hybrid system. M.Sc. thesis, November 2019.
- Tasawwar, S. Impact of water matrix on arsenic removal using ferric hydroxide-based adsorbents. M.Sc. thesis, November 2018.
- Rodrigues, J.H. Submerged membrane adsorption hybrid system for removal of arsenic from drinking water. M.Sc. thesis, October 2018.

M.Sc. Project Works

- Belkasmi, A.I. Pre-deposited dynamic membrane adsorber formed from powdered-sized iron oxyhydroxides for arsenic removal. M.Sc. project work, October 2020
- Alves, B.R.M. Adsorption characteristics of micro-sized granular ferric hydroxide (μGFH) for removing arsenate from aqueous solutions. M.Sc. project work, August 2017.

In this doctoral thesis, the adsorption of arsenic, a toxic pollutant found in surface and ground water resources, onto two fine-grained iron oxyhydroxides as adsorbents was investigated through batch adsorption tests. Moreover, arsenic adsorption in a slurry reactor was combined with a submerged microfiltration (MF) membrane unit to create an innovative and cost-effective water treatment system. Experimentally determined arsenic removal rates were modeled using a developed mathematical model. This work confirms that micro-sized iron oxyhydroxides, by-products of conventional adsorbent production processes, can successfully be employed in the proposed water treatment system to achieve arsenic maximum permissible limit of 10 µg/L in drinking water without fouling of the MF membrane.

DOI: https://doi.org/10.15480/882.3388